MAX-PLANCK-INSTITUT FÜR PLASMAPHYSIK

GARCHING BEI MÜNCHEN

SPUTTERING STUDIES WITH THE MONTE-CARLO PROGRAM TRIM SP

W. Eckstein

IPP 9/41 August 1983

Die nachstehende Arbeit wurde im Rahmen des Vertrages zwischen dem Max-Planck-Institut für Plasmaphysik und der Europäischen Atomgemeinschaft über die Zusammenarbeit auf dem Gebiete der Plasmaphysik durchgeführt.

IPP 9/41

W. Eckstein

Sputtering studies with the Monte-Carlo Program TRIM SP

Abstract

This report shows the results of an thorough investigation about the ability of the Monte-Carlo Program TRIM SP to give data on sputtering. The results show the importance of different processes leading to sputtering, they are compared with predictions of transport theory /1/, they are compared with experimental data and they give details of angular and energy distributions of sputtered particles. Many of the calculated data are given in two papers /2, 3/. The program is described in /2/.

Input parameters

Input parameters to the program are the following:

Z_1, M_1 charge and mass of the incident particle

Z_2, M_2 charge and mass of the target atom

ρ density of the target material

E_o energy of the incident particle

α angle of incidence

E_B binding energy of an atom in the bulk (always taken as zero if not stated otherwise)

E_S surface binding energy of a target atom at the surface (heat of sublimation) from /4/

interaction potential (Kr-C potential /5/ for all collisions if not stated otherwise

inelastic energy loss (equipartition of Lindhard-Scharff /6/ and Oen-Robinson /7/ for all particles heavier than He, and Andersen-Ziegler /8/ for H, and Ziegler /8/ for He, if not stated otherwise).

All these input parameters are taken from tables and publications and no fitting to experimental data has been done.

For the calculation of the data the TRIM sputtering version TRSPCR1 was used. This version neglects additional scattering with more distant atoms especially at low energy and underestimates surface scattering. This leads to sputtering yields which are larger (30 % for Ne → Ni, 5% for H → Ni) than those calculated with the new corrected version TRSP1C (see the discussion in /2/). Other small deviations arise in the angular distributions at grazing exit angles and for heavy particles at low energies.

Calculated data

Y, total sputtering yield

Y_E, sputtered energy

Number of sputtered particles for four sputtering processes 1) Ion in, PKA; 2) Ion in, SKA; 3) Ion out, PKA and 4) Ion out, SKA.

Number of sputtered particles (all sputtered particles and PKA's alone) versus the energy, E, of the sputtered particles and the polar exit angle, ß, in form of a matrix.

Number of sputtered particles (all sputtered particles and PKA's alone) versus the polar exit angle, ß, and the azimuthal exit angle, ϕ ($\equiv \varphi$), in form of a matrix.

Number of sputtered particles versus the exit energy, E, and the polar exit angle, ß, in an azimuthal exit-angle range, $\Delta\phi = 15^{o}$, again in form of a matrix.

Number of sputtered particles (all sputtered particles and PKA's alone) versus the exit energy, E, and the depth of origin, in form of a matrix.

In addition the program gives some data on reflection: Particle (R_N) and energy (R_E) reflection coefficients. Number of backscattered particles versus the exit angle, E, and the polar exit-angle, ß, in form of a matrix. Number of backscattered particles versus the azimuthal exit angle, ϕ ($\equiv \varphi$) and the polar exit-angle, ß, in form of a matrix.

The program gives also some data on particle and energy deposition in the solid:
Depth distribution of implanted particles and the first four moments.
Total pathlength distribution of implanted particles.
Depth distribution of energy lost in elastic as well as in inelastic collisions.

The energy resolution is in most cases 1 eV, the angular resolution in ß as well as ϕ is 3^{o}. The depth resolution for the depth or origin of the sputtered particles is given in Å, the resolution for the depth distribution of implanted particles larger or equal than 1 Å, depending on the maximum penetratiion depth.

Further calculated data and comparisons with experimental data are given in /11-16/.

Results

Here only a collection of the calculated sputtering data are given. For a discussion of the results see /2/ and /17/.

Fig. 1 Range of target atoms

Fig. 2-3 Sputtering yield versus incident energy: dependence on interaction potential and inelastic energy loss.

Fig. 4-17 Contribution of different processes to the sputtering yield for several incident ions on Ni: dependence on incident energy and angle.

Fig. 18 Dependence of the sputtering yield on the surface binding energy.

Fig. 19 Dependence of the sputtering yield on the bulk binding energy.

Fig.20-21 Comparison of the sputtering yield versus incident energy and angle with experimental data.

Fig. 22-23 Total angular distributions for normal and non-normal incidence.

Sputtering in one binary collision /17/

a) Angular distributions

The occurrence of the ridge in the angular distribution is shown to be due to PKA in fig. 28. In addition it can be demonstrated that the ridge is mainly due to sputtering in one binary collision. From fig. 61 the polar exit angle ß after refraction (planar surface potential) is found to be

$$tg^2\beta = \frac{E_{\parallel}}{E_{\perp}} \qquad (1)$$

with

$$E_{\parallel} = T \sin^2\beta'$$
$$E_{\perp} = T \cos^2\beta' - E_S$$

where T is the transferred energy in a binary collision and ß' is the emission angle before refraction.
The transferred energy is

$$T = \gamma E_o \cos^2 \delta_R$$

where

$$\gamma = \frac{4M_1M_2}{(M_1+M_2)^2}$$

The recoil angle δ_R can be determined from fig. 60

$$\cos\delta_R = \sin\alpha \sin\beta' \cos\phi - \cos\alpha \cos\beta' \qquad (2)$$

From these relations the polar exit angle ß is calculated by

$$tg^2\beta = \frac{A[\sin\alpha \sin\beta' \cos\phi - \cos\alpha \cos\beta']^2 \sin^2\beta'}{A[\sin\alpha \sin\beta' \cos\phi - \cos\alpha \cos\beta']^2 \cos^2\beta' - 1} \qquad (3)$$

$$\text{with } A = \gamma E_o/E_S$$

Due to the limitation of ß' caused by a maximum recoil angle, $\delta_R = 90^o$, ß must have a minimum value, β_{min}. Differentiation leads to the following transzendental equation for β'_{min}

$$A = \frac{\sin\alpha \sin 2\beta'_{min} \cos\phi - \cos\alpha \cos 2\beta'_{min}}{(\sin\alpha \sin\beta'_{min} \cos\phi - \cos\alpha \cos\beta'_{min})^3 \cos\beta'_{min}} \qquad (4)$$

Putting β'_{min} into equation (3) gives β_{min}. An example of β versus β' is shown in fig. 34. The assumption is made that the angle β_{min} occurs with the highest intensity for a binary collision sputtering process, which is justified by taking the cross section into account /17/.

As seen from fig. 34, β' has a lower and an upper limit, β'_1 and β'_2. They can be calculated from equation (3) by putting the denominator in (3) to zero. The result is

$$\cos^2\beta'_{1,2} = \frac{-[2B\cos\alpha - \sin^2\alpha \cos^2\phi] + \sin\alpha \cos\phi [\sin^2\alpha \cos^2\phi - 4B(B+\cos\alpha)]^{1/2}}{2[\cos^2\alpha + \sin^2\alpha \cos^2\phi]}$$

$$\text{with } B = A^{-1/2} \qquad (5)$$

Figure 35 shows β_{min}, β'_{min}, β'_1 and β'_2 versus the azimuthal angle, ϕ, for a chosen value of A. The next figures 36-38 show β_{min} versus ϕ, α and A.

There is an upper limit for the azimuthal angle which is determined from (5) by putting the square root to zero:

$$\cos^2\phi_c = \frac{4B(B + \cos\alpha)}{\sin^2\alpha} \qquad (6)$$

There is also a lower limit for α and A which follows from $\phi_c = 0$:

$$\cos\alpha_c = 1 - 2B \qquad \text{or} \qquad A_c = [\sin\tfrac{\alpha}{2}]^{-4} \qquad (7)$$

The critical value, ϕ_c, is shown in fig. 39, 40 versus α and A, the relation between α_c and A in fig. 41.

If one assumes a scalar potential (no refraction) there is also a lower limit for the exit angle: starting from

$$E_S = T = \gamma E_o \cos^2 \delta_R \tag{8}$$

the exit angle β_{min} in this case is determined by (8) and (2)

$$\cos\beta_{min} = \frac{-B\cos\alpha + \sin\alpha\cos\phi[\cos^2\alpha+\sin^2\alpha\cos^2\phi - B^2]^{1/2}}{\cos^2\alpha+\sin^2\alpha\cos^2\phi} \tag{9}$$

The lower limit of β_{min}, $\bar{\beta}$, is determined for $\delta_R = 90^o$ or $B = 0$

$$\cos\bar{\beta} = \frac{\sin\alpha\cos\phi}{[\cos^2\alpha + \sin^2\alpha\cos^2\phi]^{1/2}} \tag{10}$$

Again, as above, for the planar potential the upper limit for ϕ , ϕ_c, is determined by $\beta_{min} = 90^o$ in (9) with the result

$$\phi_c = \frac{B}{\sin\alpha} \tag{11}$$

and the lower limit for α, α_c, is found by $\phi_c = 0$

$$\sin\alpha_c = A^{-1/2} = B \tag{12}$$

Curves for β_{min}, ϕ_c, α_c determined for several values of A are shown in fig. 42, 43.

b) Energy distributions

The second peak in the energy distributions in the forward direction can be related to the sputtering in one binary collision.

The energy, E, a particle has after sputtered in a binary collision is

$$E = T - E_S$$

The emission angle, ß, after refraction is given by taking (1) into account.

$$tg^2\beta = \frac{(E'+1)\sin^2\beta'}{(E'+1)\cos^2\beta'-1} \qquad (13)$$

where $E' = \frac{E}{E_S}$.

The relation between ß and E is determined by calculating ß' from

$$\cos\beta' = \frac{-\sqrt{\frac{E'+1}{A}}\ \cos\alpha + \sin\alpha\ \cos\phi\ \sqrt{\cos^2\alpha + \sin^2\alpha\ \cos^2\phi - \frac{E'+1}{A}}}{\cos^2\alpha + \sin^2\alpha\ \cos^2\phi} \qquad (14)$$

The curve resulting from (13) and (14) is shown for some examples in figs. 56-58.

For the case of a scalar surface potential, the relation between E and ß is

$$\begin{aligned} E &= E_S\ [A\ \cos^2\ \delta_R - 1] \\ &= E_S\ [A\ (\sin\alpha\ \sin\beta\ \cos\phi - \cos\alpha\ \cos\beta)^2 - 1] \end{aligned} \qquad (15)$$

References

/1/ P. Sigmund, Phys.Rev. 184 (1969) 383, and 187 (1969) 768

/2/ W. Eckstein and J. Biersack, Appl.Phys.

/3/ W.Eckstein, J.Biersack, Nucl.Instr.Meth.

/4/ N.Matsunami, Y.Yamamura, Y.Itikawa, N.Itoh, Y.Kazumata, S.Myagawa, K.Morita and R.Shimizu, IPPJ-AM-14, Institute of Plasma Physics, Nagoya University, Nagoya, Japan (1980)

R. Hultgren, J.P. Desai, D.T. Hawkins, M.Gleiser, K.K. Kelley, D.D. Wagman: Selected Values of the Thermodynamic Properties of the Elements (American Society for Metals, Metals Park, Ohio, USA 1973)

/5/ W.Wilson, L.Haggmark, J.Biersack, Phys.Rev. B15, (1977) 2458

/6/ J.Lindhard, M.Scharff, Mat.-Fys.Medd., Dan.Vid.Selsk. 27 (1953) 15

/7/ O.S. Oen and M.T. Robinson, Nucl.Instr.Meth. 132 (1976)647

/8/ J.F. Ziegler, (ed) Stopping Powers and Ranges in Matter, Vol. 3 and 4, Pergamon Press, N.Y., 1977

/9/ H.H. Andersen, H.Bay, in "Sputtering by Ion Bombardment", ed. R. Behrisch, Topics in Applied Physics, Springer, Berlin-Wien, 1980

/10/ J.Roth, J.Bohdansky, W. Ottenberger, IPP-Report 9/26, 1979

/11/ J.Roth, Proc. of the Symposium on Sputtering (Varga, Betz, Viehböck, eds.) Techn. Univers. Wien, 1980, p. 773

/12/ J. Bohdansky, G.L. Chen, W.Eckstein and J.Roth, J.Nucl.Mater. 103&104 (1981) 339

/13/ W. Eckstein, IPP-JET Report No. 4 (1981)

/14/ J. Bohdansky, G.L. Chen, W.Eckstein, J.Roth, B.M.U.Scherzer, R.Behrisch, J.Nucl.Mat. 111&112 (1982) 717

/15/ R.Becerra-Acevedo, J.Roth, W.Eckstein and J.Bohdansky, to be published

/16/ P.-J. Schneider, W.Eckstein, H.Verbeek, to be published in Nucl.Instr. Meth.

/17/ J.Roth, W.Eckstein and J.Bohdansky, Nucl.Instr.Meth.

Figure Captions

Fig. 1 Sputtered particles per incident particle versus the depth, x_o, of the starting particle for 100 eV Ni in Ni.
The fraction of escaping starting particles are given for two different inelastic energy losses:
LS (+) and OR (x).
The fraction of sputtered SKA are given for the same two inelastic energy loss models:
LS (o) and OR (●).
Indicated in the figure is also the range parameter R (and 2 R) applied in TRIM to reduce computer time.
The Kr-C potential was applied for the calculations.

Fig. 2 Ne bombardment of Ni at normal incidence, $\alpha = 0^o$.
Sputtering yield, Y, versus the incident energy, E_o, for different interatomic potentials and inelastic energy loss models. Comparison with experimental data (o)/9/.

a) Moliére potential for Ne-Ni, Kr-C potential for Ni-Ni (solid lines). Moliére potential for both kinds of collisions (dashed lines).

b) Kr-C potential for both Ne-Ni and Ni-Ni collisions.

Lines drawn to guide the eye.

Fig. 3 H bombardment of Ni at normal incidence, $\alpha = 0^o$.
Sputtering yield, Y, versus the incident energy, E_o, for different interatomic potentials and inelastic energy loss models.

a) Moliére potential for H-Ni, Kr-C potential for Ni-Ni.

b) Kr-C potential for both kinds of collisions.

Lines drawn to guide the eye.

Fig. 4 H bombardment of Ni at normal incidence, $\alpha = 0^{o}$.

a) Sputtering yield, Y, and particle reflection coefficient, R_N, versus the incident energy, E_o.

b) Relative contribution of primary knock-on atoms, PKA (ion in and ion out), and secondary knock-on atoms, SKA (ion in and ion out), to the total sputtering yield, Y, versus the incident energy, E_o

Lines drawn to guide the eye.

Fig. 5 D bombardment of Ni at normal incidence, $\alpha = 0^{o}$.

a) Sputtering yield, Y, and particle reflection coefficient, R_N, versus the incident energy, E_o.

b) Relative contribution of primary knock-on atoms, PKA (ion in and ion out), and secondary knock-on atoms, SKA (ion in and ion out), to the total sputtering yield, Y, versus the incident energy, E_o

Lines drawn to guide the eye.

Fig. 6 T bombardment of Ni at normal incidence, $\alpha = 0^{o}$.

a) Sputtering yield, Y, and particle reflection coefficient, R_N, versus the incident energy, E_o.

b) Relative contribution of primary knock-on atoms, PKA (ion in and ion out), and secondary knock-on atoms SKA (ion in and ion out), to the total sputtering yield, Y, versus the incident energy, E_o

Lines drawn to guide the eye.

Fig. 7 ^{3}He bombardment of Ni at normal incidence, $\alpha = 0^{o}$.

a) Sputtering yield, Y, and particle reflection coefficient, R_N, versus the incident energy, E_o.

b) Relative contribution of primary knock-on atoms, PKA (ion in and ion out), and secondary knock-on atoms, SKA (ion in and ion out), to the total sputtering yield, Y, versus the incident energy, E_o

Lines drawn to guide the eye.

Fig. 8 Comparison of the sputtering yield, Y, of Ni with T and ^{3}He versus the incident energy, E_o, for normal incidence, $\alpha = 0^o$.
Lines drawn to guide the eye.

Fig. 9 ^{4}He bombardment of Ni at normal incidence, $\alpha = 0^o$.

a) Sputtering yield, Y, and particle reflection coefficient, R_N, versus the incident energy, E_o.

b) Relative contribution of primary knock-on atoms, PKA (ion in and ion out), and secondary knock-on atoms, SKA (ion in and ion out), to the total sputtering yield, Y, versus the incident energy, E_o.

Lines drawn to guide the eye.

Fig.10 Ne bombardment of Ni at normal incidence, $\alpha = 0^o$.

a) Sputtering yield, Y, and particle reflection coefficient, R_N, versus the incident energy, E_o.

b) Relative contributions of primary knock-on atoms, PKA (ion in and ion out), and secondary knock-on atoms, SKA (ion in and ion out), to the total sputtering yield, Y, versus the incident energy, E_o.

Lines drawn to guide the eye.

Fig.11 Ar bombardment of Ni at normal incidence, $\alpha = 0^o$.

a) Sputtering yield, Y, and particle reflection coefficient, R_N, versus the incident energy, E_o. In addition, the sputtering yield is shown as calculated from Sigmund's theory, using $F_D(x=0) = \alpha \cdot S_n(E_o)$ for both the Molière and the Kr-C potential.

b) Relative contributions of primary knock-on atoms, PKA (ion in and ion out) and secondary knock-on atoms, SKA (ion in and ion out) to the total sputtering yield, Y versus the incident energy E_o.

Lines drawn to guide the eye.

Fig.12 Xe bombardment of Ni at normal incidence, $\alpha = 0^{o}$.

a) Sputtering yield, Y, versus the incident energy, E_o.

b) Relative contributions of primary knock-on atoms, PKA (ion in and ion out), and secondary knock-on atoms, SKA (ion in and ion out) to the total sputtering yield, Y, versus the incident energy, E_o

Lines drawn to guide the eye.

Fig.13 H bombardment of Ni at an incident energy E_o = 1 keV:

a) Sputtering yield, Y, and particle reflection coefficient, R_N, versus the angle of incidence, α.

b) Relative contributions of primary knock-on atoms, PKA (ion in and ion out), and secondary knock-on atoms, SKA (ion in and ion out), to the total sputtering yield, Y, versus the angle of incidence, α.

Lines drawn to guide the eye.

Fig.14 ^{4}He bombardment of Ni at an incident energy, E_o = 1 keV

a) Sputtering yield, Y, and particle reflection coefficient, R_N, versus the angle of incidence, α.

b) Relative contributions of primary knock-on atoms, PKA (ion in and ion out), and secondary knock-on atoms, SKA (ion in and ion out), to the sputtering yield, Y, versus the angle of incidence, α.

Lines drawn to guide the eye.

Fig.15 Ne bombardment of Ni at an incident energy E_o = 1 keV:

a) Sputtering yield, Y, for three different inelastic energy loss models, and particle reflection coefficient, R_N, versus angle of incidence, α.

b) Relative contributions of primary knock-on atoms, PKA (ion in and ion out), and secondary knock-on atoms, SKA (ion in and ion out), to the total sputtering yield, Y, versus the angle of incidence, α.

Lines drawn to guide the eye.

Fig.16 Ar bombardment of Ni at an incident energy, E_o = 1 keV:

a) Sputtering yield, Y, and particle reflection coefficient, R_N, versus the angle of incidence, α.

b) Relative contributions of primary knock-on atoms, PKA (ion in and ion out), and secondary knock-on atoms, SKA (ion in and ion out), to the total sputtering yield, Y, versus the angle of incidence, α.

Lines drawn to guide the eye.

Fig.17 Xe-bombardment of Ni at an incident energy E_o = 1 keV:

a) Sputtering yield, Y, and particle reflection coefficient, R_N, versus the angle of incidence, α.

b) Relative contributions of primary knock-on atoms, PKA (ion in and ion out), and secondary knock-on atoms, SKA (ion in and ion out), to the total sputtering yield, Y, versus the angle of incidence, α.

Fig.18 a) Sputtering yield, Y, versus surface binding energy, E_s, for 1 keV Ar on Ni at normal incidence. The dashed line gives $Y \propto E_s^{-1}$ /1/.

b) Sputtering yield, Y, versus surface binding energy, E_s, for 0.08, 0.3 and 2 keV D on C at normal incidence.
The dashed line gives $Y \propto E_s^{-1}$.

Fig.19 Sputtering yield, Y, versus the normalized ion energy, E', where $E' = E/E_{th}$ with E_{th} defined in /10/ for D on Ni at normal incidence. The curves show the influence of various choices of bulk binding energies. The curve is determined from the semi-empirical formula (7) from Ref. /10/.

Fig.20 Comparison of experimental /9,10/ and calculated values of the sputtering yield, Y, versus incident energy, E_o, for H, D, ^{4}He, Ne, Ar and Xe on Ni at normal incidence.
Lines connect the calculated points and are drawn to guide the eye.

Fig.21 Comparison of experimental /10/and calculated values of the sputtering yield, Y, versus the angle of incidence, α, for H on Ni.
a) incident energies from 0.2 keV to 1 keV.
b) incident energies from 4 keV and to 8 keV.

Fig.22 Angular distribution of sputtered particles for 1 keV H bombardment of Ni at normal incidence. The polar angle distribution is azimuthally symmetric. The total angular distribution (solid line), a cosine distribution (circle) and the contribution of primary knock-ons (dashed line) are shown.

Fig.23 Azimuthal distribution (integrated over polar angles) of sputtered particles for 1 keV H bombardment of Ni at an angle of incidence, $\alpha = 80^o$.

Fig.24 Angular distributions in the incident plane of the sputtered particles (azimuthal angular range $0^o \leq \phi \leq 15^o$) for 1 keV H bombardment of Ni at several angles of incidence. The distributions are normalized to give the same maximum value.

Fig.25 Angular distributions of sputtered particles in the incident plane (azimuthal angular range $0^o \leq \phi \leq 15^o$) for H bombardment of Ni at an angle of incidence, $\alpha = 80^o$, and for several incident energies E_o. The distributions are normalized to give the same maximum value.

Fig.26 Angular distributions of sputtered particles in the incident plane (azimuthal angular range $0^{\circ} < \phi < 15^{\circ}$) for the bombardment of Ni with different incident particles with an incident energy, E_o = 1 keV, and an angle of incidence, $\alpha = 80^{\circ}$. The distributions are normalized to give the same maximum value.

Fig.27 Angular distribution of sputtered particles in the incident plane (azimuthal angular range $0 < \phi < 15^{\circ}$) for D bombardment of Ni, Mo and W with an incident energy, E_o = 4 keV, and an angle of incidence, $\alpha = 80^{\circ}$. The distributions are normalized to give the same maximum value.

Fig.28 Contour plots (lines of equal intensity: sputtered atoms per solid angle) of the angular distribution of sputtered particles for D bombardment of Ni at an incident energy of 4 keV and an angle of incidence of $\alpha = 80^{\circ}$.

a) angular distribution of all sputtered particles
b) angular distribution of primary knock-on atoms (PKA)
c) angular distribution of secondary knock-on atoms (SKA)

Fig.29 Contourplot (lines of equal intensity: sputtered atoms per solid angle) of the angular distribution of sputtered particles for D bombardment of Mo at an incident energy of 4 keV and an angle of incidence of $\alpha = 80^{\circ}$.

Fig.30 Contourplot (lines of equal intensity: sputtered atoms per solid angle) of the angular distribution of sputtered particles for D bombardment of W at an incident energy, E_o = 4 keV and an angle of incidence of $\alpha = 80^{\circ}$.

Fig.31 Contour plots (lines of equal intensity: sputtered atoms per solid angle) of the angular distribution of sputtered particles for Ne bombardment of Ni at an incident energy of 3 keV and an incident angle, $\alpha = 75^{\circ}$.

a) angular distribution of all sputtered particles
b) angular distribution of primary knock-on atoms (PKA)
c) angular distribution of secondary knock-on atoms (SKA).

Fig.32 Contour plots (lines of equal intensity: sputtered atoms per solid angle) of the angular distribution of sputtered particles for 350 eV D bombardment of C at an incident angle, $\alpha = 80^{\circ}$.

a) planar potential, surface binding energy, $E_s = 7.4$
b) without refraction, (scalar potential) surface binding energy, $E_s = 7.4$ eV.

Fig.33 Angular distributions of sputtered particles in the incident plane (azimuthal angular range $0 < \phi < 15^{\circ}$) for 350 eV D bombardment of C at an incident angle, $\alpha = 80^{\circ}$.

- planar potential, surface binding energy, $E_s = 7.4$ e
-- without refraction, (scalar potential), surface binding energy, $E_s = 7.4$ eV.

Fig.34 Polar angle ß of sputtered particles (after refraction) versus the starting polar angle ß' (in a binary collision) in the incident plane ($\phi = 0^{\circ}$) calculated by formula (3).
The example is determined for 4 keV D bombardment of Ni at an incident angle, $\alpha = 80^{\circ}$.

Fig.35 The polar angles $\bar{\beta}$, β', β'_{min} versus the azimuthal angle, ϕ, calculated by formula (3,5, 10). The example is determined for 4 keV D bombardment of Ni at an incident angle, $\alpha = 80^{o}$.

Fig.36 Polar angle, β_{min}, versus the azimuthal angle, , for several values of $A = \gamma E_o/E_s$ and an incident angle, $\alpha = 80^{o}$.

Fig.37 Polar angle, β_{min}, versus the incident angle, α, in the incident plane ($\phi = 0^{o}$) for several values of A

Fig.38 Polar angle, β_{min}, versus the value A in the incident plane for several values of the incident angle, α.

Fig.39 The critical azimuthal angle, ϕ_c, versus the angle of incidence, α, for several values of A.

Fig.40 The critical azimuthal angle, $_c$, versus the value A for several angles of incidence, α.

Fig.41 The critical angle of incidence, α_c (critical value, A_c), versus the value A (angle of incidence, α).

Fig.42 Polar angle, β_{min}, versus the azimuthal angle, ϕ, for several values of A. The curves are calculated for an incident angle, $\alpha = 80^{o}$, and without refraction.

Fig.43 Critical azimuthal angle, ϕ_c, and critical angle of incidence, α_c, versus the value A. ϕ_c is determined for several angles of incidence, α.

Fig.44 Comparison of the polar angle, β_{min}, with the polar angle of maximum intensity in the angular distribution of sputtered particles in the incident plane for several ion target combinations at an angle of incidence, $\alpha = 80^{o}$.

Fig.45 Angular distributions of sputtered particles in the incident plane (azimuthal angular range, $0^{\circ} <$ $< 15^{\circ}$) for different ion target combinations but with the same value $A = \gamma E_o/E_s = 19.7$ and an angle of incidence, $\alpha = 80^{\circ}$. The distributions are normalized to give the same maximum value.

Fig.46 Contour plots (lines of equal intensity: sputtered atoms per solid angle) of the angular distribution of sputtered particles for 350 eV D bombardment of C at an incident angle, $\alpha = 80^{\circ}$. Inserted is the line β_{min} versus calculated from formula ( ).

a) planar potential, $E_s = 7.4$ eV

b) without refraction (scalar potential) $E_s = 7.4$ eV.

Fig.47 Contour plot (lines of equal intensity: sputtered atoms per solid angle) of the angular distribution of sputtere particles for 4 keV D bombardment of Ni at an incident angle, $\alpha = 80^{\circ}$. Inserted in the line β_{min} versus ϕ calculated from formula ( ).

Fig.48 Energy distributions of sputtered particles (particles per eV and incident particle) for 0.35 keV D bombardment of C at an incident angle, $\alpha = 80^{\circ}$.
Planar potential: all sputtered particles (——),
and primary knock-on atoms, PKA (---).
Scalar potential (without refraction): all sputtered particles (-·-)

Fig.49 Energy distributions of sputtered particles in several azimuthal directions (integrated over the polar angle, ß). C was bombarded with 0.35 keV D at an incident angle, $\alpha = 80^{\circ}$.

Fig.50 Energy distribution of sputtered particles for 3 keV Ne bombardment of Ni at an incident angle, $\alpha = 75^{\circ}$. Shown are the energy distributions of all sputtered particles (—) and of the PKA (---).

Fig. 51 Energy distributions of sputtered particles in several azimuthal directions (integrated over the polar angle, ß). Ni was bombarded with 3 keV Ne at an incident angle, $\alpha = 75^{\circ}$.

Fig. 52 Contour plots (lines of equal intensity: sputtered atoms per solid angle and energy interval) of the energy - polar angle distribution of sputtered particles for different azimuthal angle intervals 350 eV D bombardment of C at an incident angle, $\alpha = 80^{\circ}$. c gives the intensity step between adjacent contour lines.

a) integrated over the azimuthal angle, ϕ
b) azimuthal angular range, $0^{\circ} < \phi < 15^{\circ}$
c) " $15^{\circ} < \phi < 30^{\circ}$
d) " $30^{\circ} < \phi < 45^{\circ}$
e) " $45^{\circ} < \phi < 60^{\circ}$
f) " $60^{\circ} < \phi < 75^{\circ}$
g) " $75^{\circ} < \phi < 90^{\circ}$
h) " $90^{\circ} < \phi < 105^{\circ}$
i) " $105^{\circ} < \phi < 120^{\circ}$
j) " $120^{\circ} < \phi < 135^{\circ}$
k) " $135^{\circ} < \phi < 150^{\circ}$
l) " $150^{\circ} < \phi < 165^{\circ}$
m) " $165^{\circ} < \phi < 180^{\circ}$

Fig. 53 Energy distributions of sputtered particles in the incident plane ($0^{\circ} < \phi < 15^{\circ}$) in several polar-angle intervals for D bombardment of C. Incident energy, $E_o = 0.35$ keV; incident angle, $\alpha = 80^{\circ}$.

a) $12^{\circ} < ß < 15^{\circ}$ and $27^{\circ} < ß < 30^{\circ}$

b) $42^{\circ} < ß < 45^{\circ}$, $57^{\circ} < ß < 60^{\circ}$ and $72^{\circ} < ß < 75^{\circ}$.

Fig. 54 Contour plots (lines of equal intensity: sputtered particles per solid angle and energy interval) of the energy-polar angle distribution of sputtered particles for different azimuthal-angle intervals. 3 keV Ne bombardment of Ni at an incident angle, $\alpha = 75^{\circ}$. c gives the intensity step between adjacent contour lines.

a) integrated over the azimuthal angle,
b) azimuthal angular range, $0^{\circ} < \phi < 15^{\circ}$
c) " $15^{\circ} < \phi < 30^{\circ}$
d) " $30^{\circ} < \phi < 45^{\circ}$
e) " $45^{\circ} < \phi < 60^{\circ}$
f) " $60^{\circ} < \phi < 75^{\circ}$
g) " $75^{\circ} < \phi < 90^{\circ}$
h) " $90^{\circ} < \phi < 105^{\circ}$
i) " $105^{\circ} < \phi < 120^{\circ}$
j) " $120^{\circ} < \phi < 135^{\circ}$
k) " $135^{\circ} < \phi < 150^{\circ}$
l) " $150^{\circ} < \phi < 165^{\circ}$
m) " $165^{\circ} < \phi < 180^{\circ}$

Fig. 55 Energy distributions of sputtered particles in the incident plane ($0^{\circ} < \phi < 15^{\circ}$) in several polar-angle intervals for Ne bombardment of Ni. Incident energy, $E_o = 3$ keV, incident angle, $\alpha = 75^{\circ}$.
a) $12^{\circ} < \beta < 15^{\circ}$ and $27^{\circ} < \beta < 30^{\circ}$
b) $42^{\circ} < \beta < 45^{\circ}$, $57^{\circ} < \beta < 60^{\circ}$ and $72^{\circ} < \beta < 75^{\circ}$.

Fig. 56 Exit angle, β, versus the energy, E, of C sputtered in a binary collision with D. The three curves are due to the simple binary collision, and due to an additiona scalar and planar potential.

Fig. 57 Contour plot (lines of equal intensity: sputtered particles per solid angle and energy interval) of the energy-polar angle distribution of sputtered particles in the incident plane ($0^{o} < \phi < 15^{o}$) for 350 eV D bombardment of C at an incident angle, $\alpha = 80^{o}$

a) planar potential; indicated is the curve for a binary collision, see Fig. 56

b) scalar potential; indicated is the curve for a binary collision, see Fig. 56

Fig. 58 Contour plot (lines of equal intensity: sputtered particles per solid angle and energy interval) of the energy-polar angle distribution of sputtered particles in the incident plane ($0^{o} < \phi < 15^{o}$) for 3 keV Ne bombardment of Ni at an incident angle, $\alpha = 75^{o}$. Indicated is the curve due to a binary collision (planar potential).

Fig. 59 Relative number of sputtered particles versus their depth of origin

a) H bombardment of Ni at normal incidence for three incident energies, E_o = 0.5, 5 and 50 keV.

b) Ar bombardment of Ni at normal incidence and for four incident energies, E_o = 0.1, 1, 10 and 100 keV.

Fig. 60 Definition of angles α, β, ϕ and δ_R.

Fig. 61 Surface refraction due to a planar surface potential.

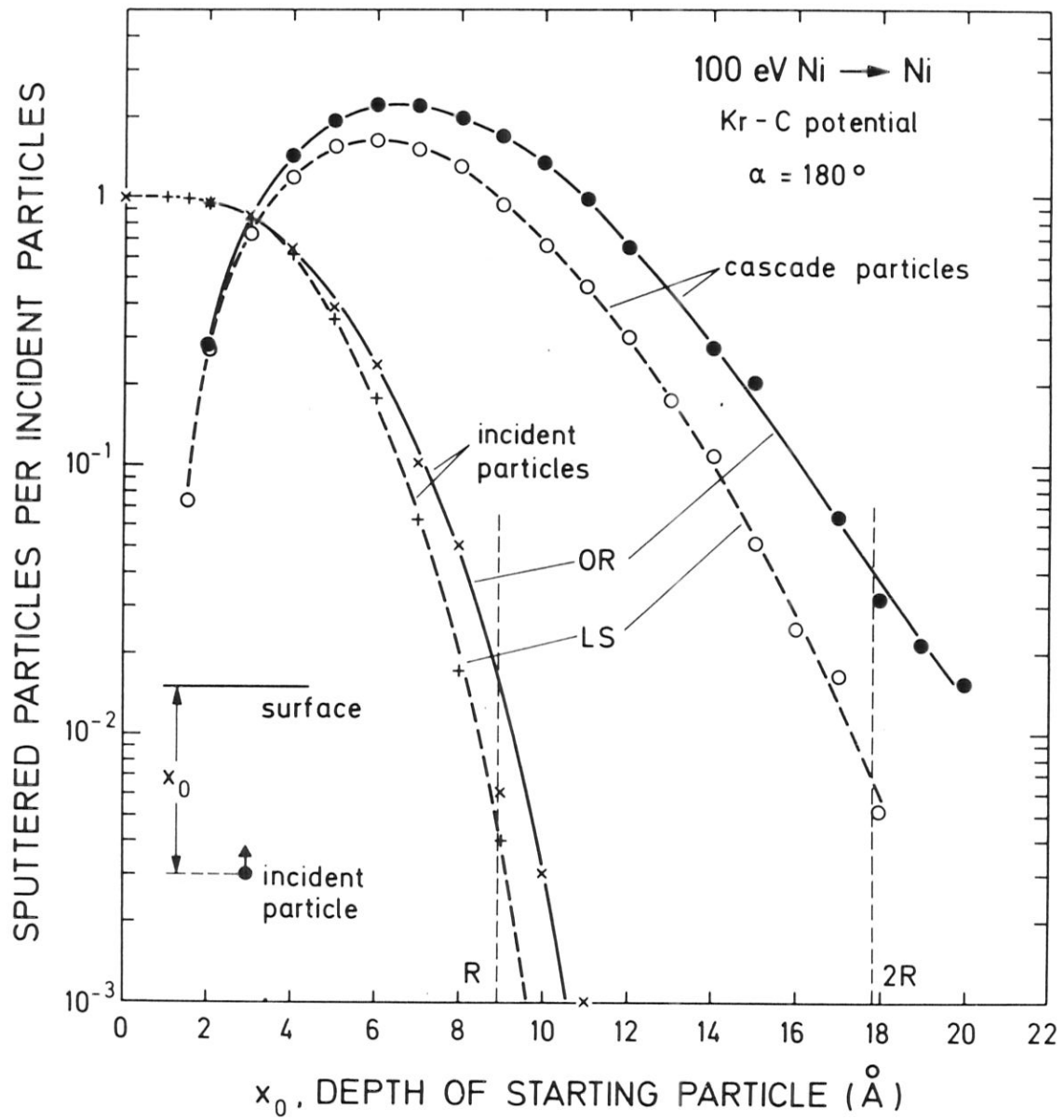
100 eV Ni → Ni
Kr - C potential
α = 180°
cascade particles
incident particles
OR
LS
surface
x_0
incident particle
R
2R
SPUTTERED PARTICLES PER INCIDENT PARTICLES
x_0, DEPTH OF STARTING PARTICLE (Å)
1
10^{-1}
10^{-2}
10^{-3}
0
2
4
6
8
10
12
14
16
18
20
22

Fig. 1

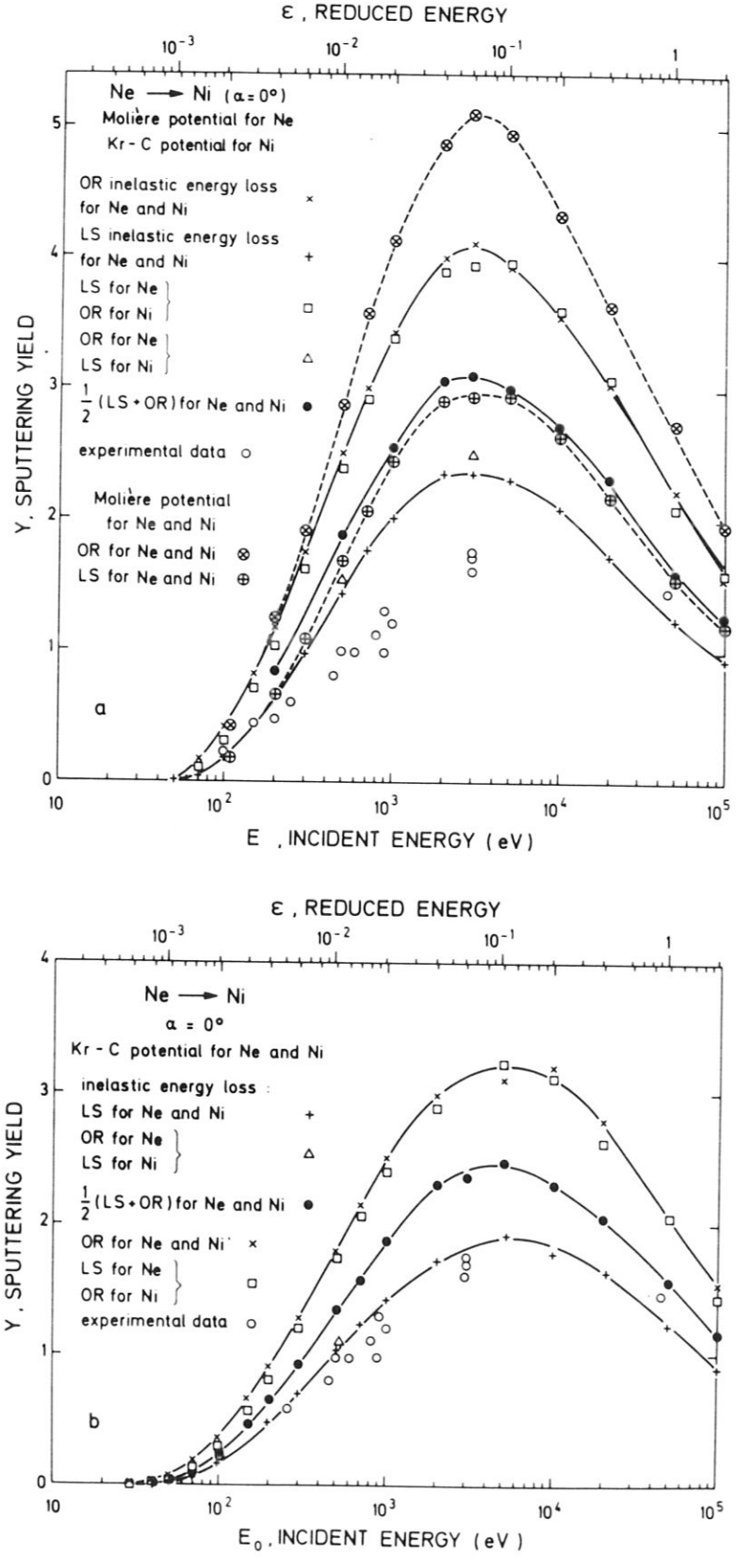
ε , REDUCED ENERGY
Ne → Ni (α = 0°)
Molière potential for Ne
Kr - C potential for Ni
OR inelastic energy loss for Ne and Ni
LS inelastic energy loss for Ne and Ni
LS for Ne
OR for Ni
OR for Ne
LS for Ni
1/2 (LS + OR) for Ne and Ni
experimental data
Molière potential for Ne and Ni
OR for Ne and Ni
LS for Ne and Ni
a
Y, SPUTTERING YIELD
E , INCIDENT ENERGY (eV)
ε , REDUCED ENERGY
Ne → Ni
α = 0°
Kr - C potential for Ne and Ni
inelastic energy loss :
LS for Ne and Ni
OR for Ne
LS for Ni
1/2 (LS + OR) for Ne and Ni
OR for Ne and Ni
LS for Ne
OR for Ni
experimental data
b
Y, SPUTTERING YIELD
E0 , INCIDENT ENERGY (eV)

Fig. 2

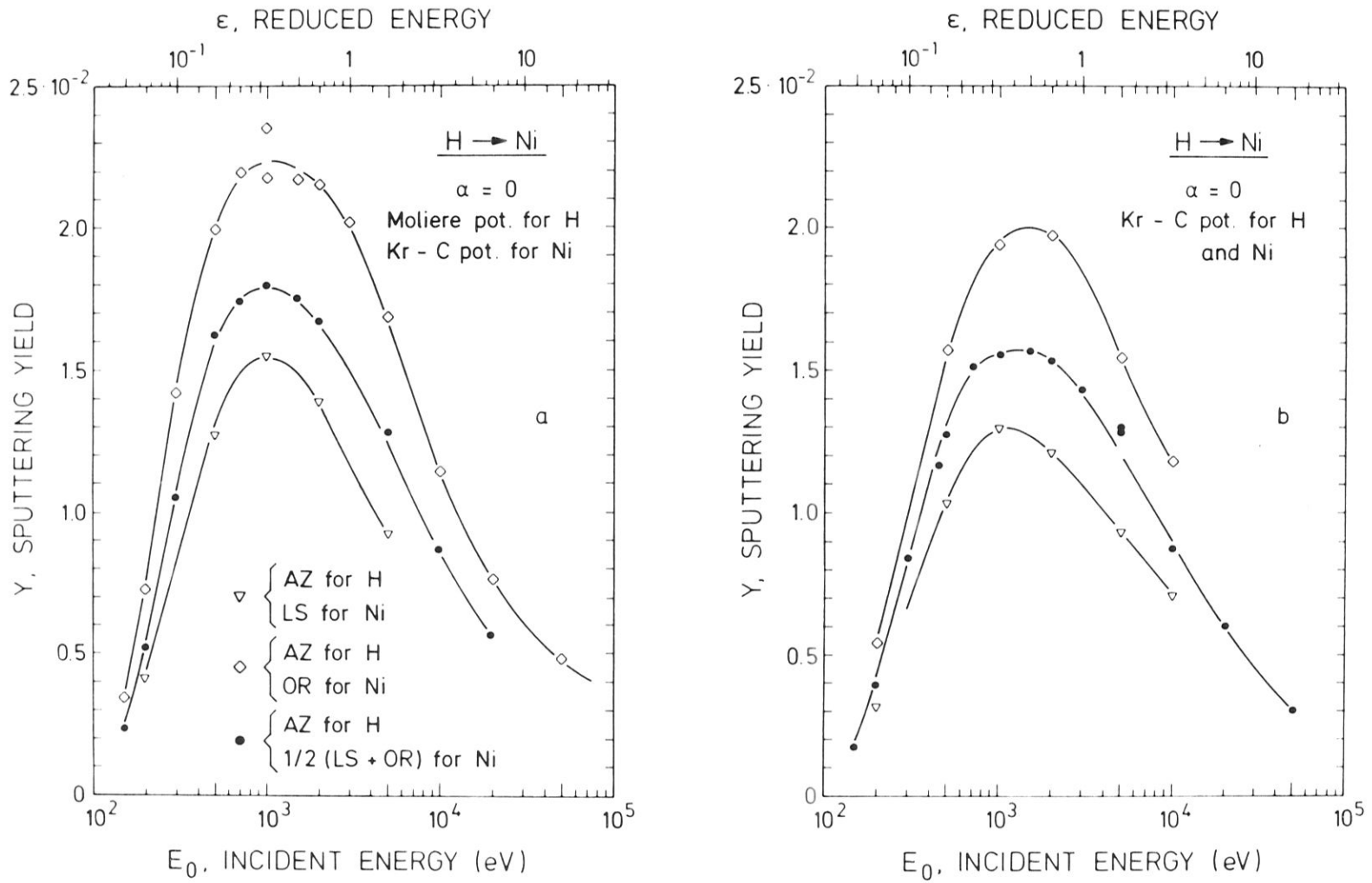
ε, REDUCED ENERGY
10⁻¹
1
10
2.5 · 10⁻²
2.0
1.5
1.0
0.5
0
Y, SPUTTERING YIELD
H → Ni
α = 0
Moliere pot. for H
Kr - C pot. for Ni
a
AZ for H
LS for Ni
AZ for H
OR for Ni
AZ for H
1/2 (LS + OR) for Ni
10²
10³
10⁴
10⁵
E₀, INCIDENT ENERGY (eV)
ε, REDUCED ENERGY
10⁻¹
1
10
2.5 · 10⁻²
2.0
1.5
1.0
0.5
0
Y, SPUTTERING YIELD
H → Ni
α = 0
Kr - C pot. for H
and Ni
b
10²
10³
10⁴
10⁵
E₀, INCIDENT ENERGY (eV)

Fig. 3

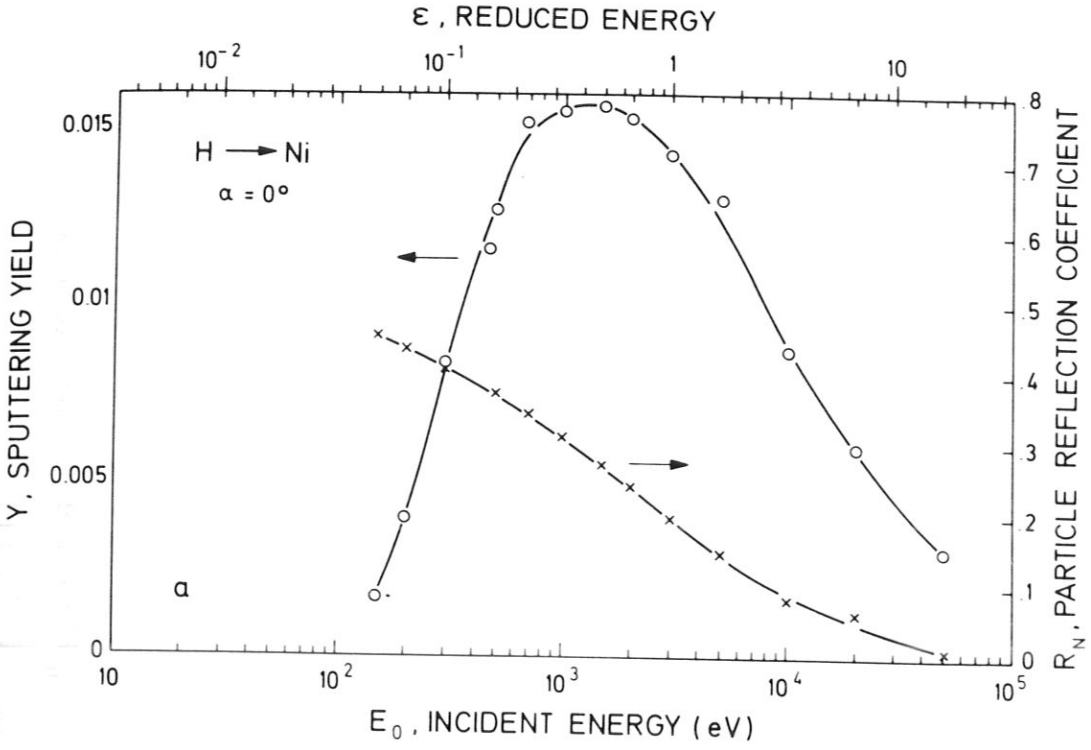
ε , REDUCED ENERGY
10^-2
10^-1
1
10
H → Ni
α = 0°
Y , SPUTTERING YIELD
R_N , PARTICLE REFLECTION COEFFICIENT
a
E_0 , INCIDENT ENERGY (eV)

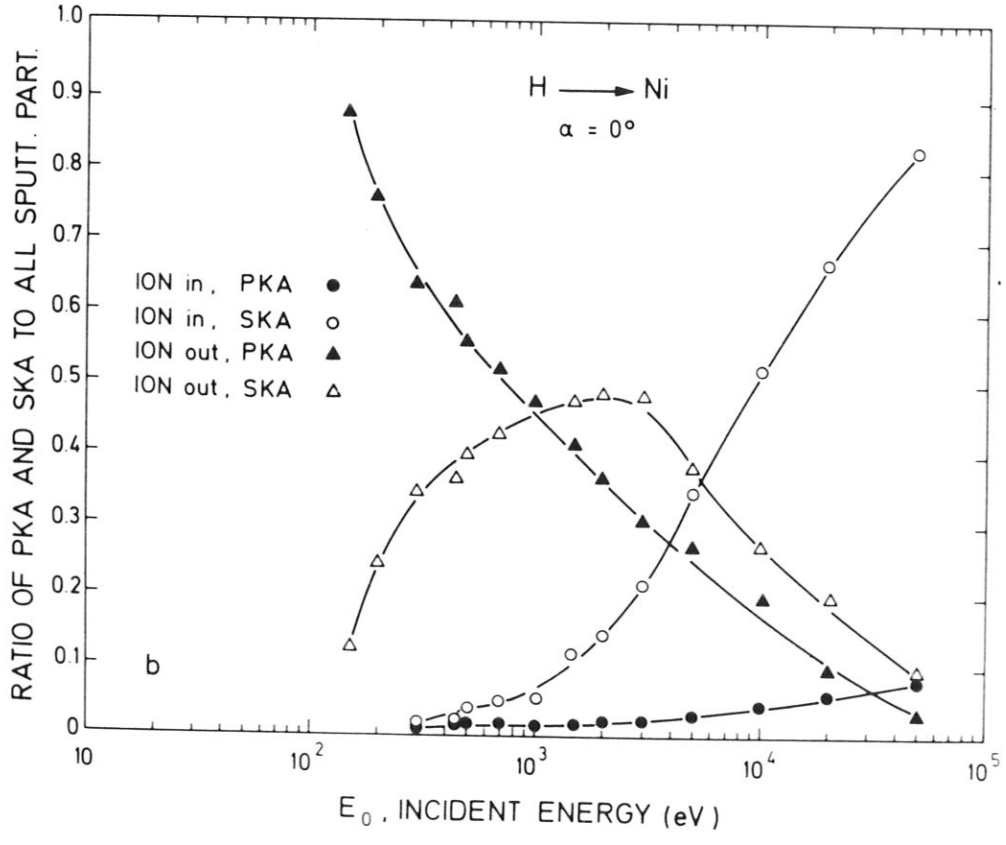
H → Ni
α = 0°
ION in , PKA
ION in , SKA
ION out , PKA
ION out , SKA
RATIO OF PKA AND SKA TO ALL SPUTT. PART.
b
E_0 , INCIDENT ENERGY (eV)

Fig. 4

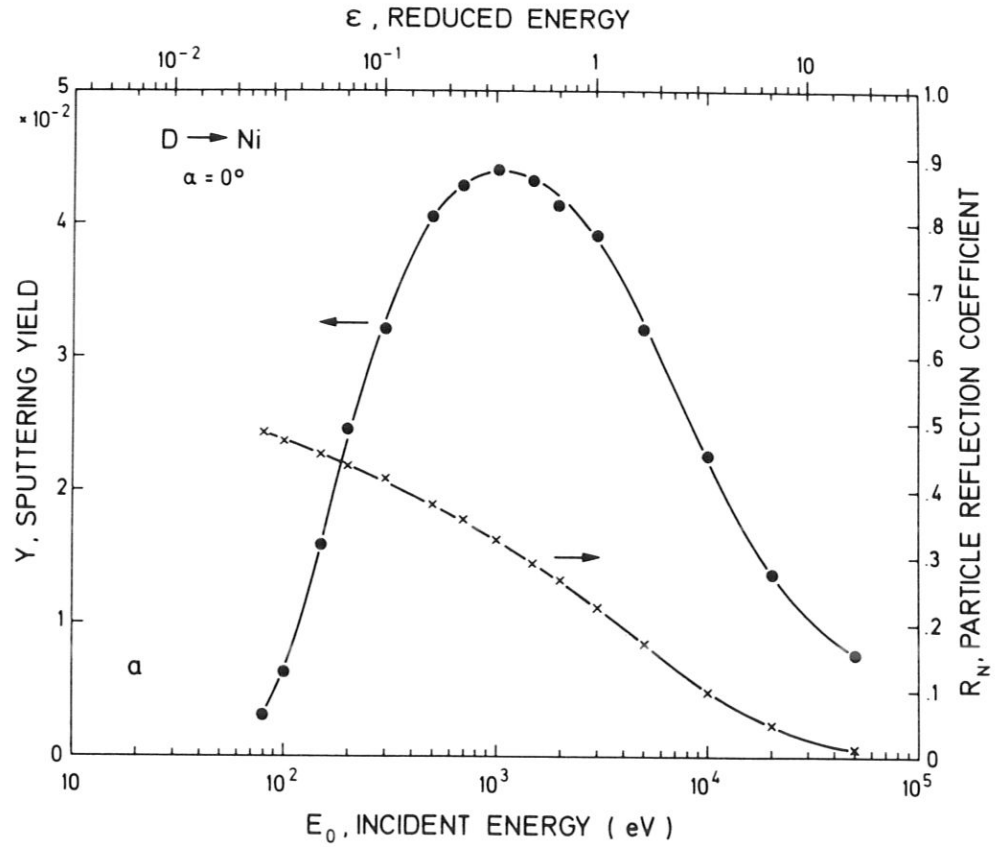
ε , REDUCED ENERGY
10⁻²
10⁻¹
1
10
D → Ni
α = 0°
Y, SPUTTERING YIELD
× 10⁻²
R_N, PARTICLE REFLECTION COEFFICIENT
a
E₀, INCIDENT ENERGY (eV)

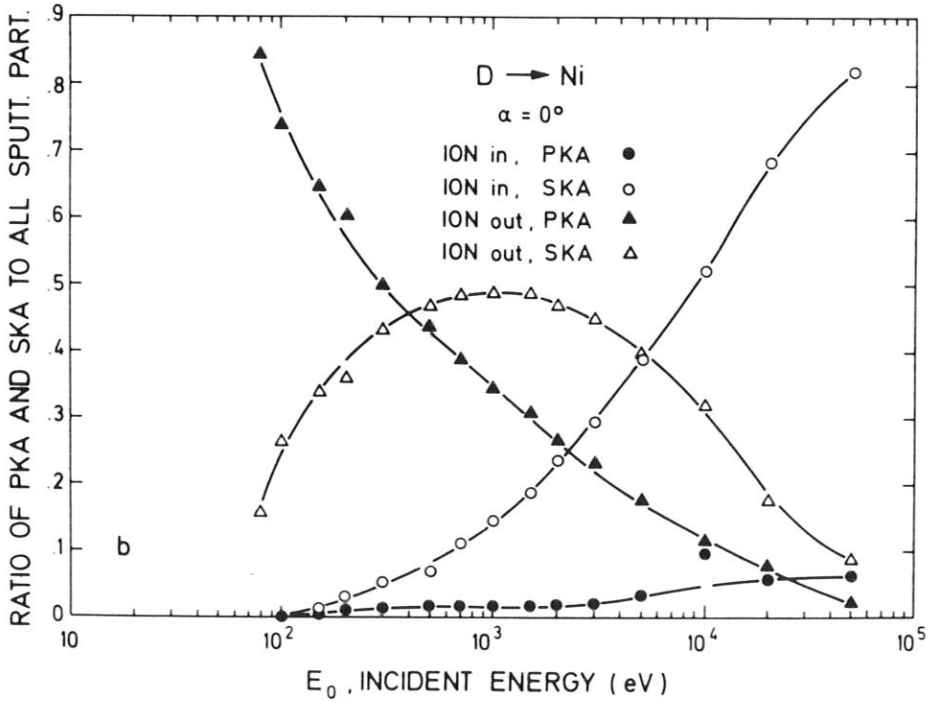
D → Ni
α = 0°
ION in, PKA
ION in, SKA
ION out, PKA
ION out, SKA
RATIO OF PKA AND SKA TO ALL SPUTT. PART.
b
E₀, INCIDENT ENERGY (eV)

Fig. 5

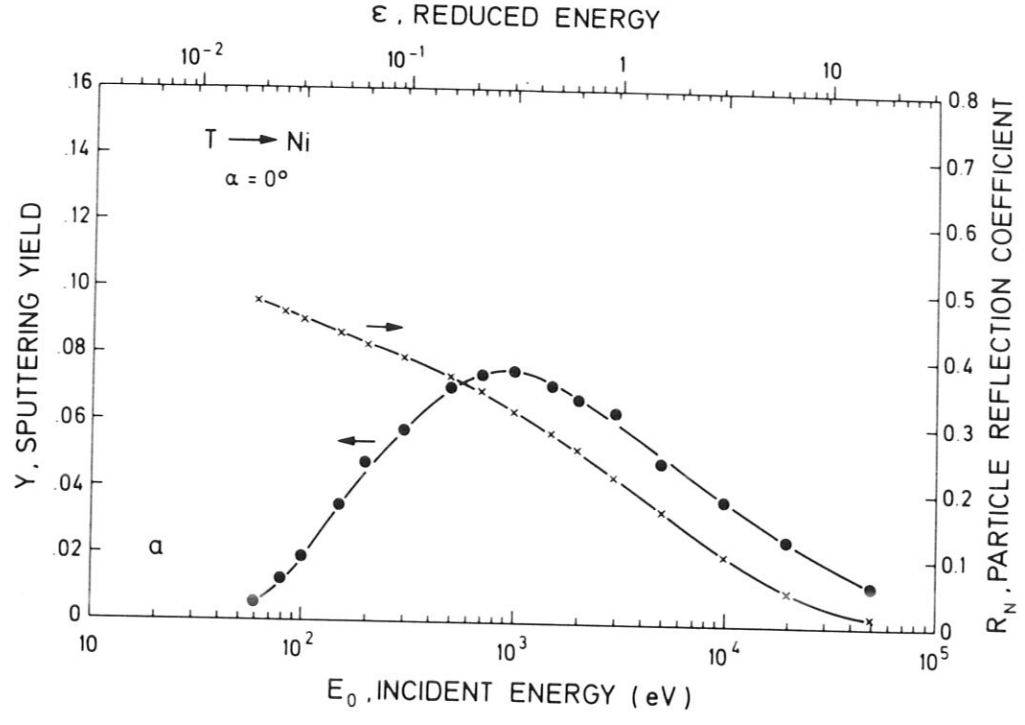
ε , REDUCED ENERGY
T → Ni
α = 0°
Y, SPUTTERING YIELD
R_N, PARTICLE REFLECTION COEFFICIENT
a
E_0 , INCIDENT ENERGY (eV)

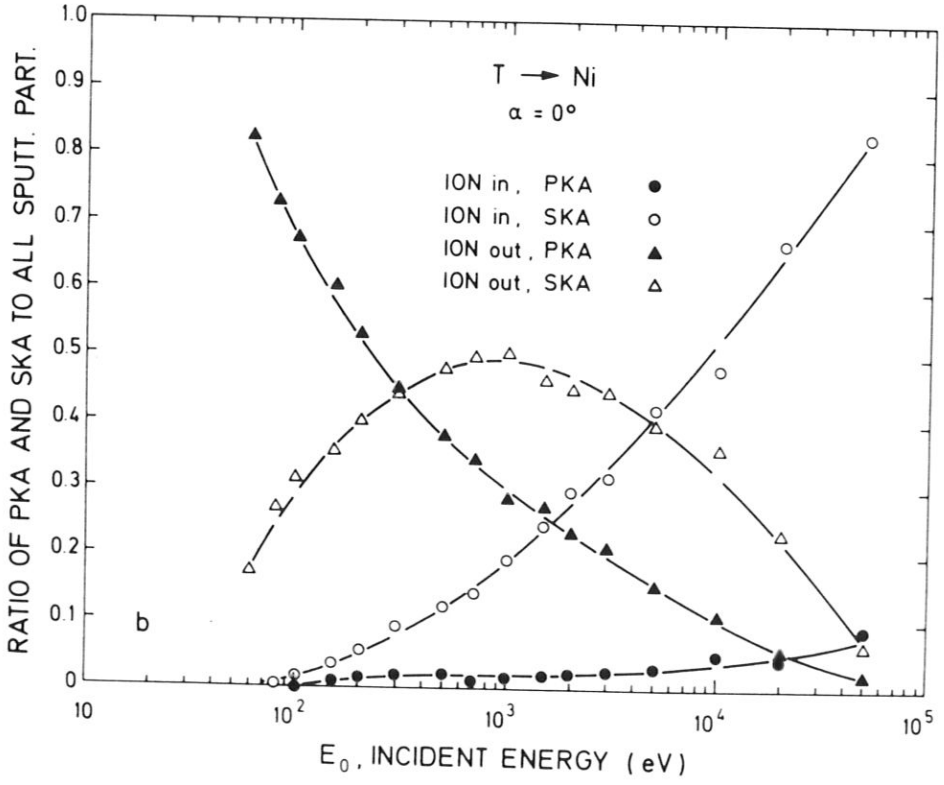
T → Ni
α = 0°
ION in , PKA
ION in , SKA
ION out , PKA
ION out , SKA
RATIO OF PKA AND SKA TO ALL SPUTT. PART.
b
E_0 , INCIDENT ENERGY (eV)

Fig. 6

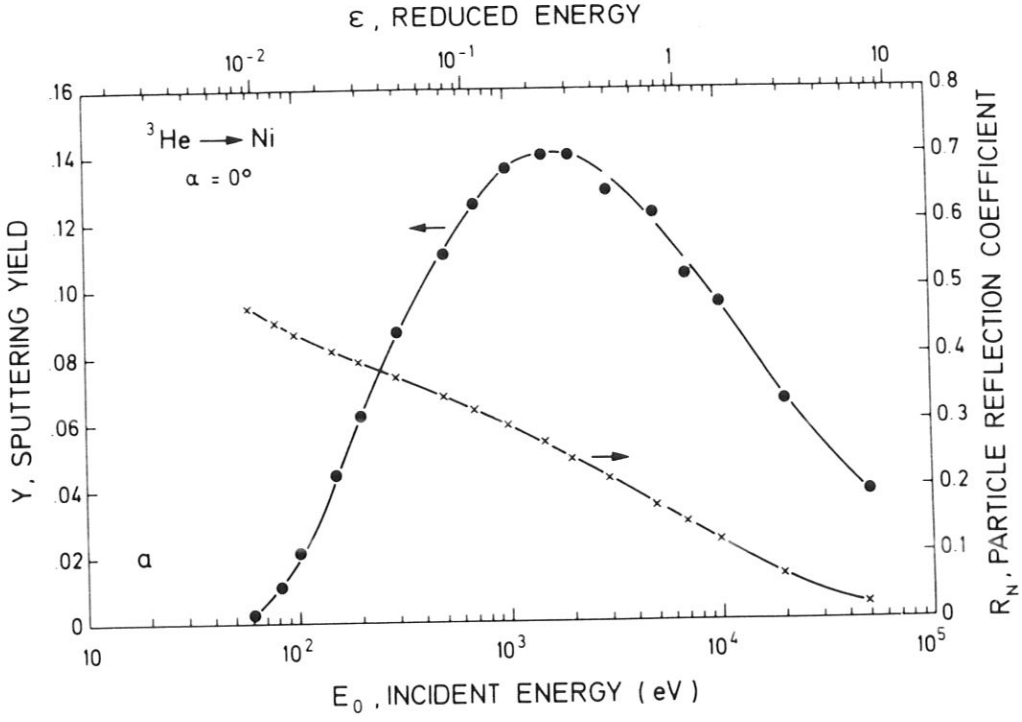
ε , REDUCED ENERGY
10^{-2}
10^{-1}
1
10
^{3}He → Ni
α = 0°
a
Y, SPUTTERING YIELD
R_N, PARTICLE REFLECTION COEFFICIENT
E_0 , INCIDENT ENERGY (eV)

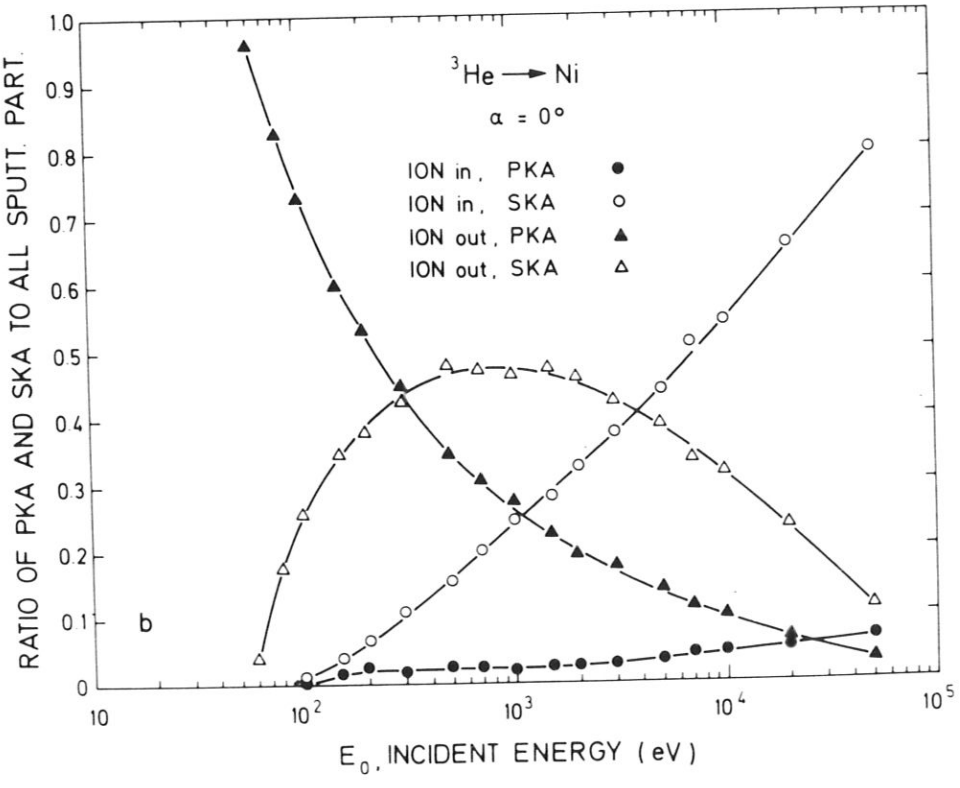
^{3}He → Ni
α = 0°
ION in , PKA
ION in , SKA
ION out , PKA
ION out , SKA
b
RATIO OF PKA AND SKA TO ALL SPUTT. PART.
E_0, INCIDENT ENERGY (eV)

Fig. 7

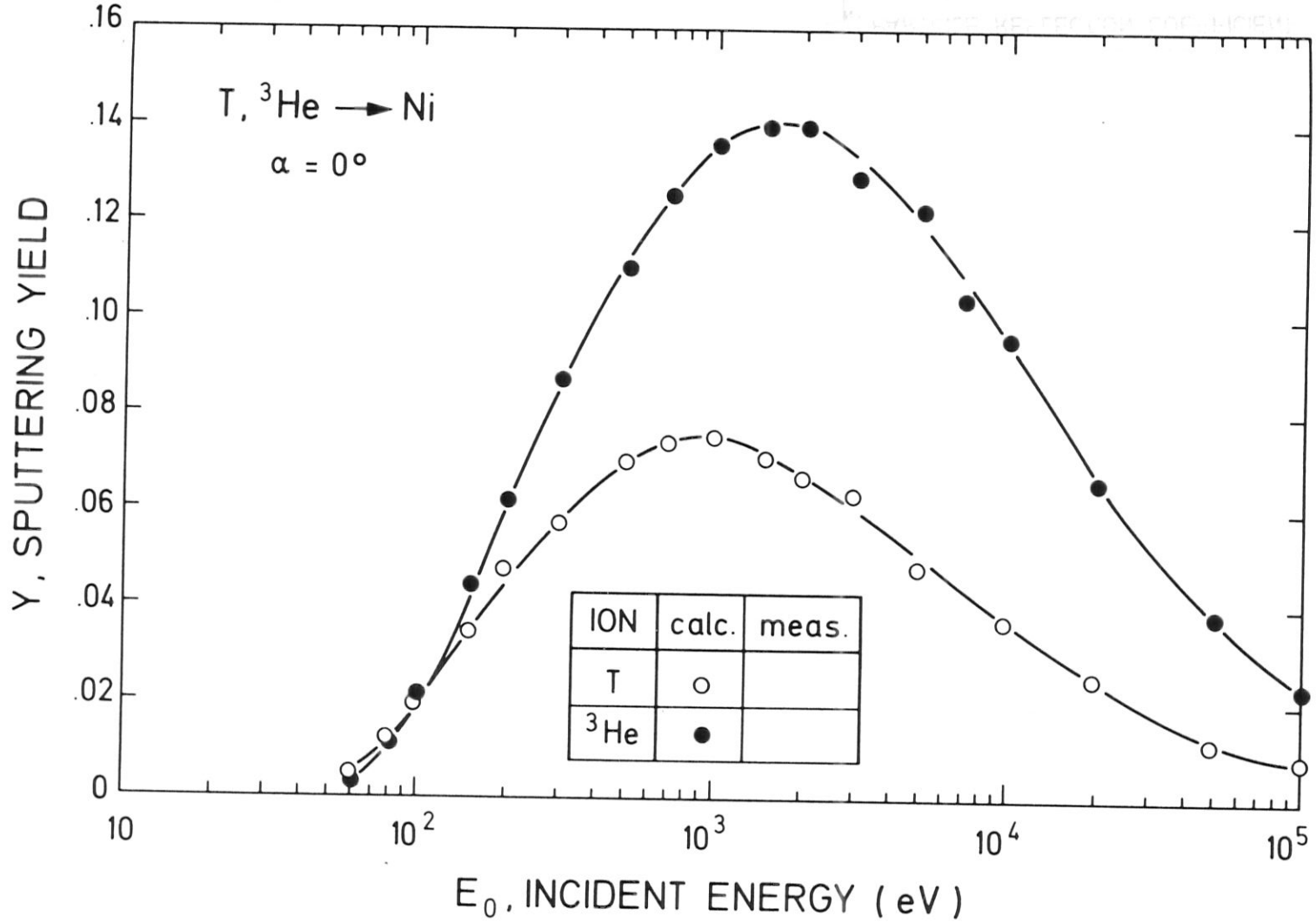
T, ^{3}He → Ni
α = 0°
Y, SPUTTERING YIELD
E$_0$, INCIDENT ENERGY (eV)
ION | calc. | meas.
T | ○ |
^{3}He | ● |
.16
.14
.12
.10
.08
.06
.04
.02
0
10
10^2
10^3
10^4
10^5

Fig. 8

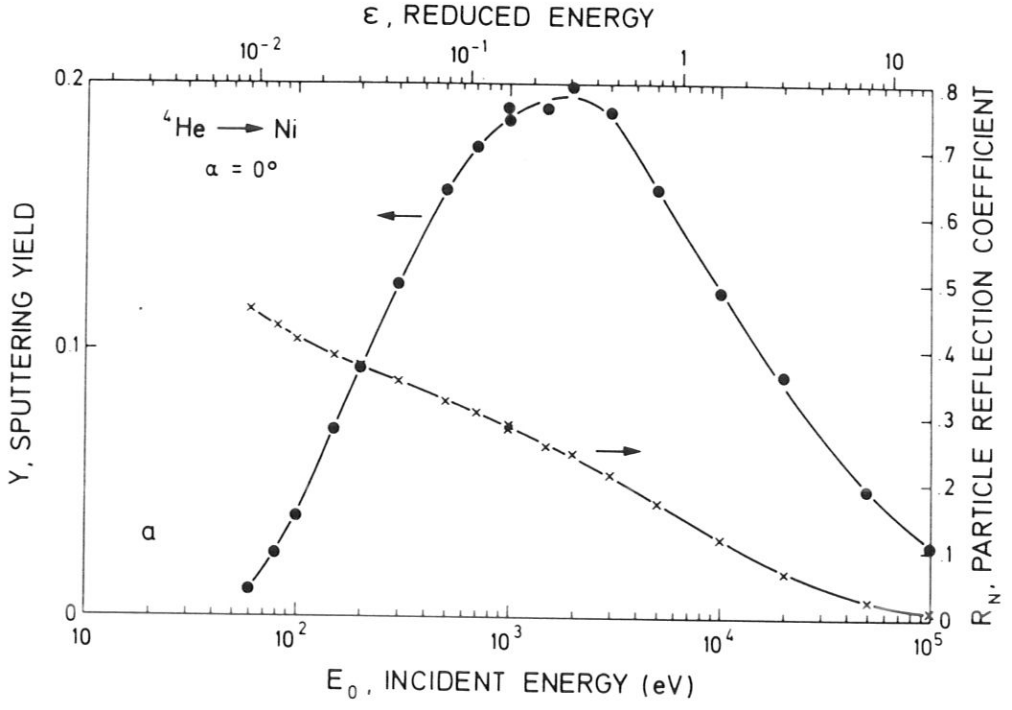
ε, REDUCED ENERGY
10^{-2}
10^{-1}
1
10
0.2
0.1
0
8
7
6
5
4
3
2
1
0
^{4}He → Ni
α = 0°
a
Y, SPUTTERING YIELD
R_N, PARTICLE REFLECTION COEFFICIENT
10
10^2
10^3
10^4
10^5
E_0, INCIDENT ENERGY (eV)

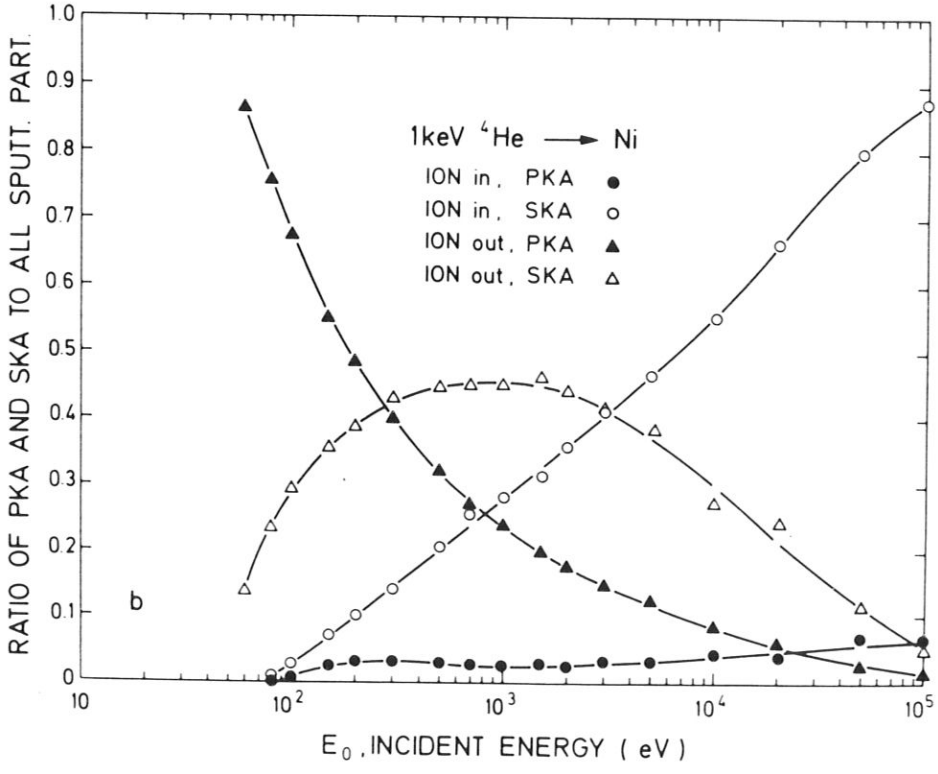
1.0
0.9
0.8
0.7
0.6
0.5
0.4
0.3
0.2
0.1
0
1keV ^{4}He → Ni
ION in, PKA ●
ION in, SKA ○
ION out, PKA ▲
ION out, SKA △
b
RATIO OF PKA AND SKA TO ALL SPUTT. PART.
10
10^2
10^3
10^4
10^5
E_0, INCIDENT ENERGY (eV)

Fig. 9

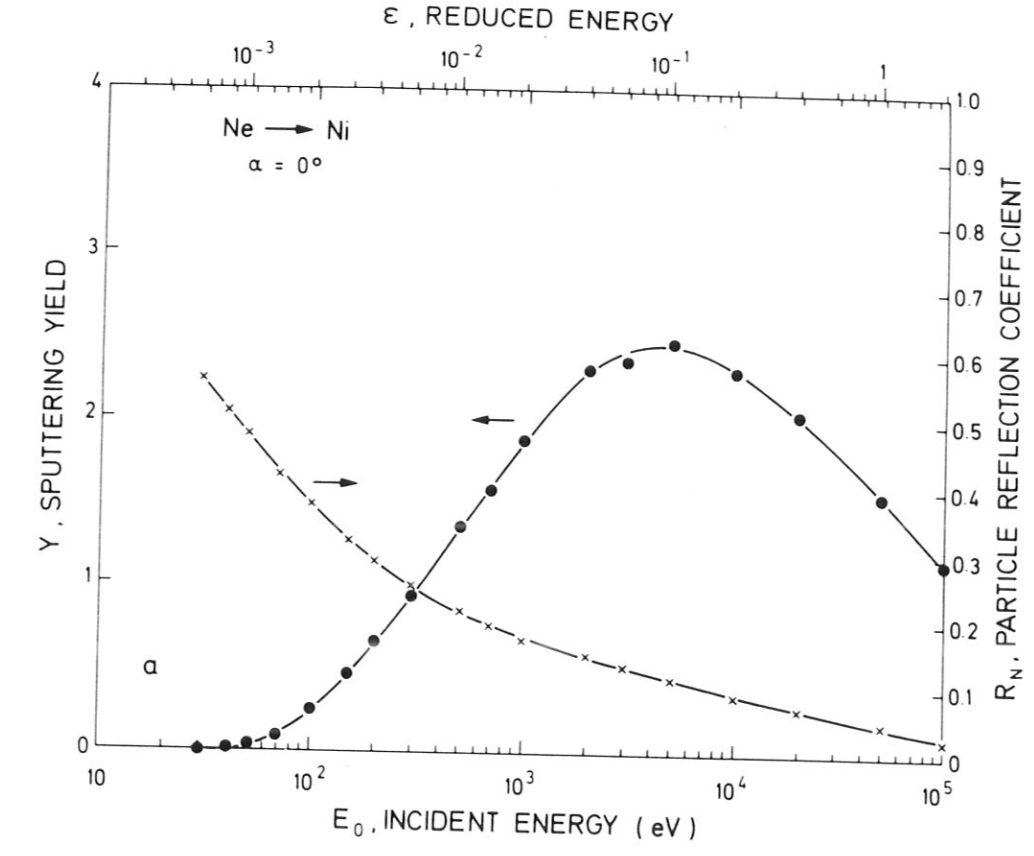
ε , REDUCED ENERGY
10^-3
10^-2
10^-1
1
Ne → Ni
α = 0°
Y , SPUTTERING YIELD
R_N , PARTICLE REFLECTION COEFFICIENT
a
E_0 , INCIDENT ENERGY (eV)

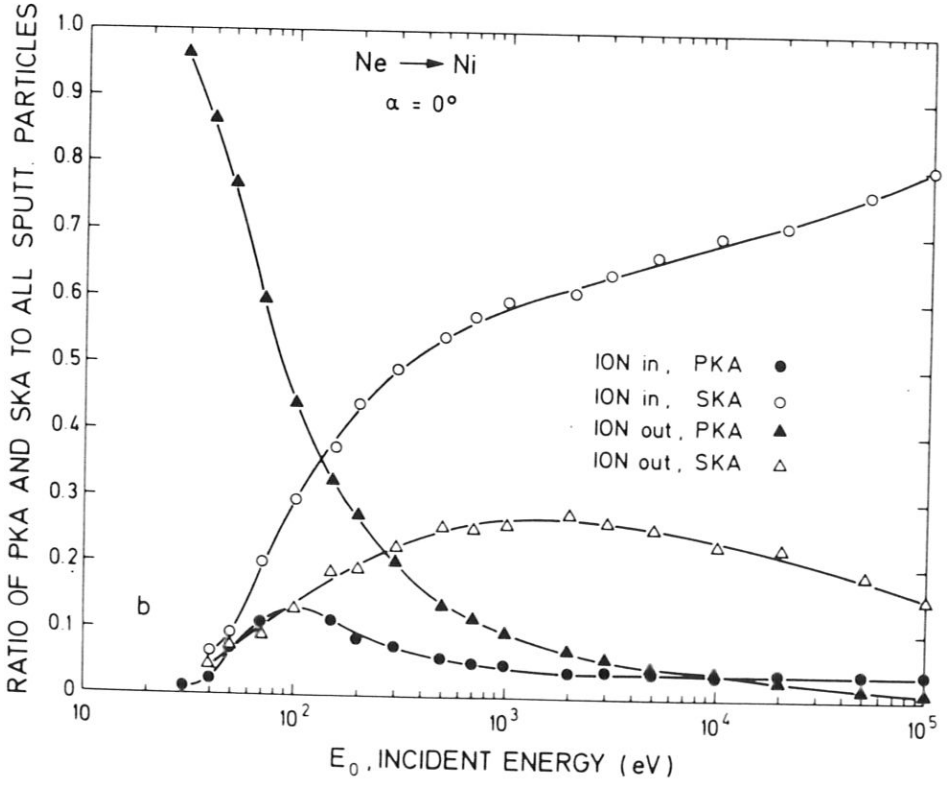
Ne → Ni
α = 0°
ION in , PKA
ION in , SKA
ION out , PKA
ION out , SKA
RATIO OF PKA AND SKA TO ALL SPUTT. PARTICLES
b
E_0 , INCIDENT ENERGY (eV)

Fig. 10

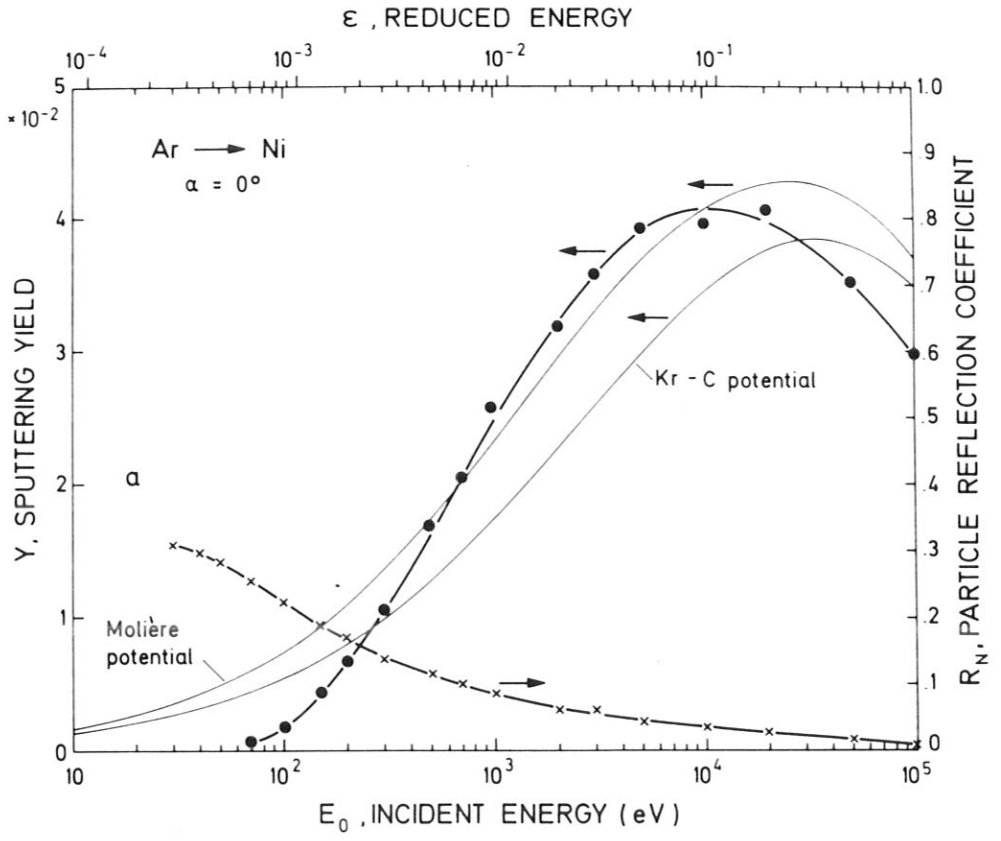
ε , REDUCED ENERGY
10⁻⁴
10⁻³
10⁻²
10⁻¹
×10⁻²
Ar → Ni
α = 0°
Y, SPUTTERING YIELD
R_N, PARTICLE REFLECTION COEFFICIENT
Kr - C potential
Molière potential
a
E₀ , INCIDENT ENERGY (eV)

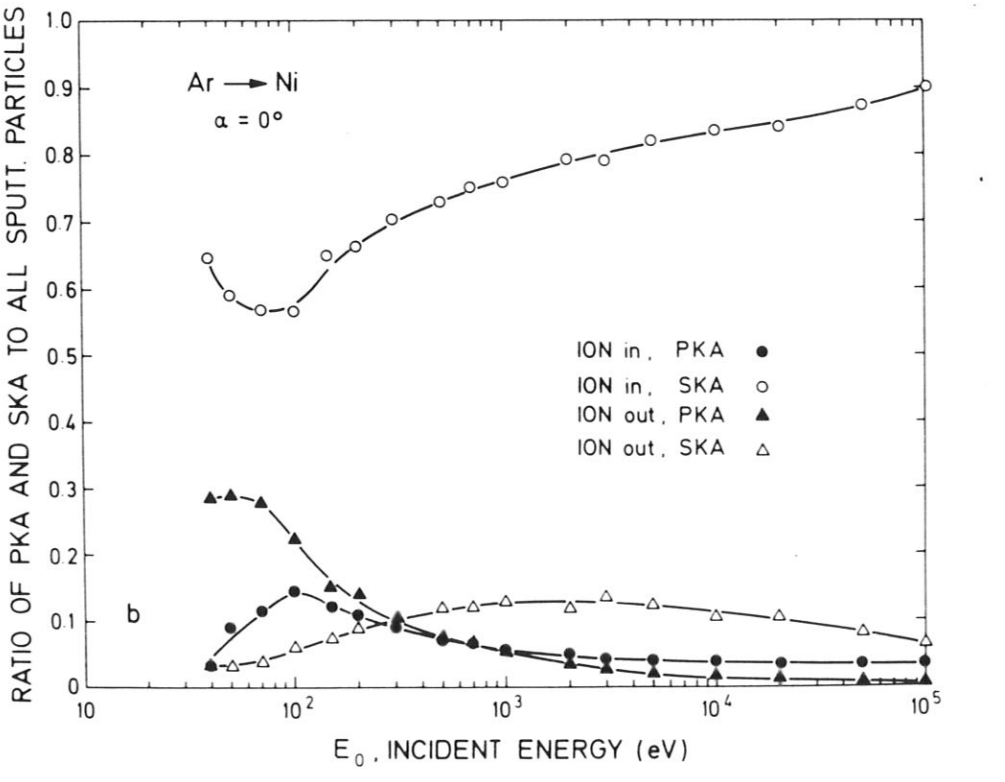
Ar → Ni
α = 0°
ION in , PKA
ION in , SKA
ION out , PKA
ION out , SKA
RATIO OF PKA AND SKA TO ALL SPUTT. PARTICLES
b
E₀ , INCIDENT ENERGY (eV)

Fig. 11

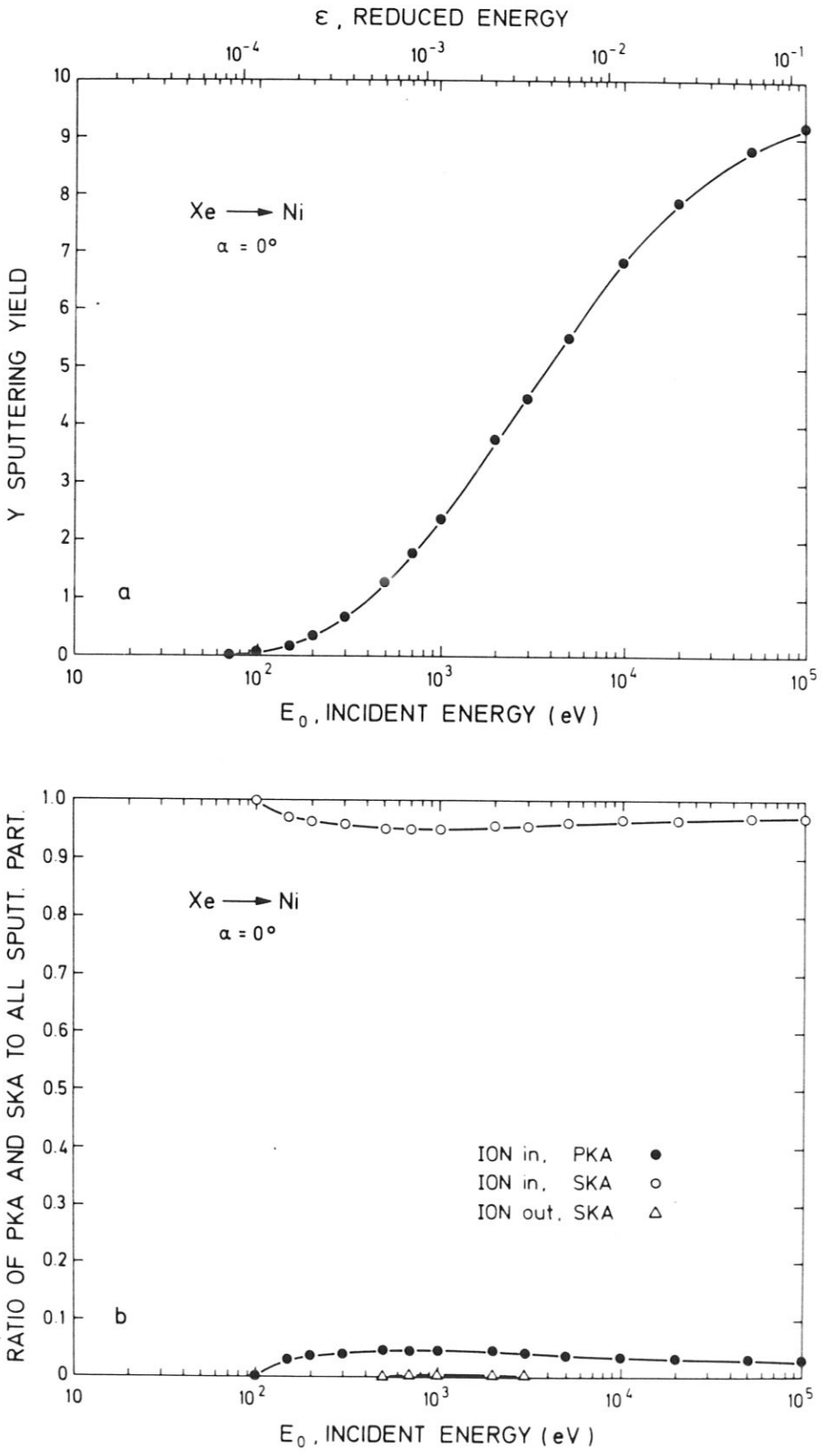
ε , REDUCED ENERGY
10^-4
10^-3
10^-2
10^-1
Y SPUTTERING YIELD
Xe → Ni
α = 0°
a
E0 , INCIDENT ENERGY (eV)
RATIO OF PKA AND SKA TO ALL SPUTT. PART.
ION in, PKA
ION in, SKA
ION out, SKA
b

Fig. 12

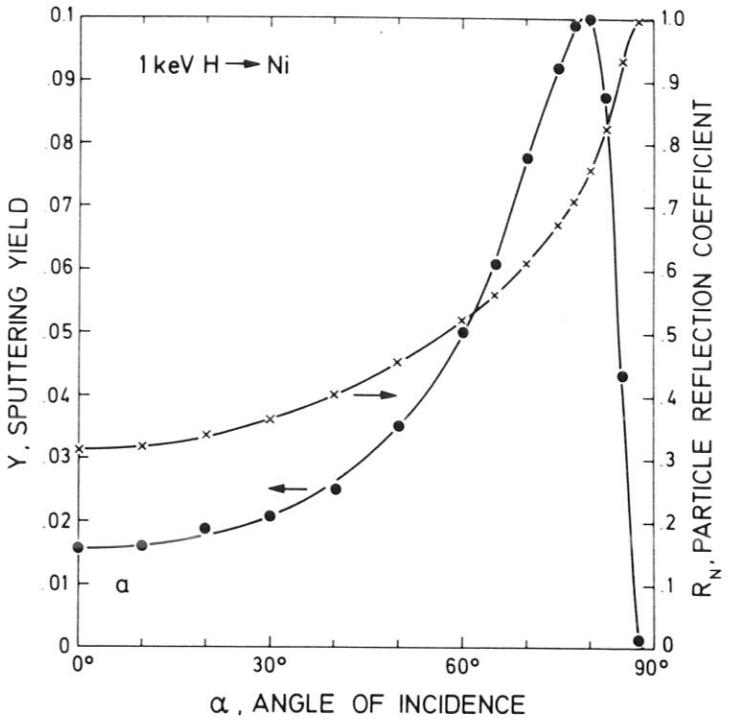
1 keV H → Ni
Y, SPUTTERING YIELD
R_N, PARTICLE REFLECTION COEFFICIENT
a
α, ANGLE OF INCIDENCE
0°
30°
60°
90°

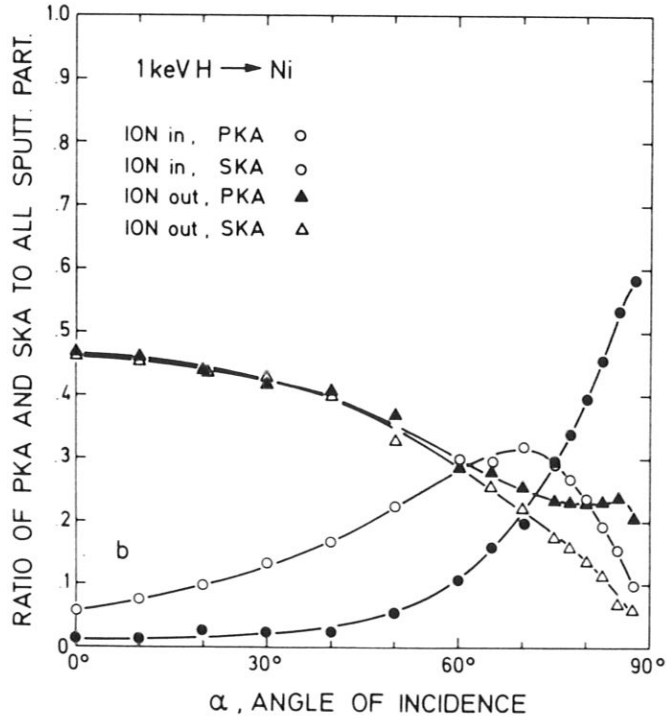
1 keV H → Ni
ION in, PKA
ION in, SKA
ION out, PKA
ION out, SKA
RATIO OF PKA AND SKA TO ALL SPUTT. PART.
b
α, ANGLE OF INCIDENCE
0°
30°
60°
90°

Fig. 13

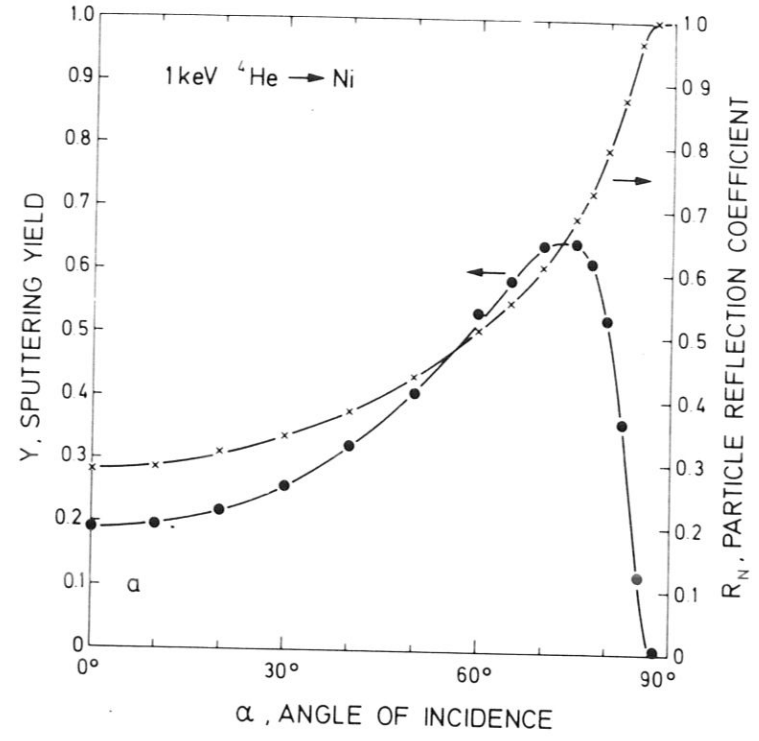
1keV ⁴He → Ni
Y, SPUTTERING YIELD
R_N, PARTICLE REFLECTION COEFFICIENT
a
0°
30°
60°
90°
α, ANGLE OF INCIDENCE

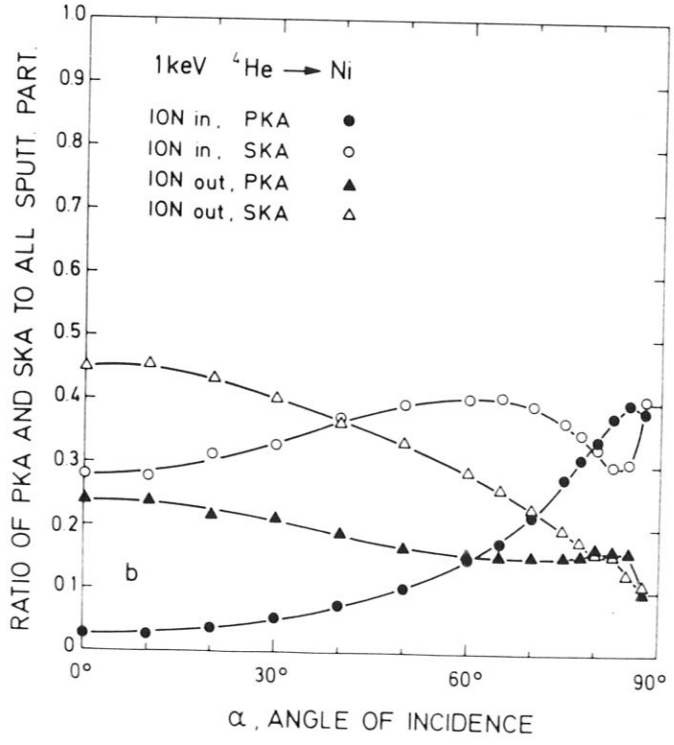
1keV ⁴He → Ni
ION in, PKA
ION in, SKA
ION out, PKA
ION out, SKA
RATIO OF PKA AND SKA TO ALL SPUTT. PART.
b
0°
30°
60°
90°
α, ANGLE OF INCIDENCE

Fig. 14

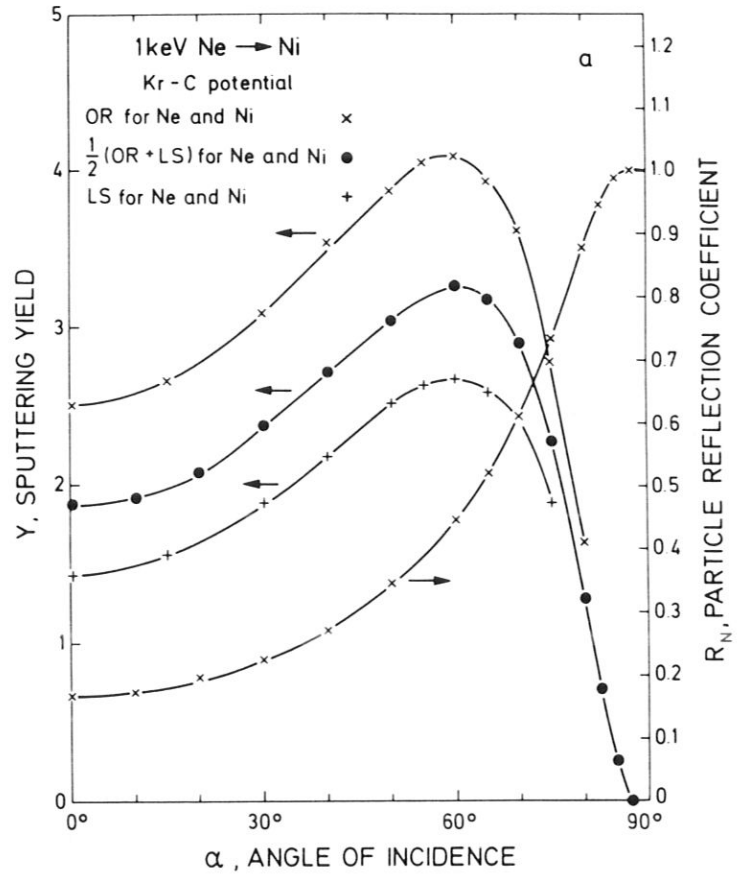
1keV Ne → Ni
Kr - C potential
OR for Ne and Ni
½ (OR + LS) for Ne and Ni
LS for Ne and Ni
a
Y, SPUTTERING YIELD
R_N, PARTICLE REFLECTION COEFFICIENT
α, ANGLE OF INCIDENCE
0°
30°
60°
90°

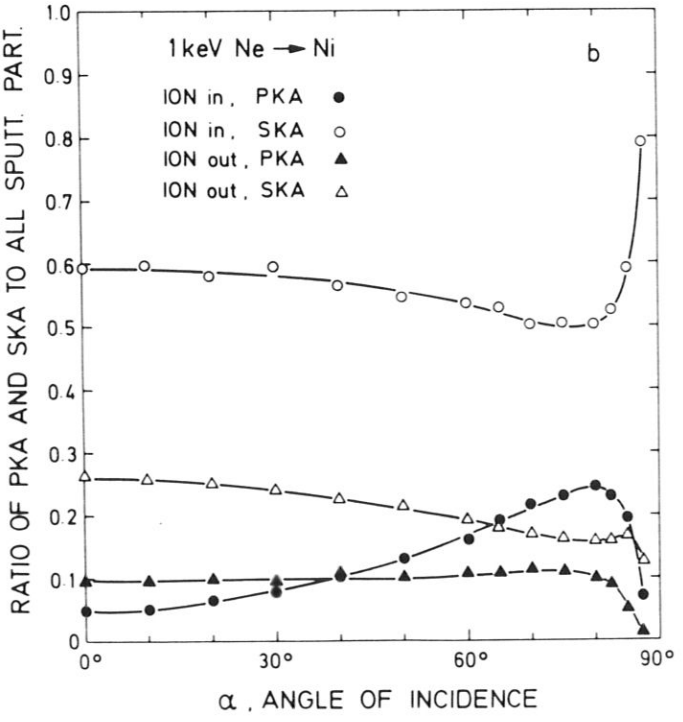
1keV Ne → Ni
b
ION in, PKA
ION in, SKA
ION out, PKA
ION out, SKA
RATIO OF PKA AND SKA TO ALL SPUTT. PART.
α, ANGLE OF INCIDENCE
0°
30°
60°
90°

Fig. 15

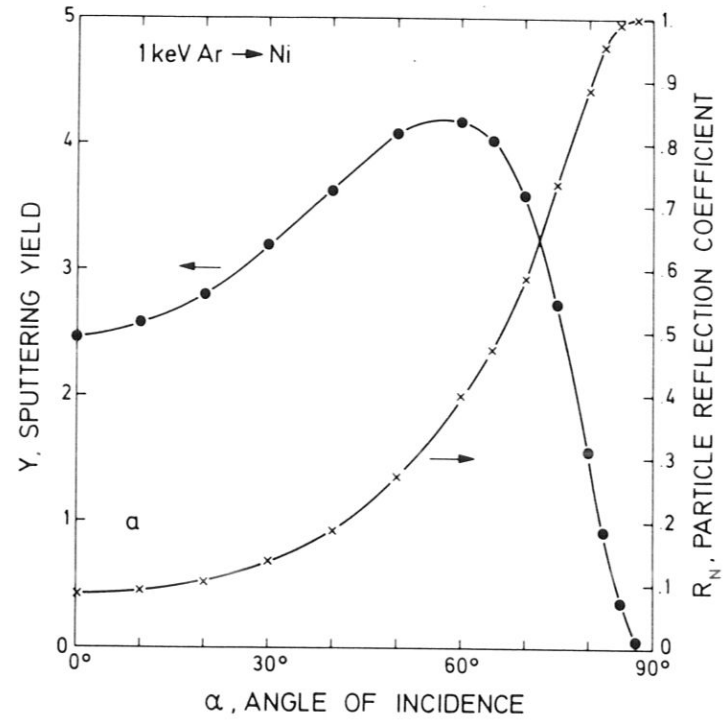
1 keV Ar → Ni
Y, SPUTTERING YIELD
R_N, PARTICLE REFLECTION COEFFICIENT
a
0°
30°
60°
90°
α, ANGLE OF INCIDENCE

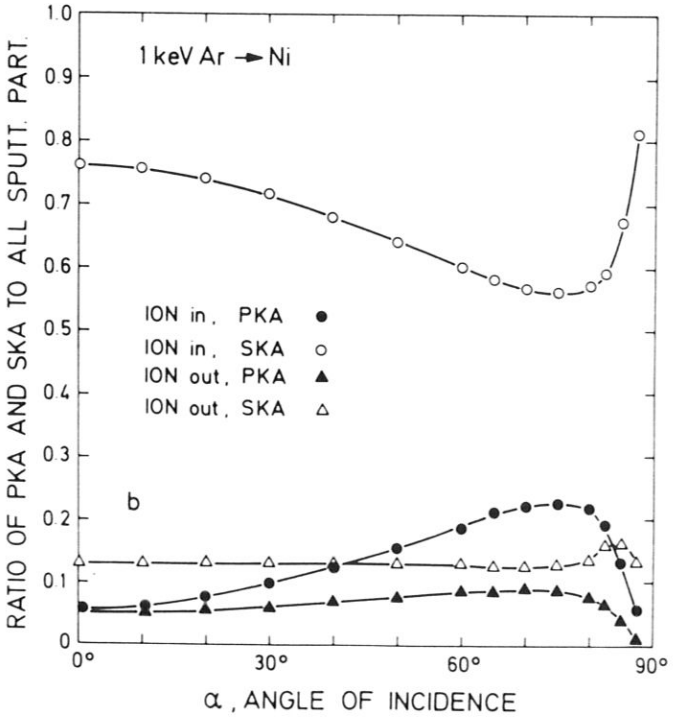
1 keV Ar → Ni
RATIO OF PKA AND SKA TO ALL SPUTT. PART.
ION in, PKA
ION in, SKA
ION out, PKA
ION out, SKA
b
0°
30°
60°
90°
α, ANGLE OF INCIDENCE

Fig. 16

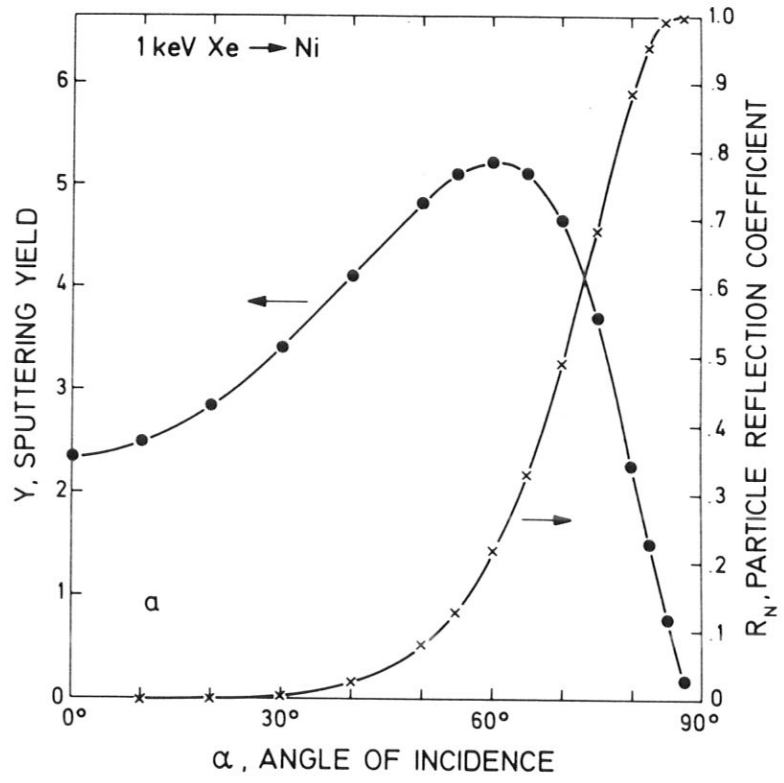
1 keV Xe → Ni
Y, SPUTTERING YIELD
R_N, PARTICLE REFLECTION COEFFICIENT
a
α, ANGLE OF INCIDENCE
0°
30°
60°
90°

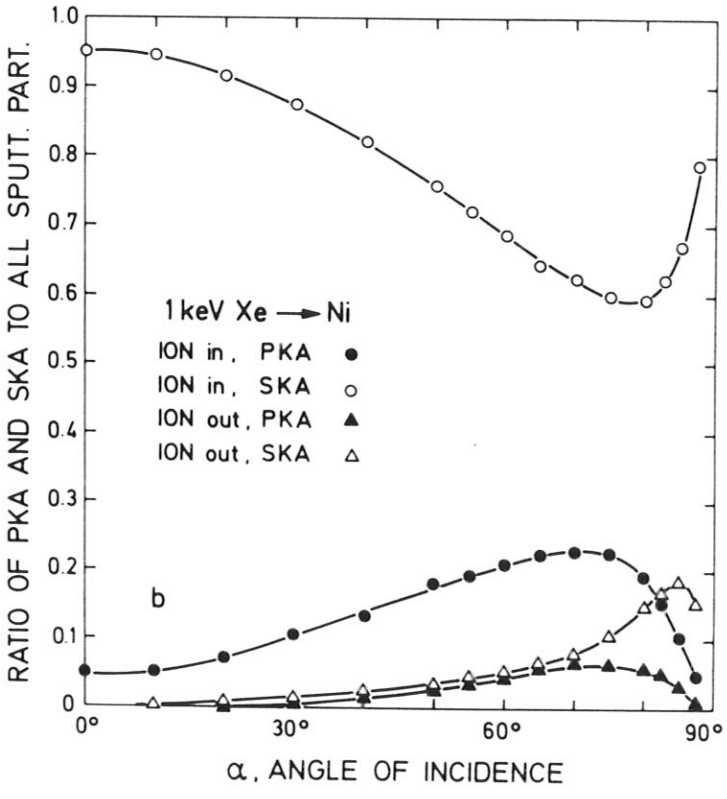
RATIO OF PKA AND SKA TO ALL SPUTT. PART.
1 keV Xe → Ni
ION in, PKA
ION in, SKA
ION out, PKA
ION out, SKA
b
α, ANGLE OF INCIDENCE
0°
30°
60°
90°

Fig. 17

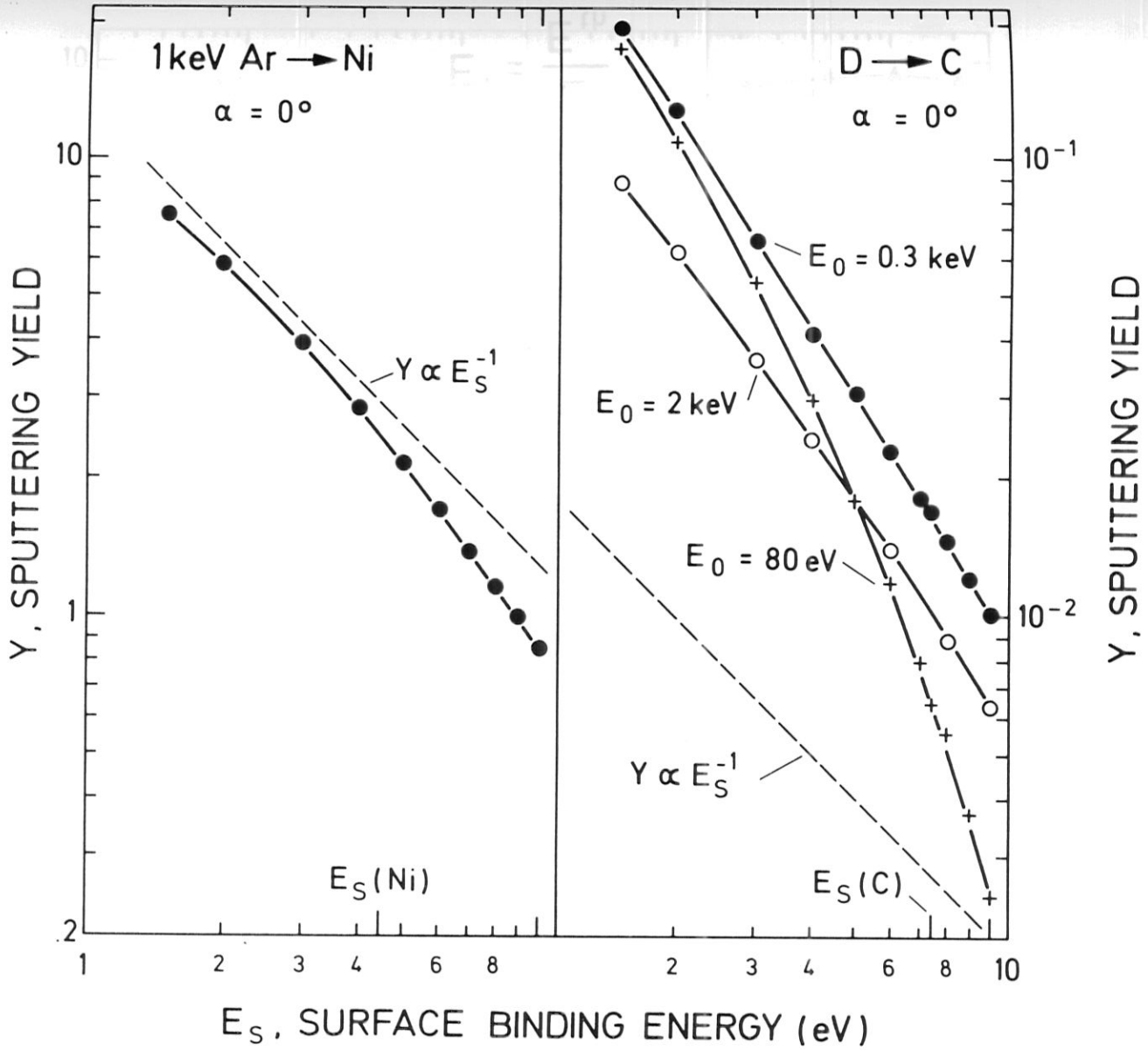
1keV Ar → Ni
α = 0°
D → C
α = 0°
Y, SPUTTERING YIELD
Y, SPUTTERING YIELD
Y ∝ E_S^-1
E_0 = 0.3 keV
E_0 = 2 keV
E_0 = 80 eV
Y ∝ E_S^-1
E_S(Ni)
E_S(C)
10
1
.2
10^-1
10^-2
1
2
3
4
6
8
2
3
4
6
8
10
E_S, SURFACE BINDING ENERGY (eV)

Fig. 18

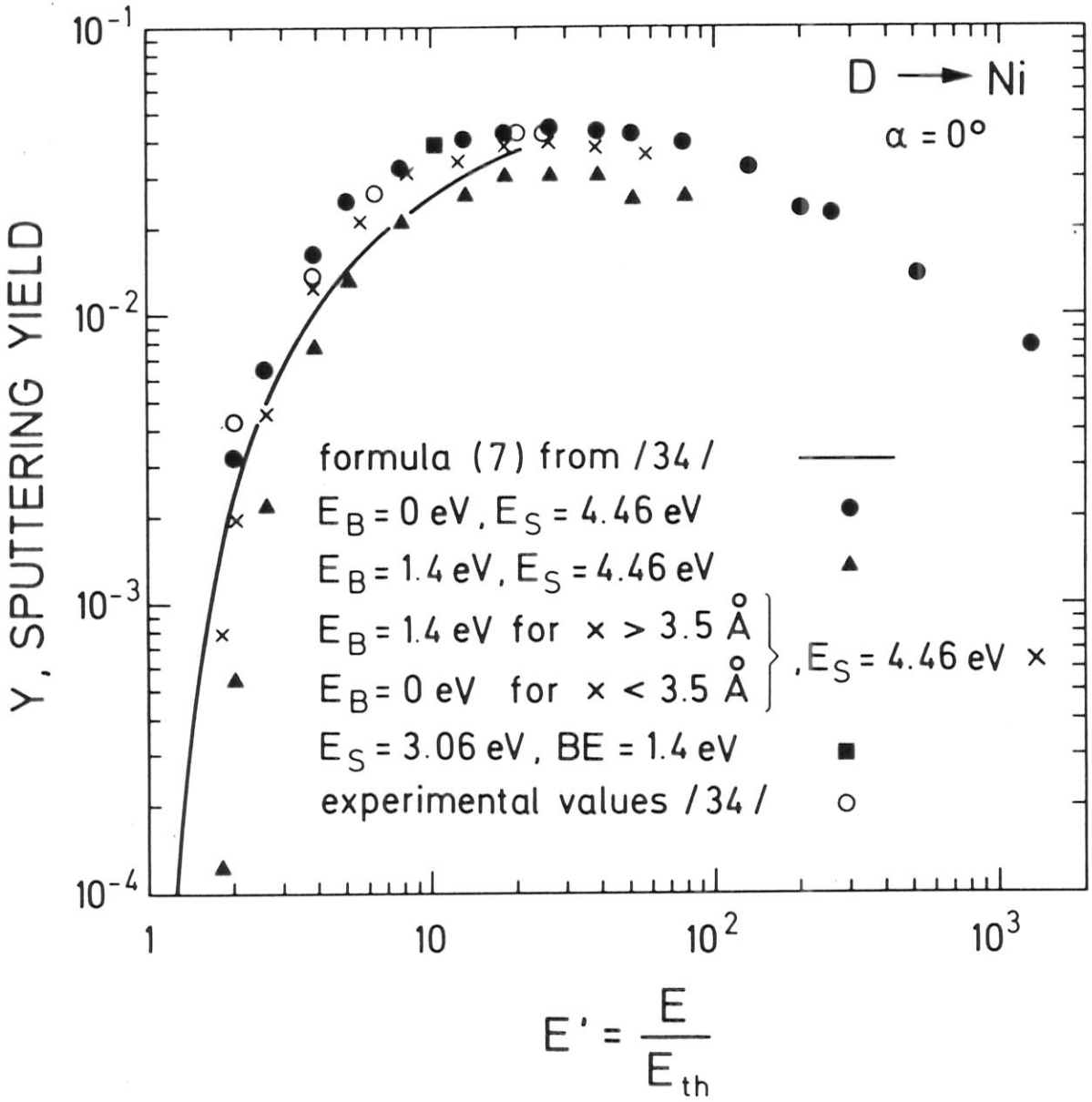
D → Ni
α = 0°
Y, SPUTTERING YIELD
formula (7) from /34/
E_B = 0 eV, E_S = 4.46 eV
E_B = 1.4 eV, E_S = 4.46 eV
E_B = 1.4 eV for x > 3.5 Å
E_B = 0 eV for x < 3.5 Å
, E_S = 4.46 eV
E_S = 3.06 eV, BE = 1.4 eV
experimental values /34/
E' = E / E_th

Fig. 19

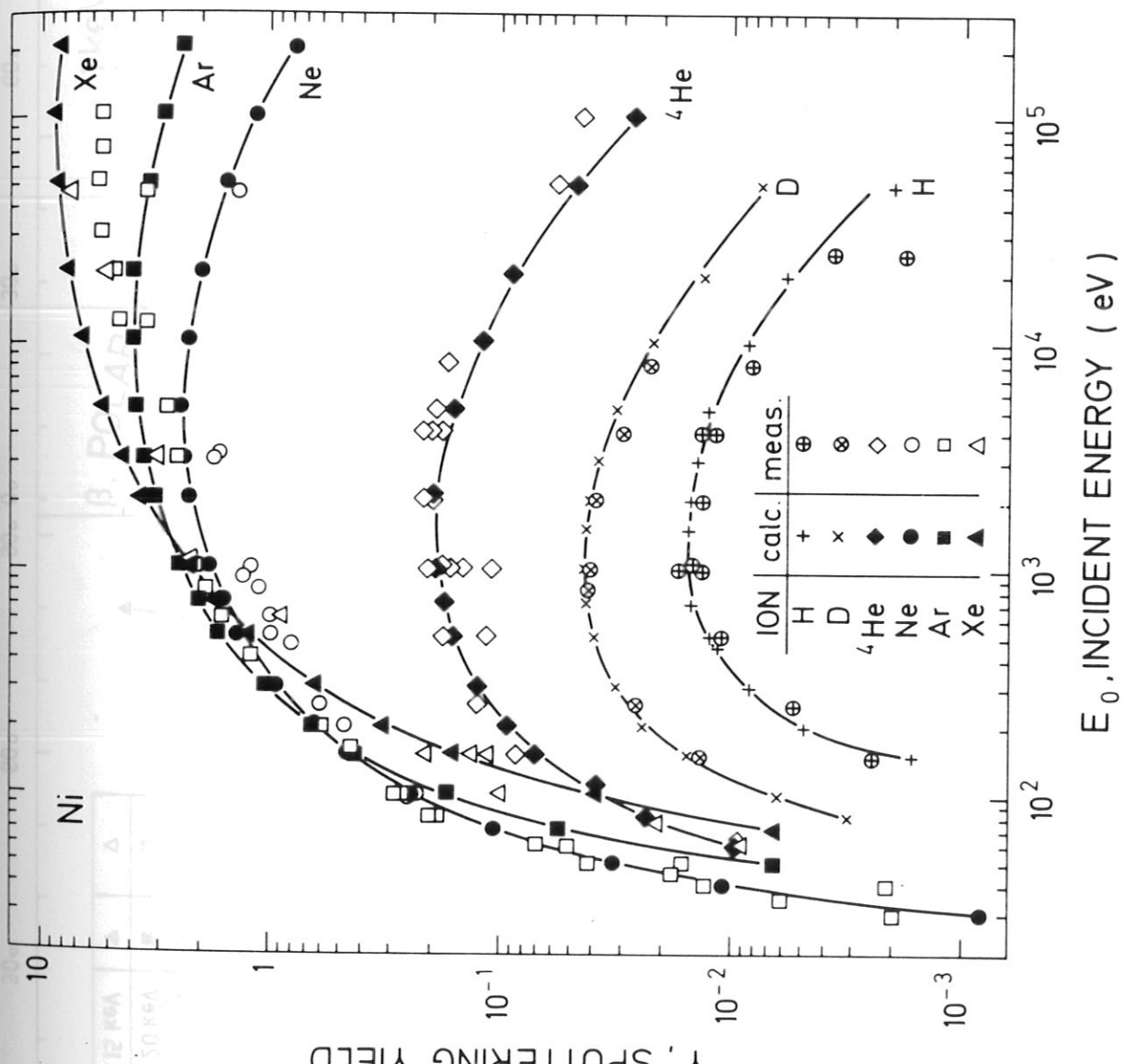
Ni
Xe
Ar
Ne
^{4}He
H
D
^{4}He
Ne
Ar
Xe
ION
calc.
meas.
Y , SPUTTERING YIELD
E_0, INCIDENT ENERGY (eV)

Fig. 20

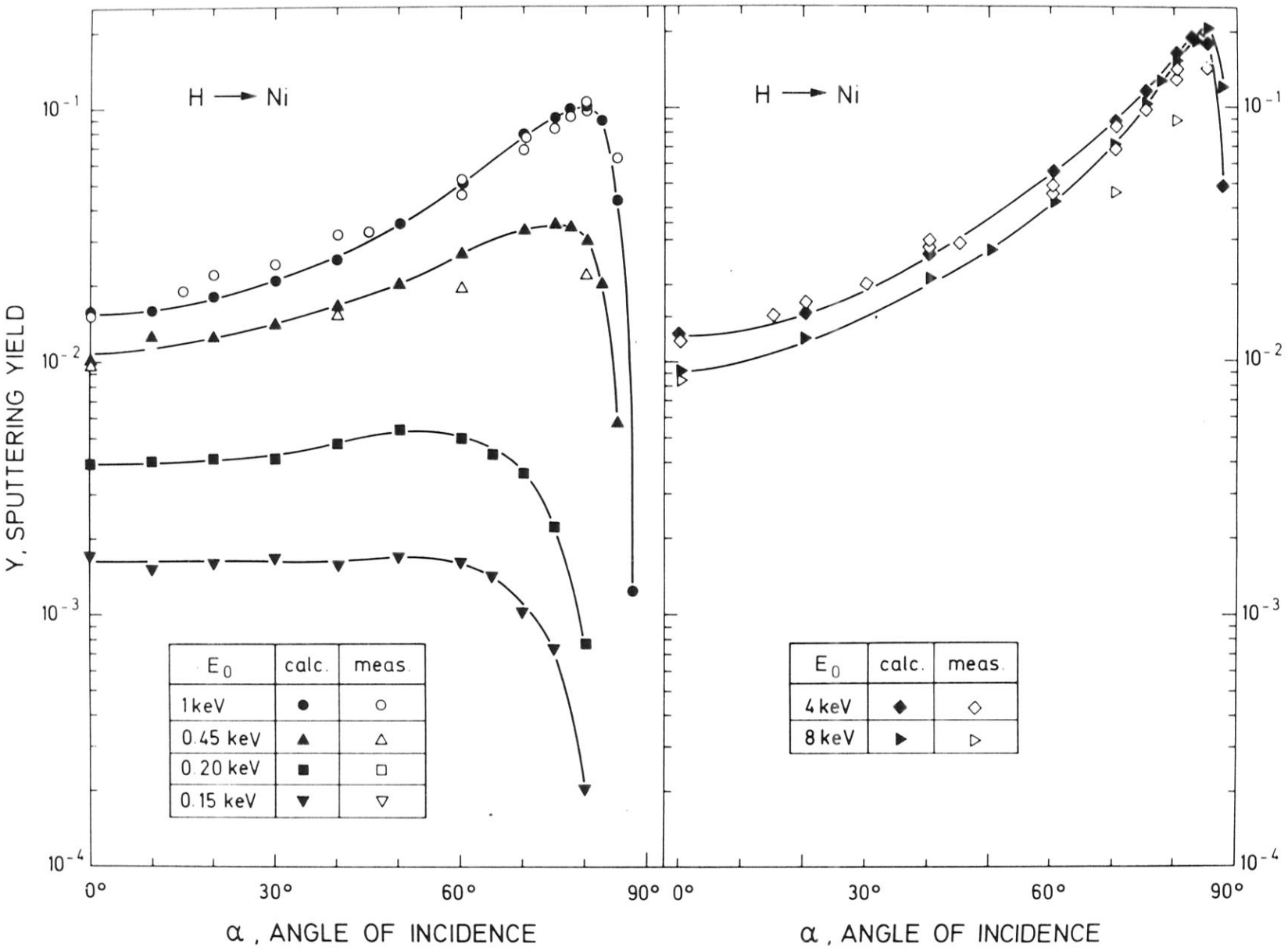
H → Ni
H → Ni
Y, SPUTTERING YIELD
10^{-1}
10^{-2}
10^{-3}
10^{-4}
0°
30°
60°
90°
α , ANGLE OF INCIDENCE
α , ANGLE OF INCIDENCE
E0 | calc. | meas.
1 keV
0.45 keV
0.20 keV
0.15 keV
E0 | calc. | meas.
4 keV
8 keV

Fig. 21

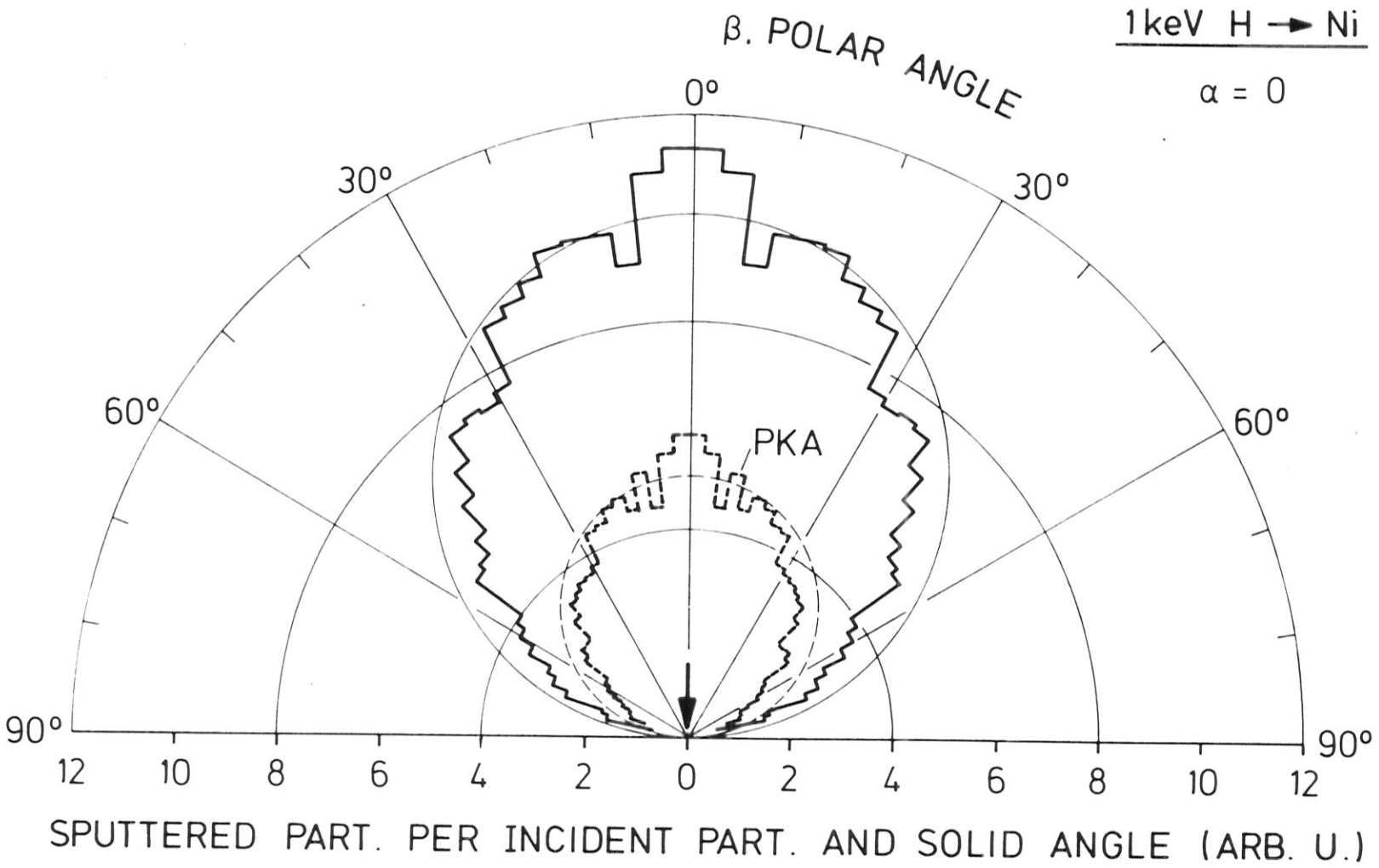
1keV H → Ni
α = 0
β. POLAR ANGLE
0°
30°
30°
60°
60°
90°
90°
PKA
12
10
8
6
4
2
0
2
4
6
8
10
12
SPUTTERED PART. PER INCIDENT PART. AND SOLID ANGLE (ARB. U.)

Fig. 22

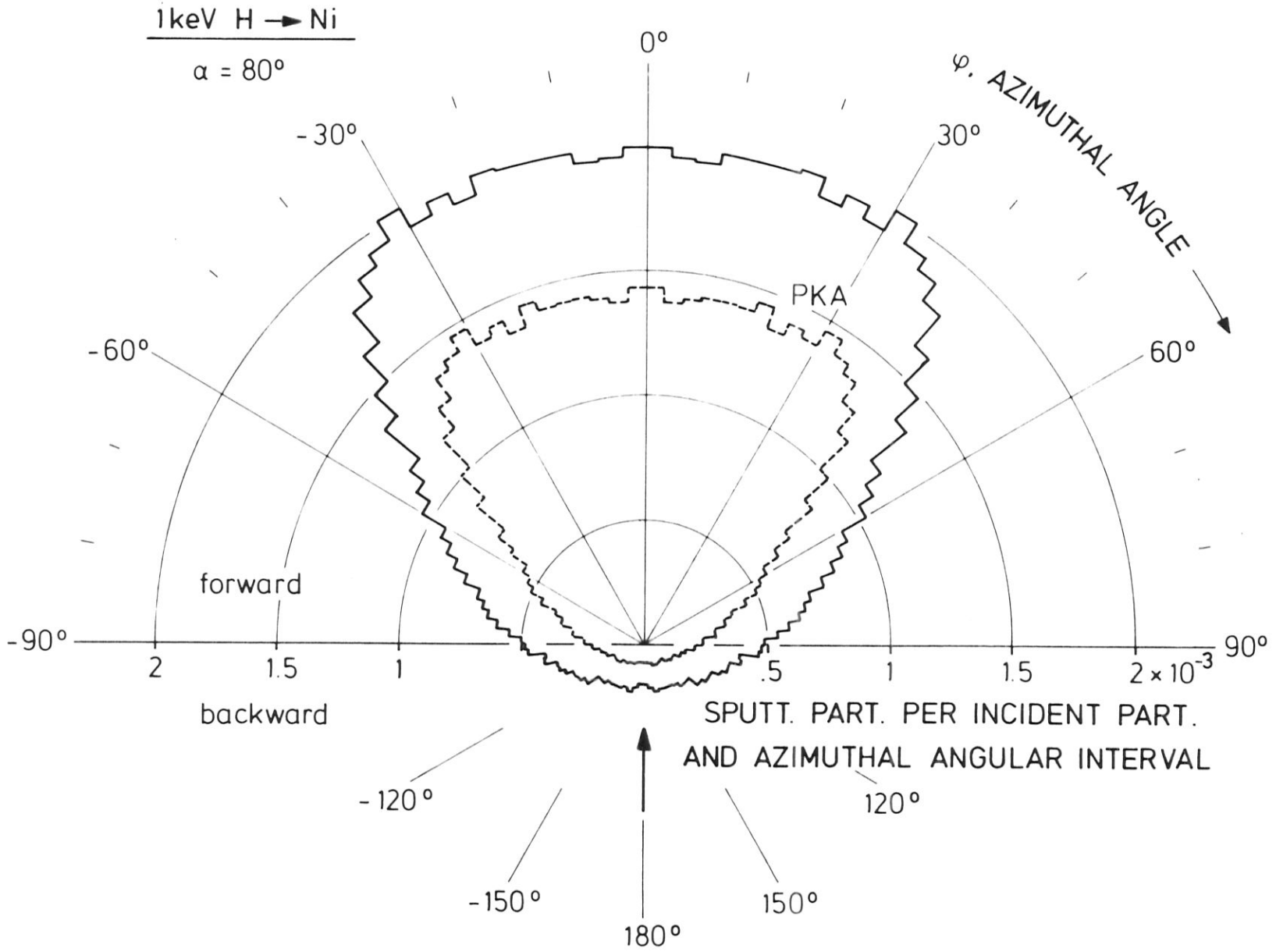
1keV H → Ni
α = 80°
0°
-30°
30°
φ. AZIMUTHAL ANGLE
PKA
-60°
60°
forward
-90°
90°
2
1.5
1
.5
1
1.5
2 × 10⁻³
backward
SPUTT. PART. PER INCIDENT PART.
AND AZIMUTHAL ANGULAR INTERVAL
-120°
120°
-150°
150°
180°

Fig. 23

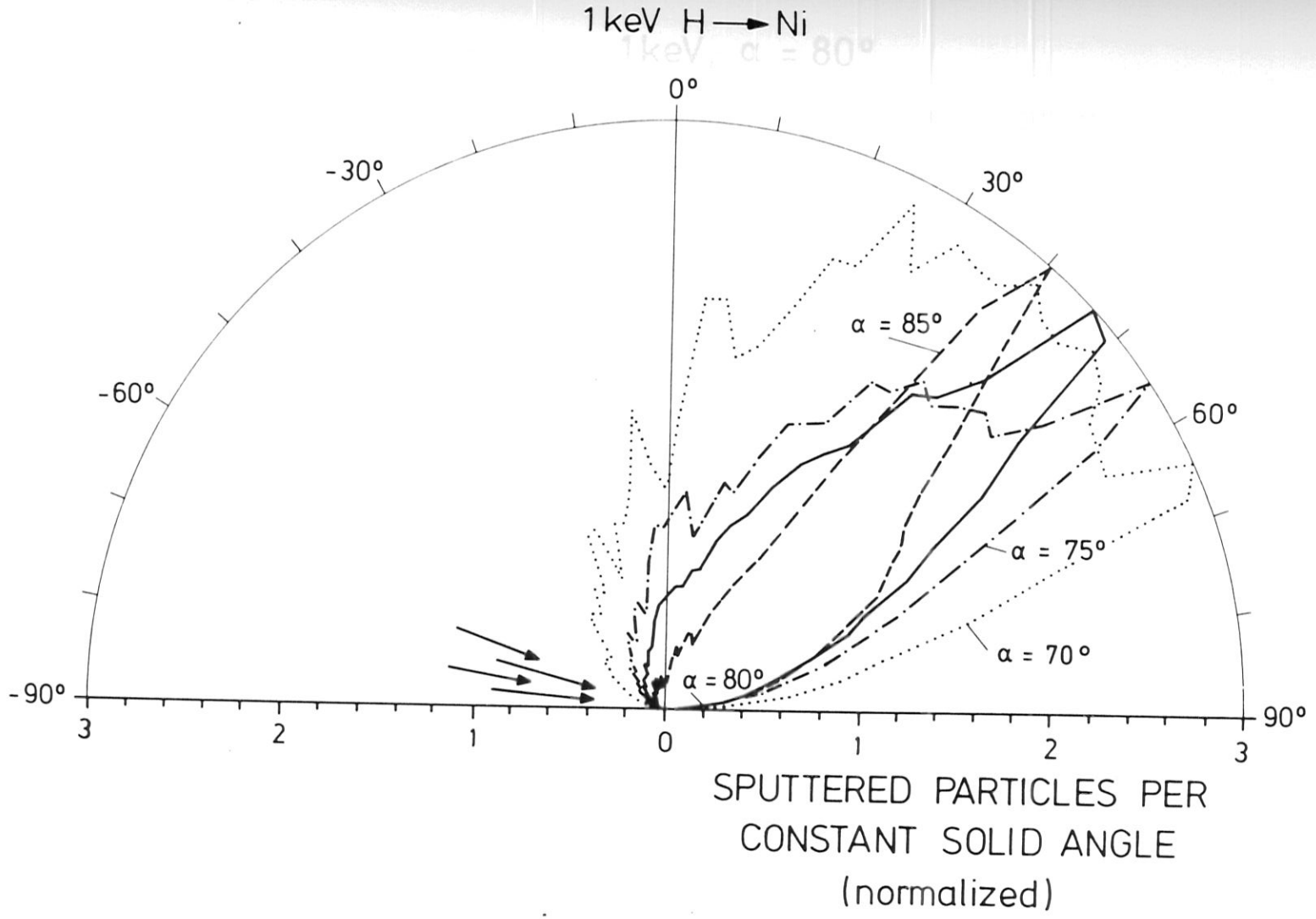
1 keV H → Ni
0°
-30°
30°
-60°
60°
-90°
90°
α = 85°
α = 75°
α = 70°
α = 80°
3
2
1
0
1
2
3
SPUTTERED PARTICLES PER
CONSTANT SOLID ANGLE
(normalized)

Fig. 24

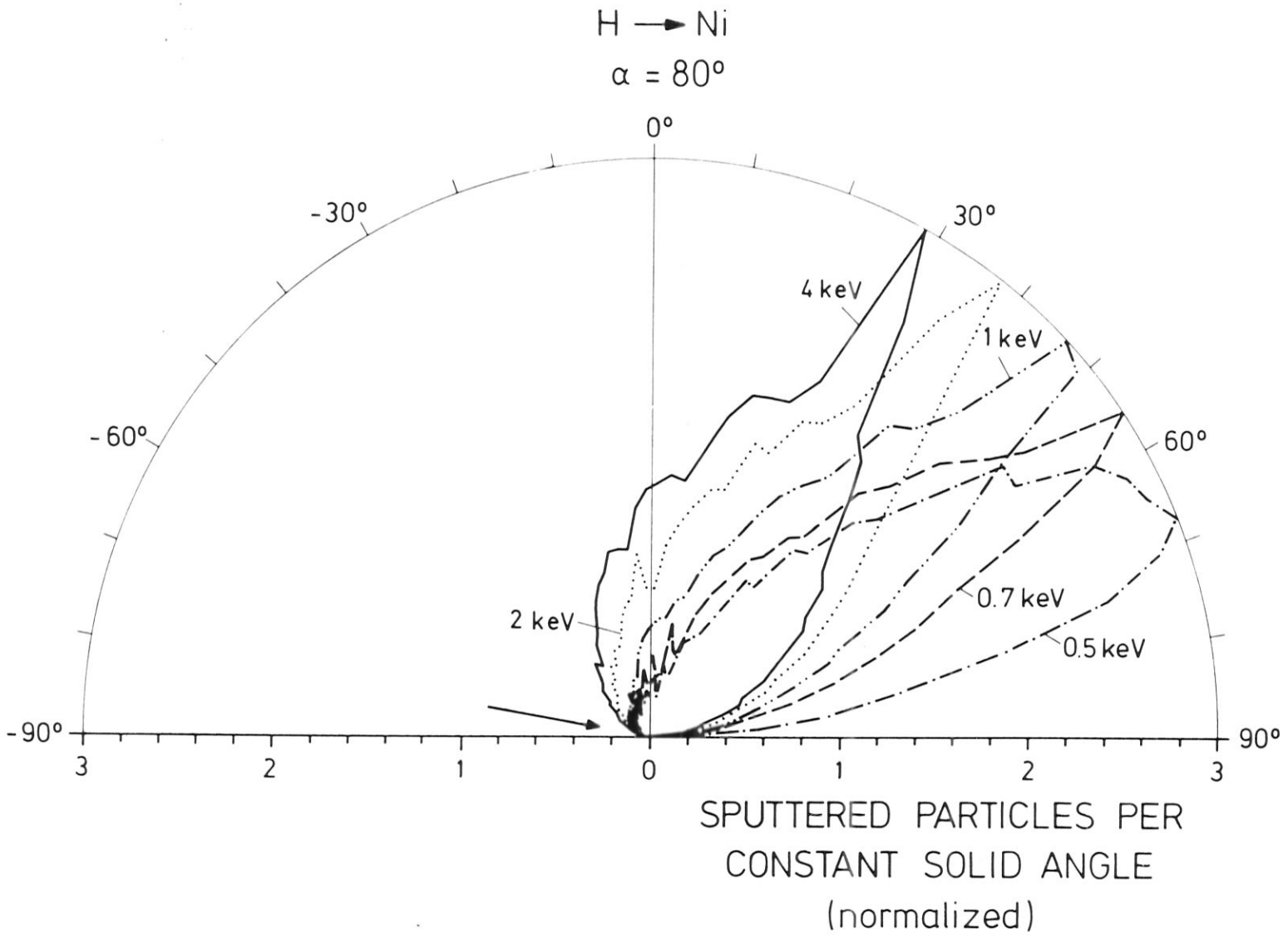
H → Ni
α = 80°
0°
-30°
30°
-60°
60°
-90°
90°
4 keV
1 keV
0.7 keV
0.5 keV
2 keV
3
2
1
0
1
2
3
SPUTTERED PARTICLES PER
CONSTANT SOLID ANGLE
(normalized)

Fig. 25

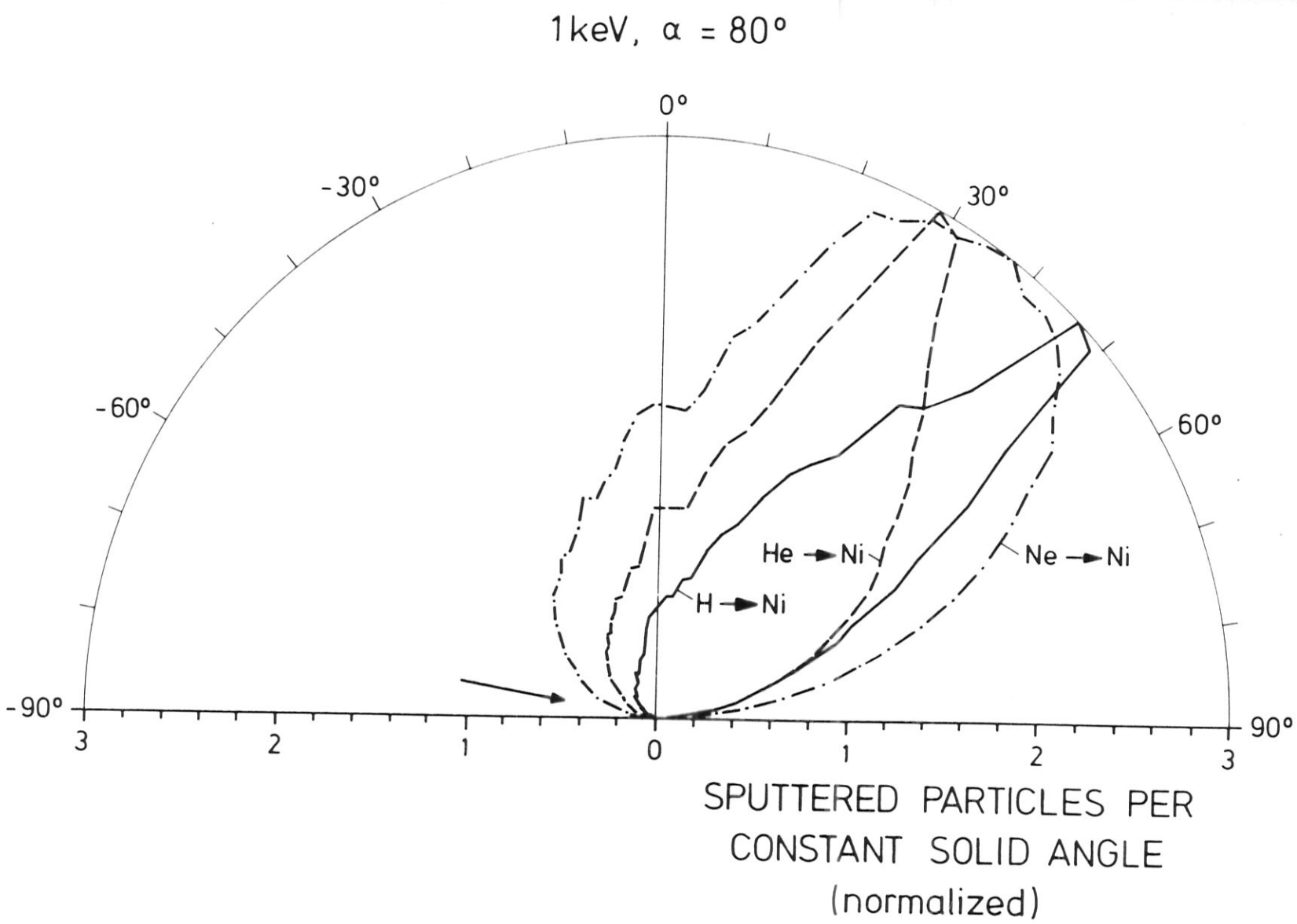
1keV, α = 80°
0°
-30°
30°
-60°
60°
-90°
90°
He → Ni
H → Ni
Ne → Ni
3
2
1
0
1
2
3
SPUTTERED PARTICLES PER
CONSTANT SOLID ANGLE
(normalized)

Fig. 26

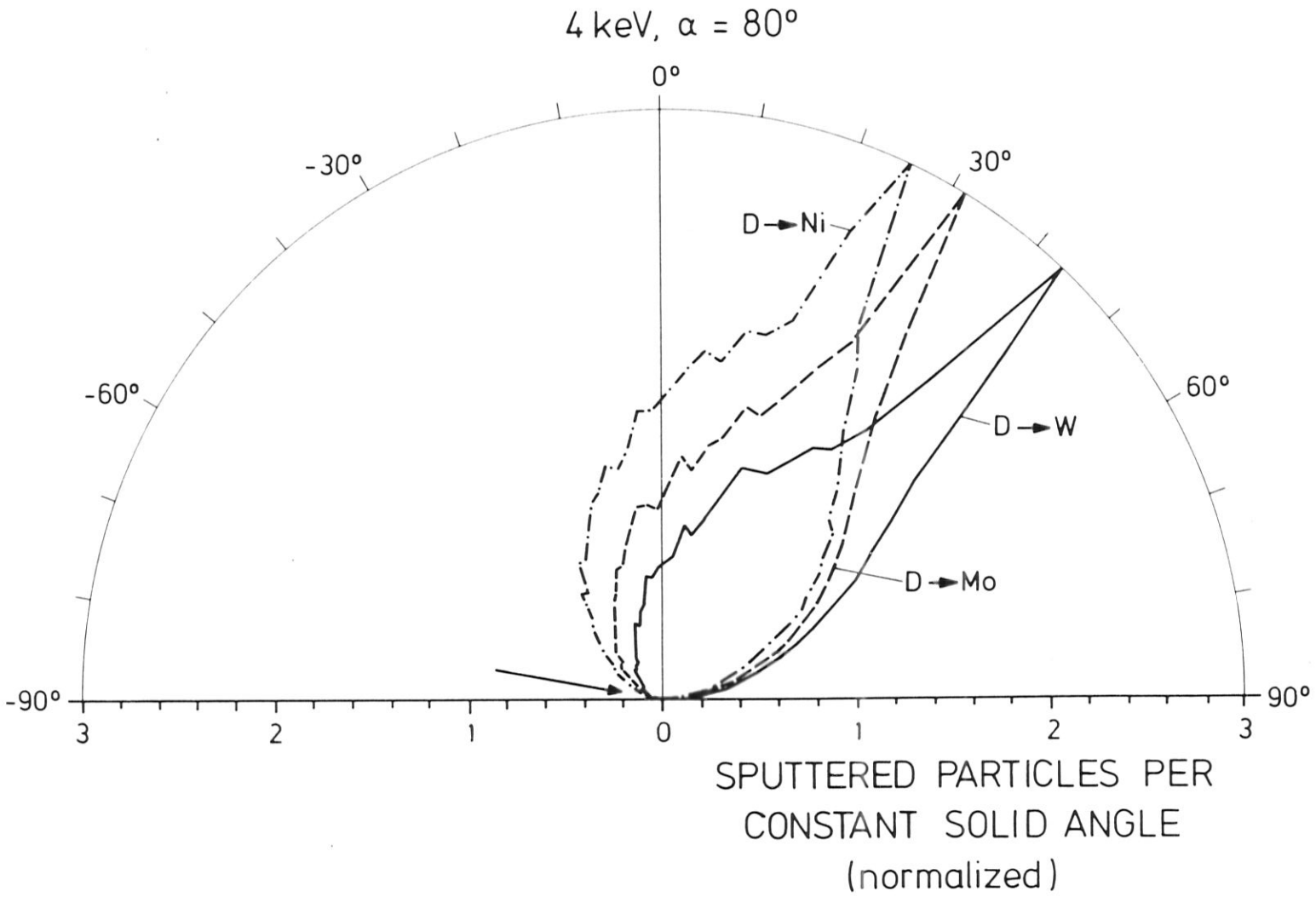
4 keV, α = 80°
0°
-30°
30°
-60°
60°
-90°
90°
D → Ni
D → W
D → Mo
3
2
1
0
1
2
3
SPUTTERED PARTICLES PER
CONSTANT SOLID ANGLE
(normalized)

Fig. 27

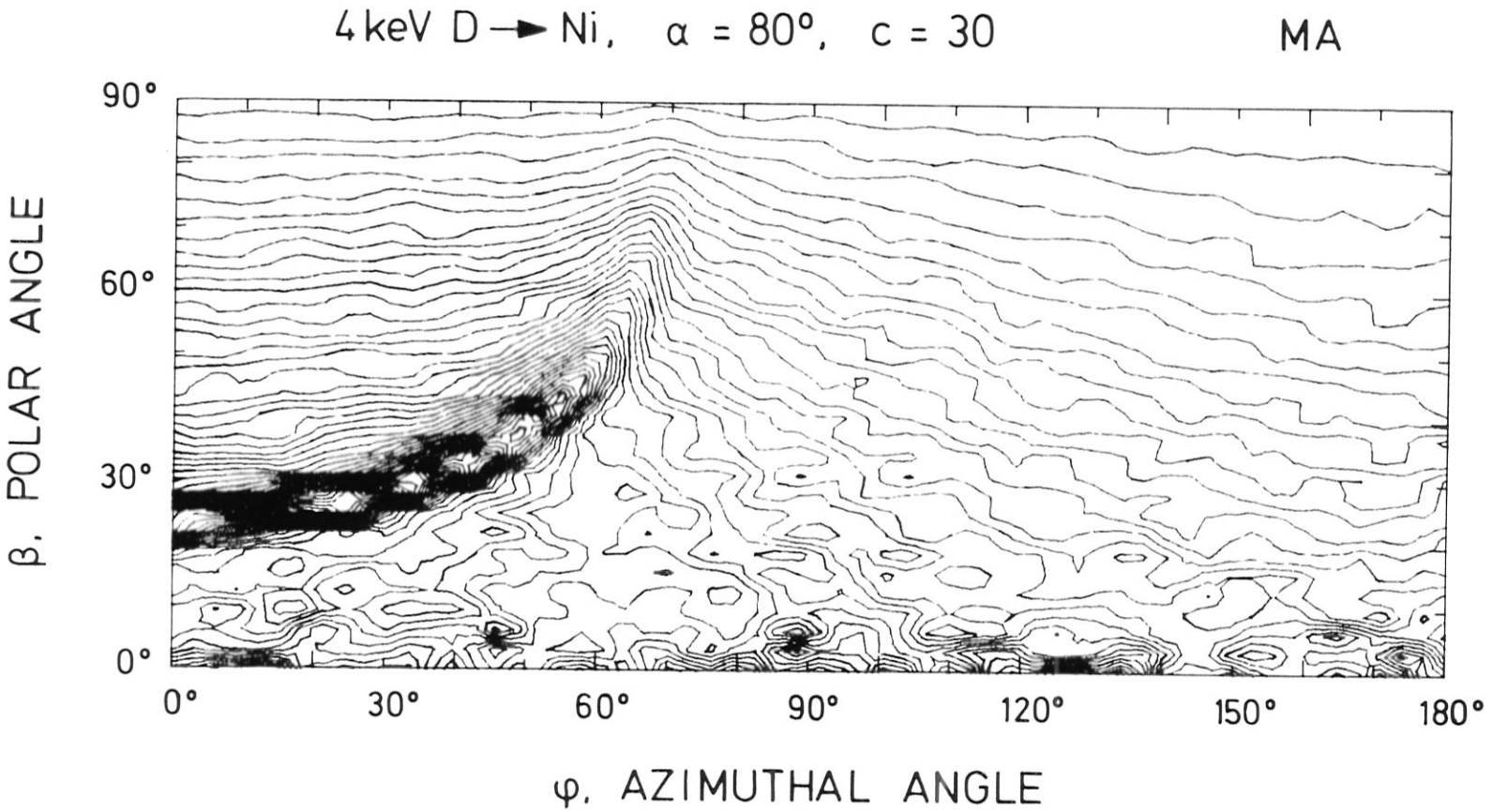
4 keV D → Ni, α = 80°, c = 30
MA
β, POLAR ANGLE
90°
60°
30°
0°
0°
30°
60°
90°
120°
150°
180°
φ, AZIMUTHAL ANGLE

Fig. 28a

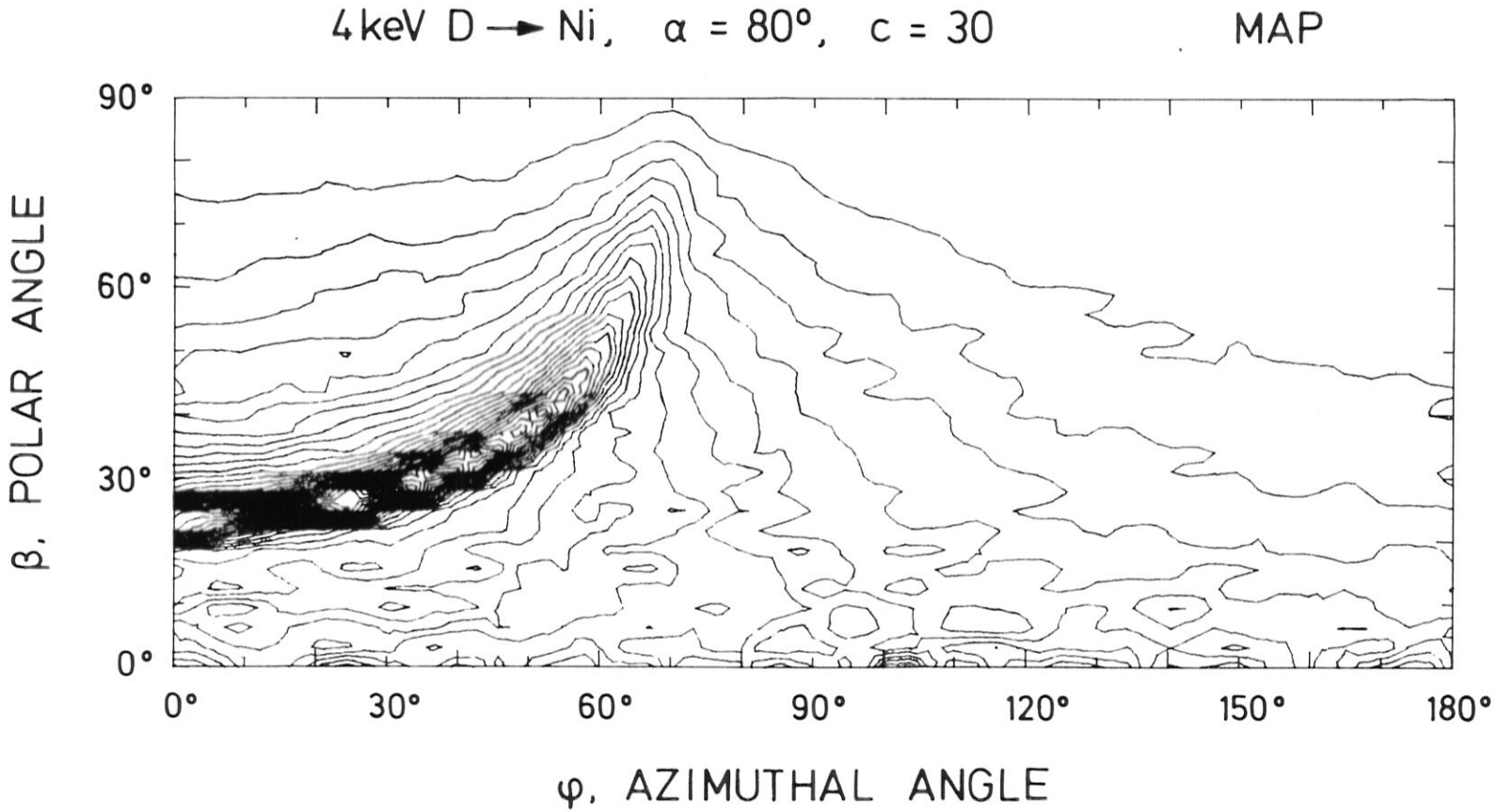
4 keV D → Ni, α = 80°, c = 30
MAP
β, POLAR ANGLE
90°
60°
30°
0°
0°
30°
60°
90°
120°
150°
180°
φ, AZIMUTHAL ANGLE

Fig. 28b

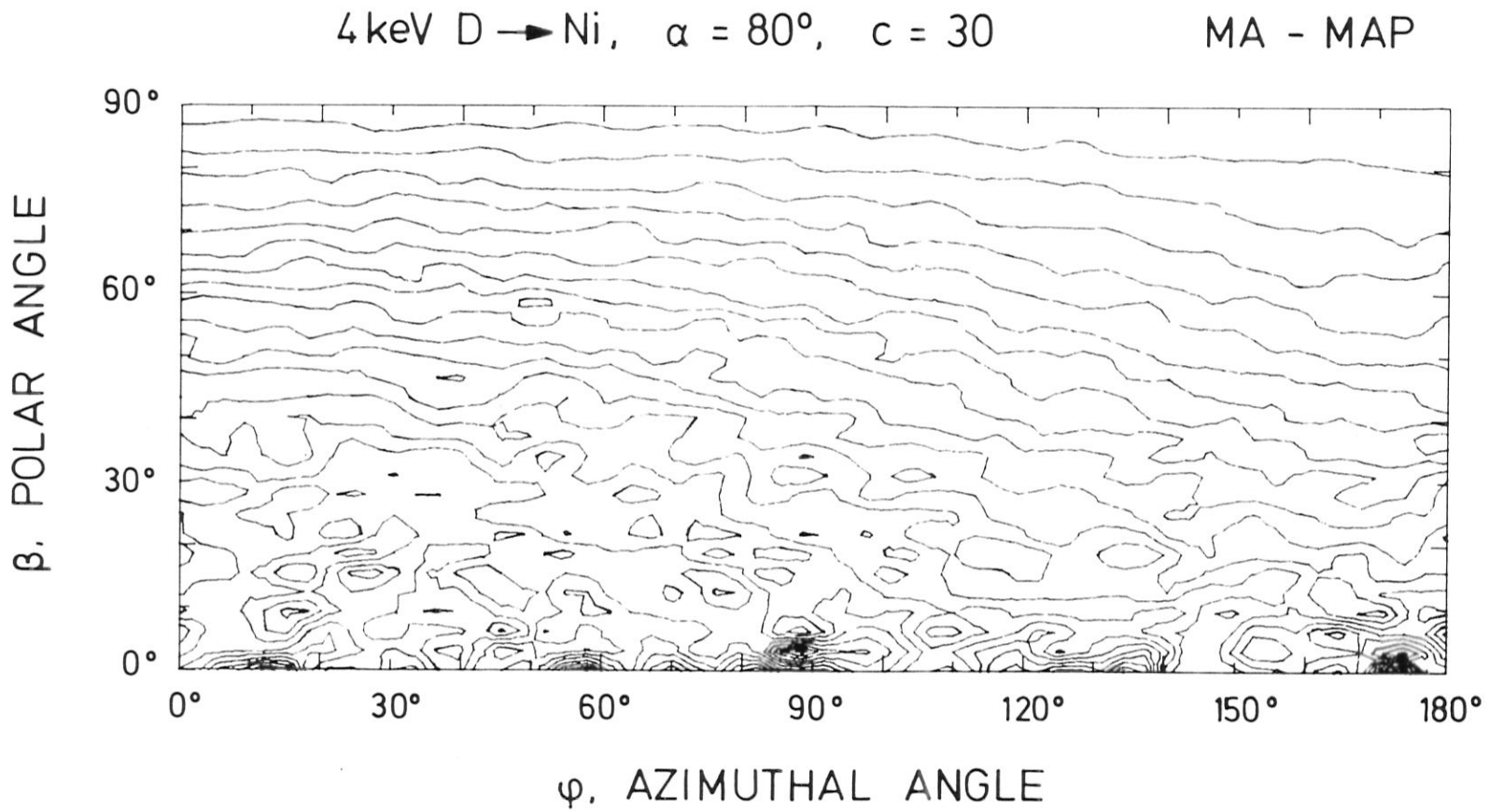
4 keV D → Ni, α = 80°, c = 30
MA - MAP
β, POLAR ANGLE
90°
60°
30°
0°
0°
30°
60°
90°
120°
150°
180°
φ, AZIMUTHAL ANGLE

Fig. 28c

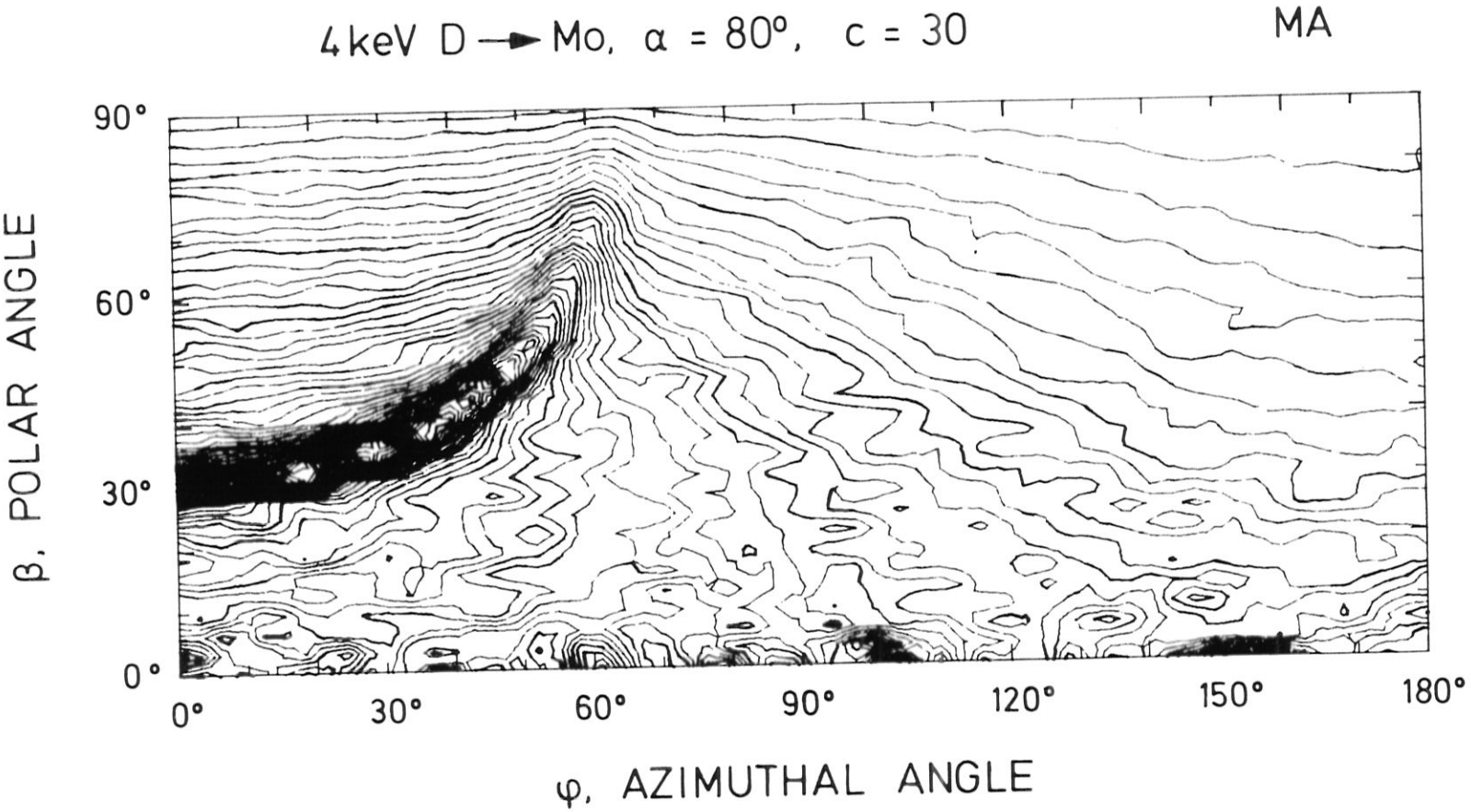
4keV D → Mo, α = 80°, c = 30
MA
β, POLAR ANGLE
90°
60°
30°
0°
0°
30°
60°
90°
120°
150°
180°
φ, AZIMUTHAL ANGLE

Fig. 29

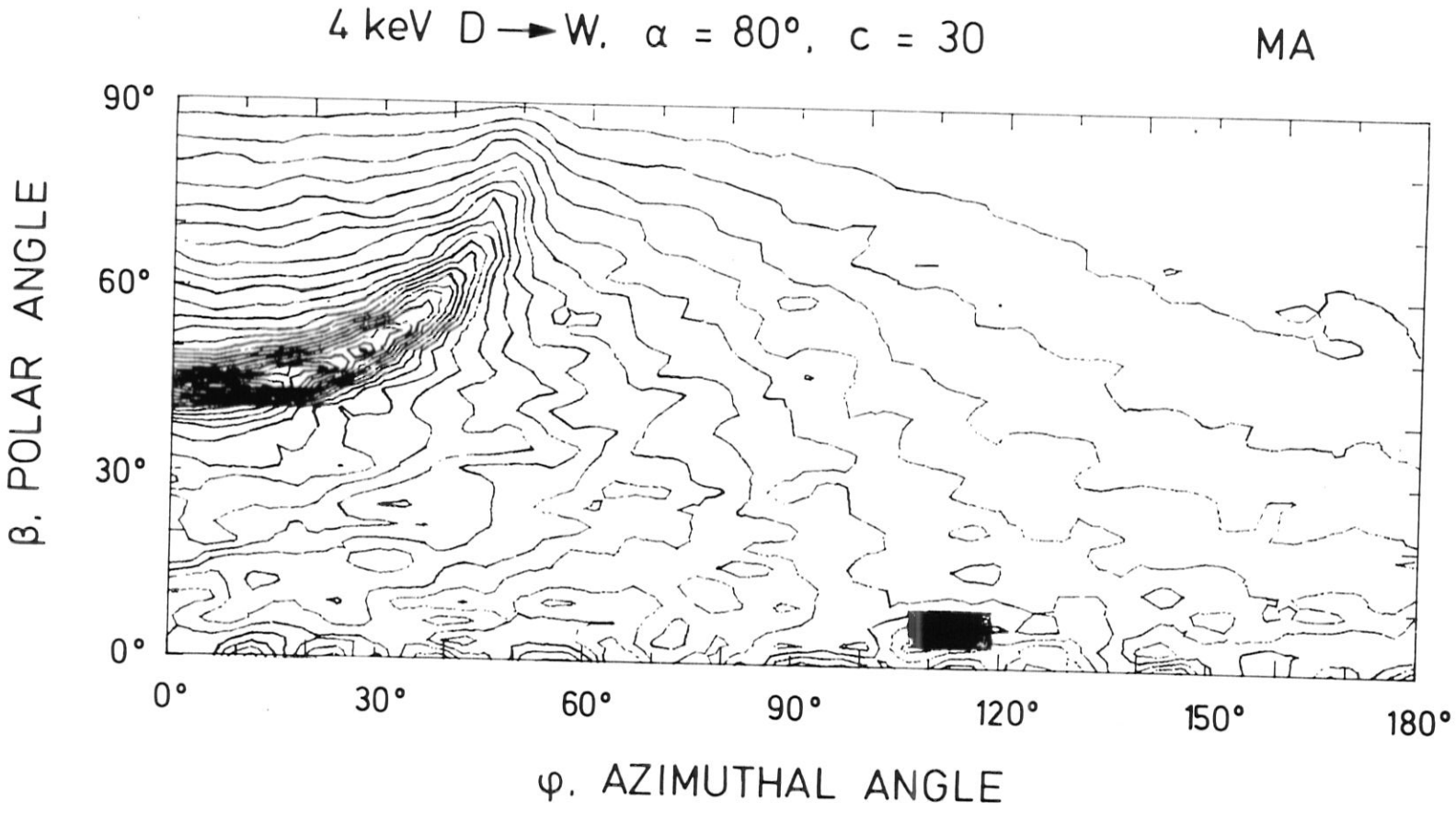
4 keV D → W. α = 80°. c = 30
MA
β. POLAR ANGLE
90°
60°
30°
0°
0°
30°
60°
90°
120°
150°
180°
φ. AZIMUTHAL ANGLE

Fig. 30

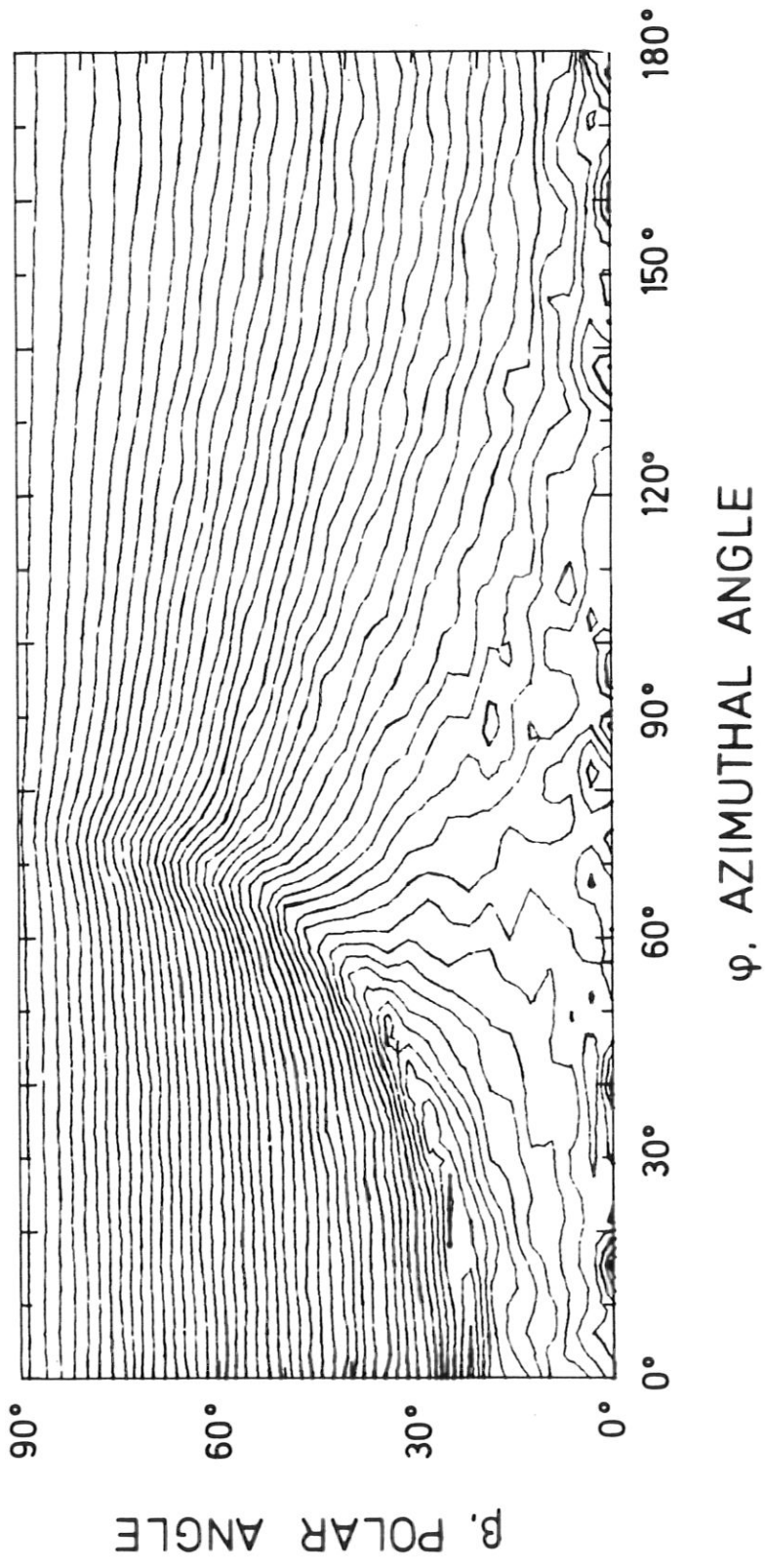
3 keV Ne → Ni, α = 75°, c = 300
MA
β, POLAR ANGLE
90°
60°
30°
0°
0°
30°
60°
90°
120°
150°
180°
φ, AZIMUTHAL ANGLE

Fig. 31a

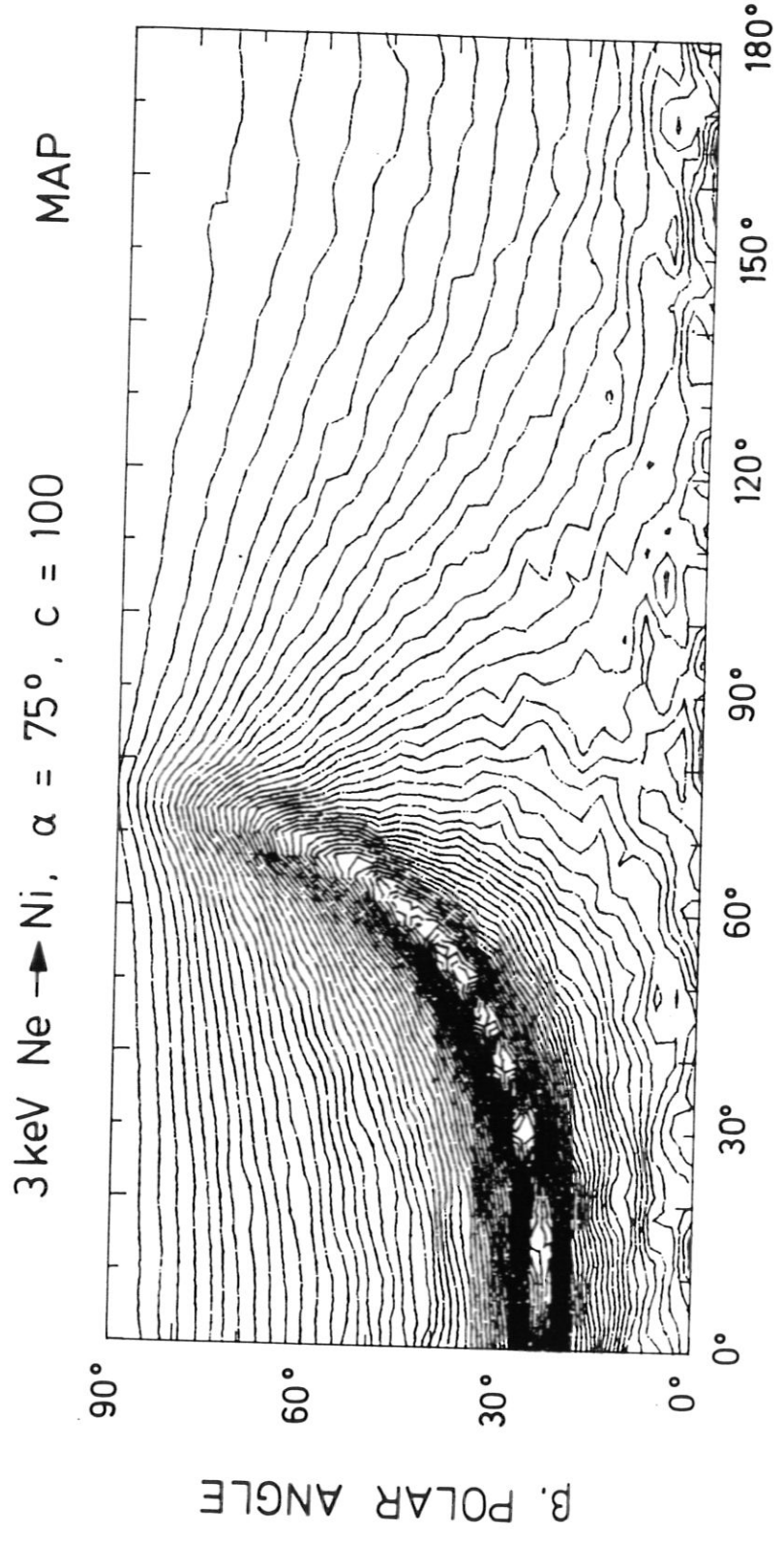
3keV Ne → Ni, α = 75°, c = 100
MAP
β, POLAR ANGLE
φ, AZIMUTHAL ANGLE
90°
60°
30°
0°
0°
30°
60°
90°
120°
150°
180°

Fig. 31b

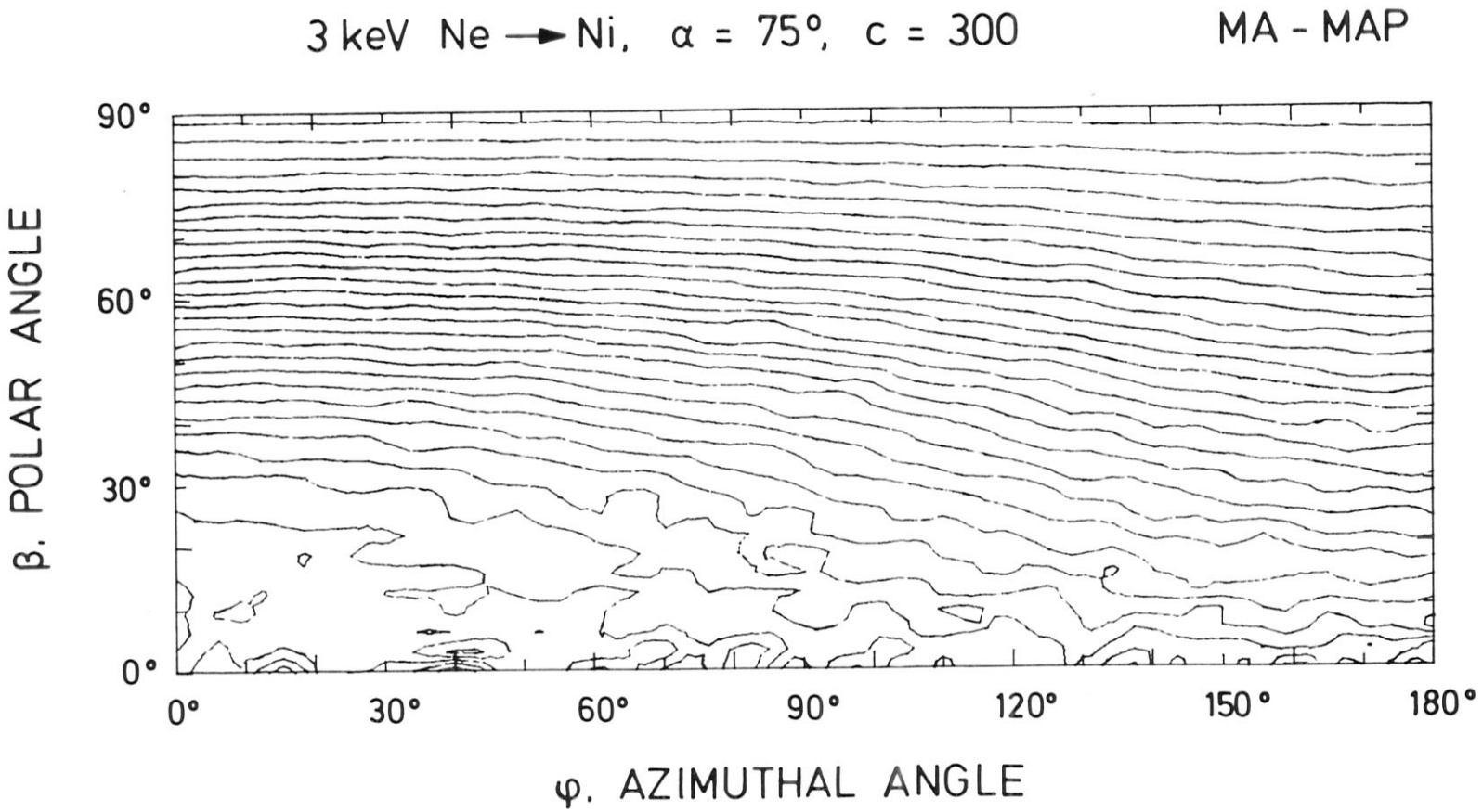
3 keV Ne → Ni, α = 75°, c = 300
MA - MAP
β. POLAR ANGLE
90°
60°
30°
0°
0°
30°
60°
90°
120°
150°
180°
φ. AZIMUTHAL ANGLE

Fig. 31c

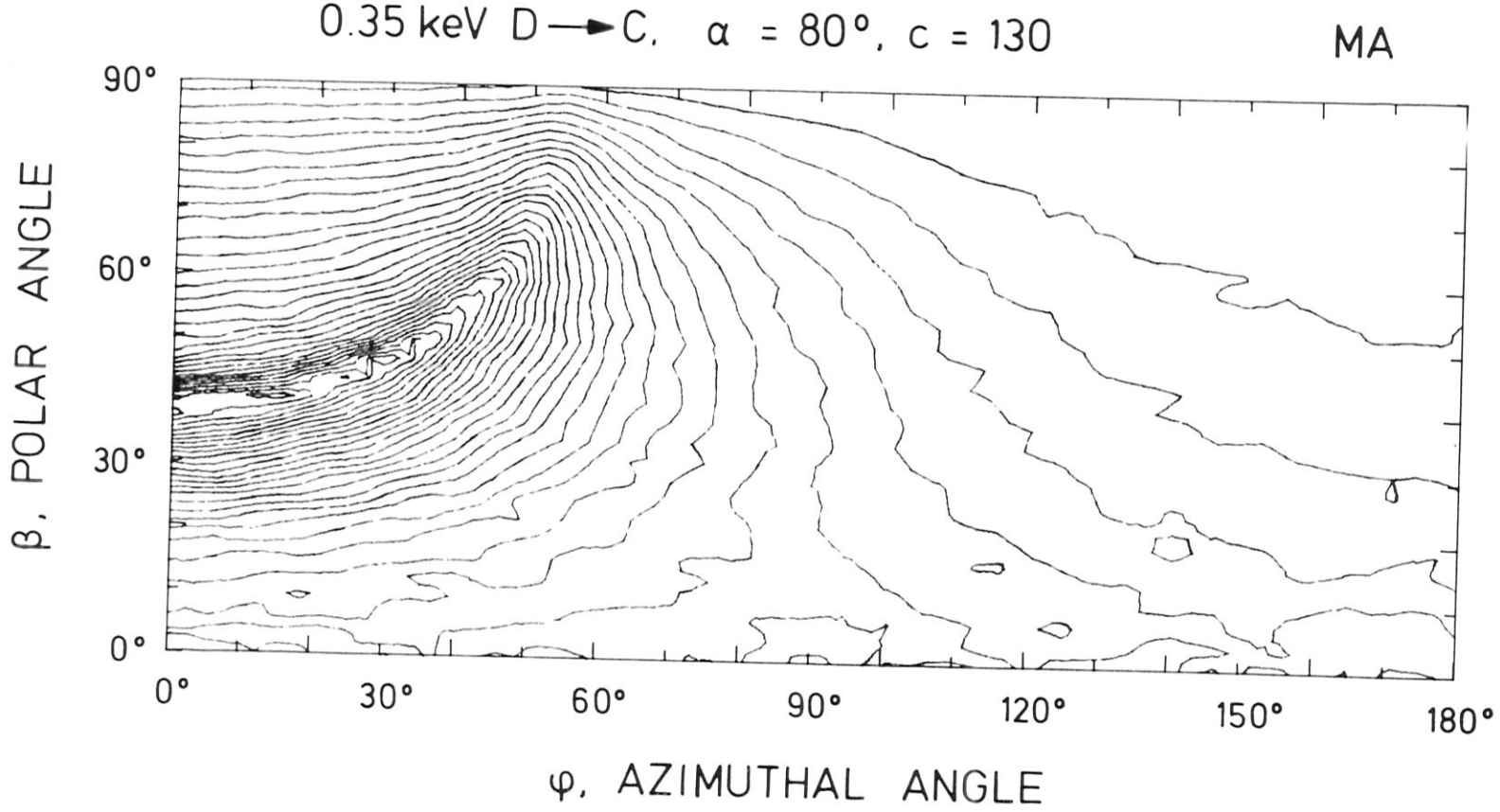
0.35 keV D → C, α = 80°, c = 130
MA
β, POLAR ANGLE
90°
60°
30°
0°
0°
30°
60°
90°
120°
150°
180°
φ, AZIMUTHAL ANGLE

Fig. 32a

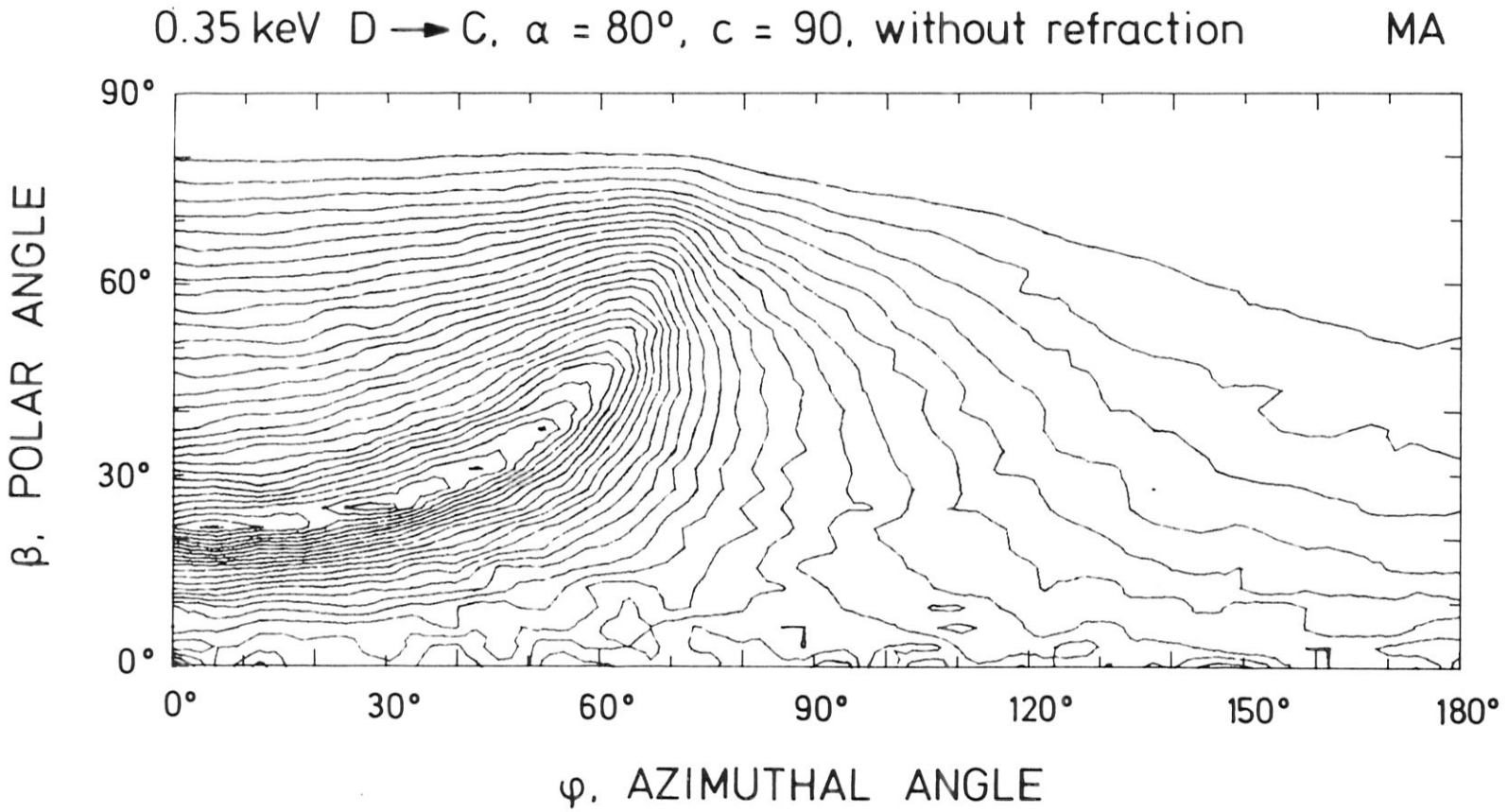
0.35 keV D → C, α = 80°, c = 90, without refraction
MA
β, POLAR ANGLE
90°
60°
30°
0°
0°
30°
60°
90°
120°
150°
180°
φ, AZIMUTHAL ANGLE

Fig. 32b

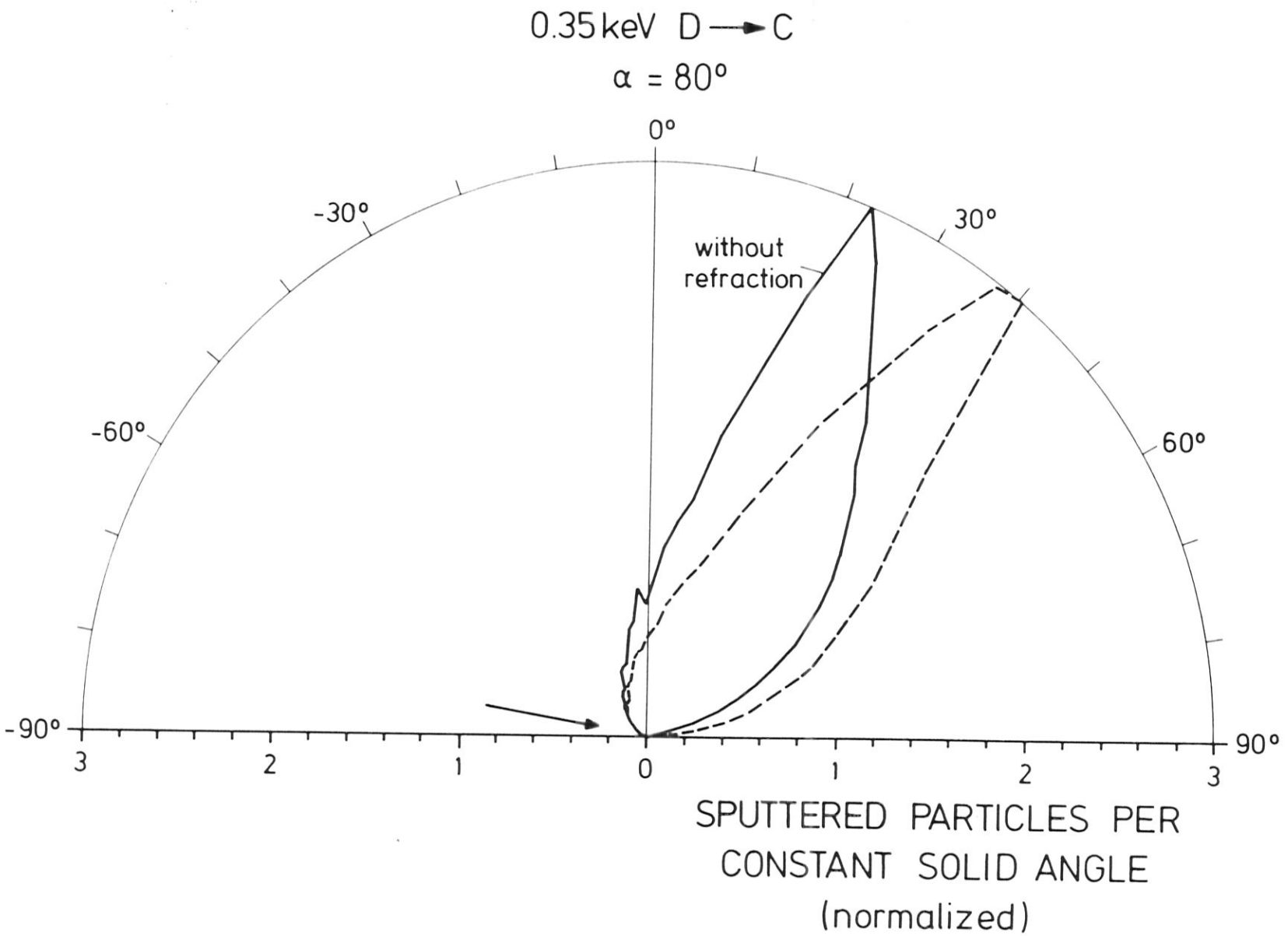
0.35 keV D → C
α = 80°
0°
-30°
30°
-60°
60°
-90°
90°
without
refraction
3
2
1
0
1
2
3
SPUTTERED PARTICLES PER
CONSTANT SOLID ANGLE
(normalized)

Fig. 33

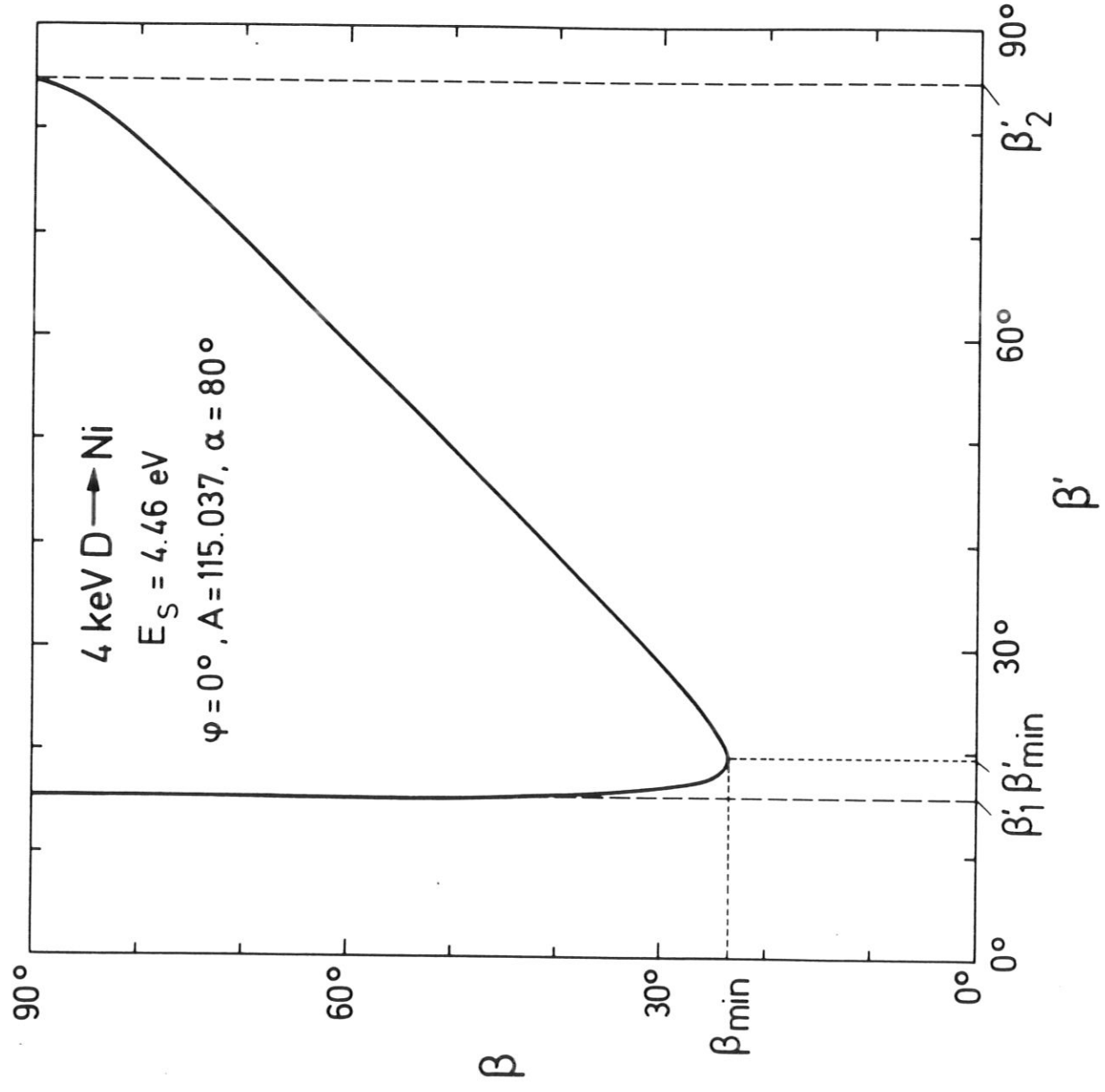
4 keV D⟶Ni
E_S = 4.46 eV
φ = 0°, A = 115.037, α = 80°
90°
60°
30°
0°
β
β_{min}
0°
30°
60°
90°
β'_1 β'_{min}
β'_2
β'

Fig. 34

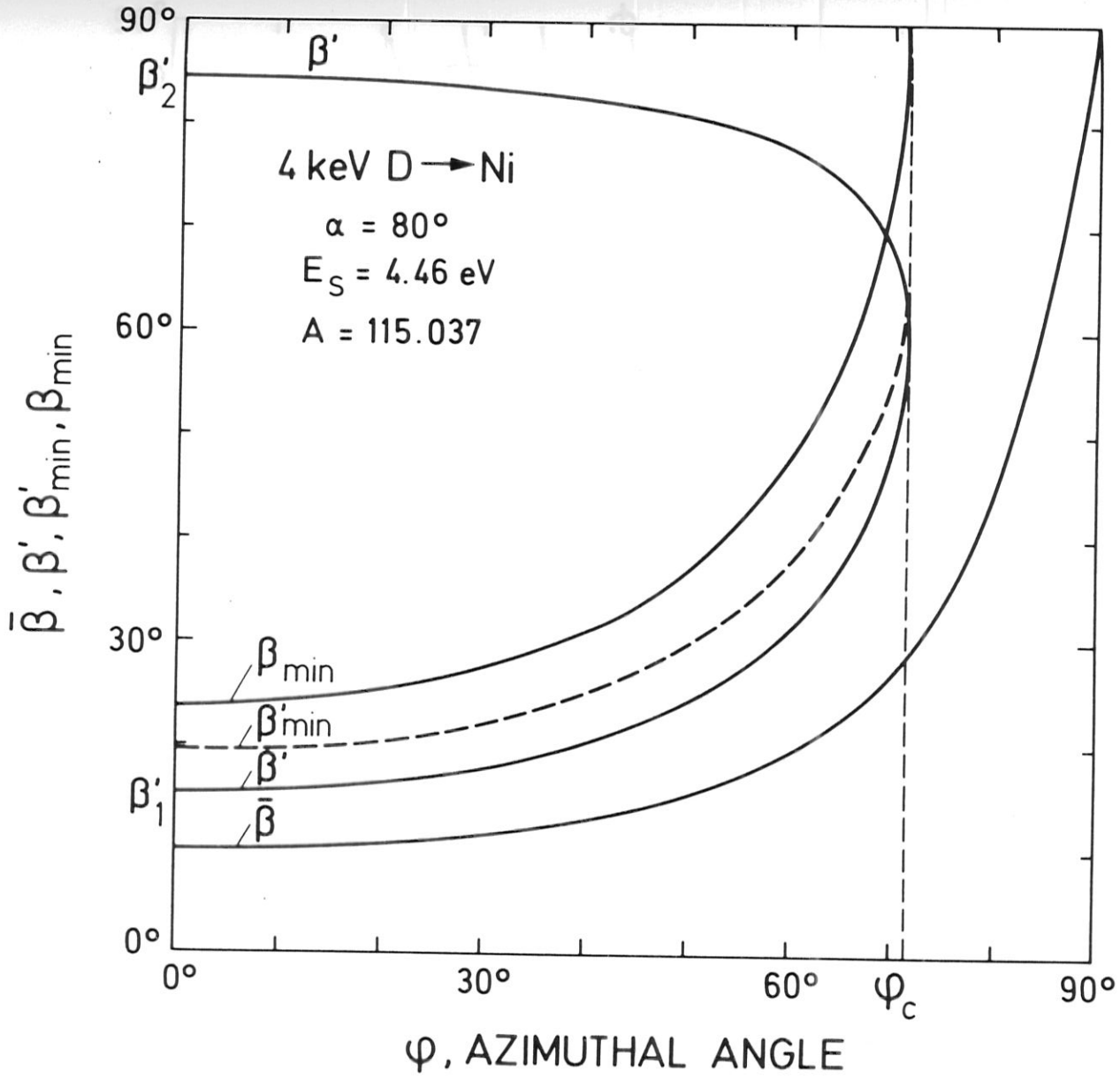
90°
β'
β'2
4 keV D → Ni
α = 80°
E_S = 4.46 eV
A = 115.037
60°
30°
β_min
β'min
β'
β̄
β'1
0°
0°
30°
60°
φc
90°
β̄, β', β'min, βmin
φ, AZIMUTHAL ANGLE

Fig. 35

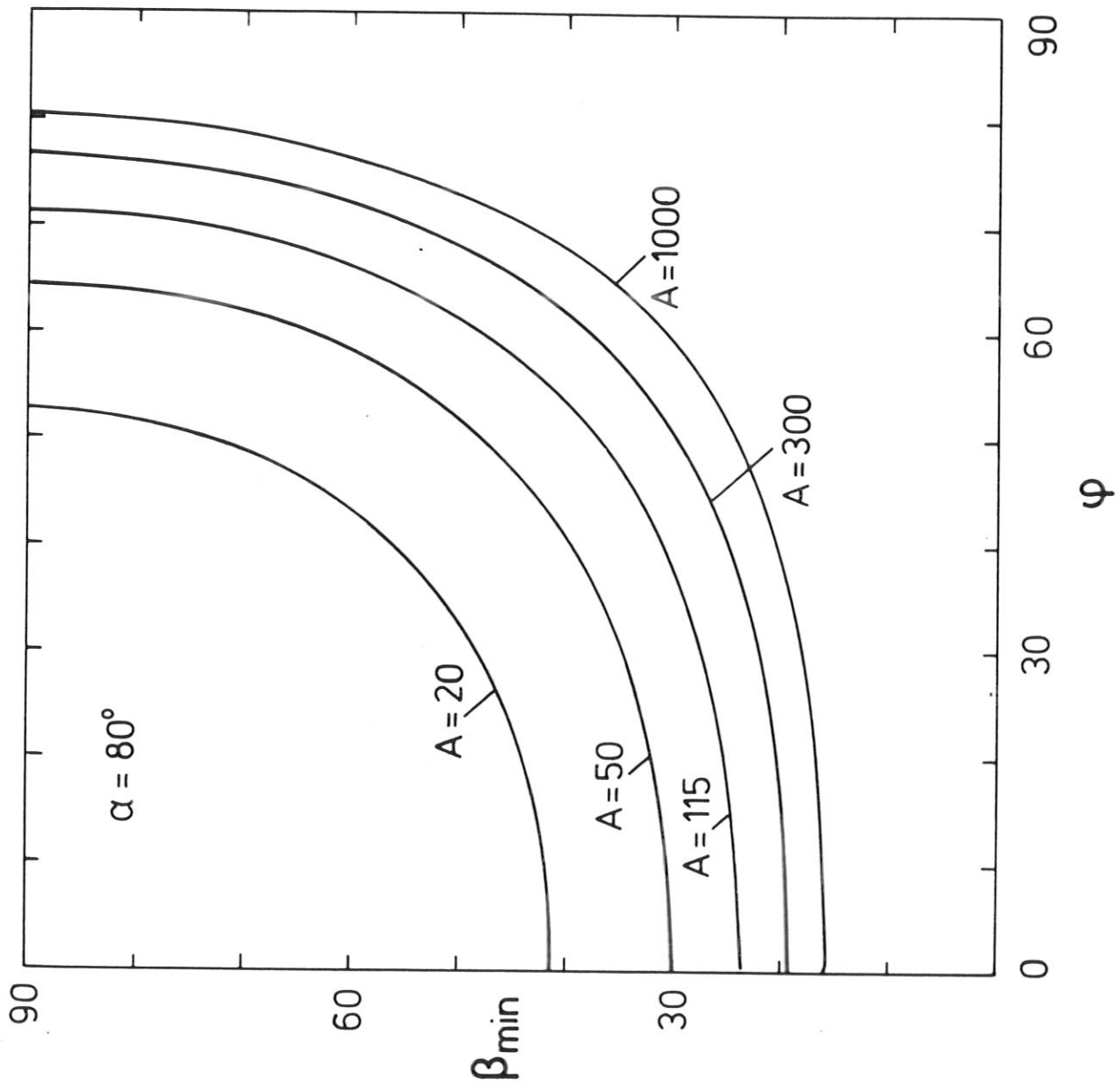
90
60
30
0
β_{min}
φ
90
60
30
$\alpha = 80°$
A = 20
A = 50
A = 115
A = 300
A = 1000

Fig. 36

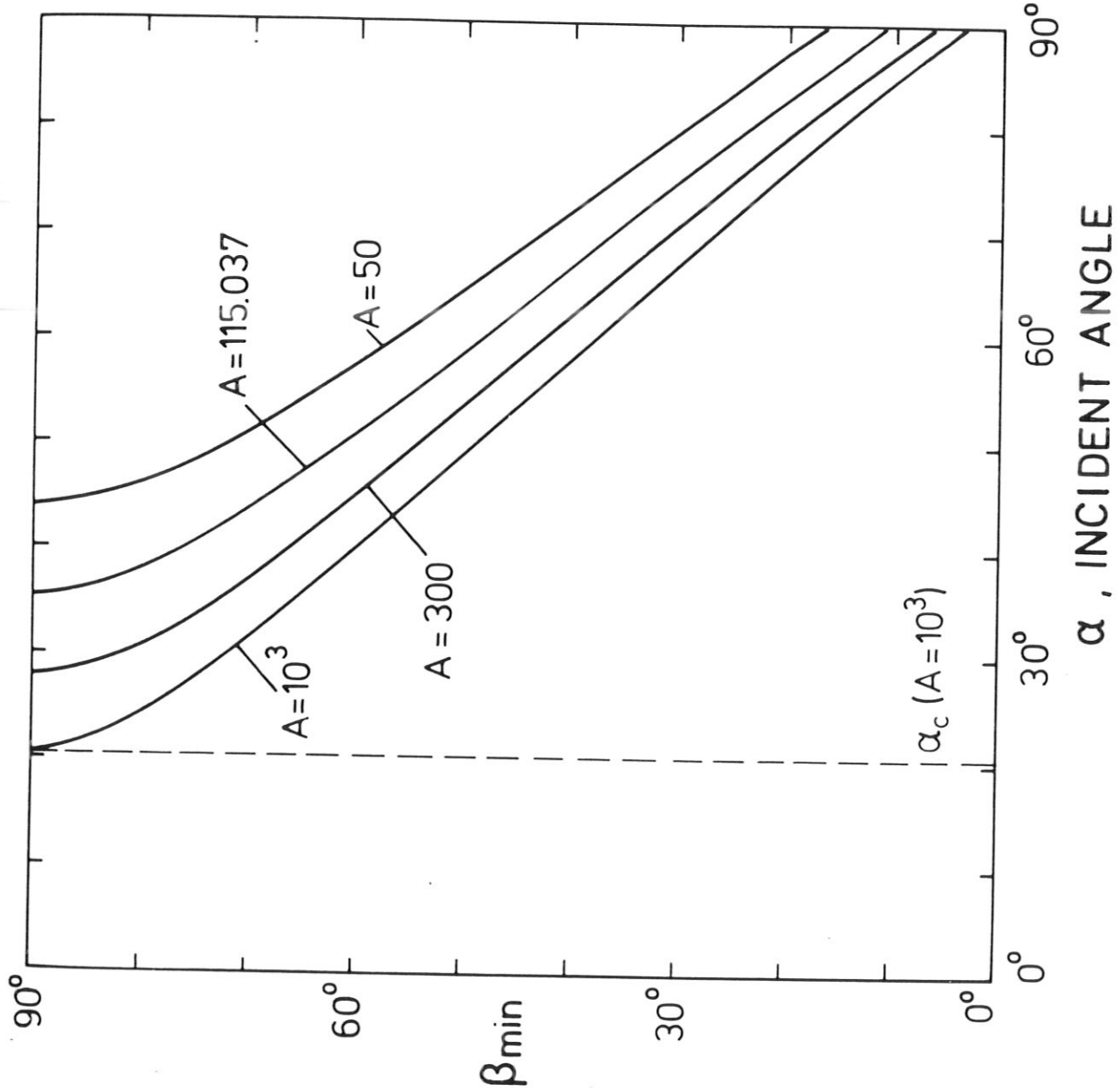
90°
60°
30°
0°
β_{min}
A=115.037
A=50
A=300
A=10³
α_c (A=10³)
0°
30°
60°
90°
α , INCIDENT ANGLE

Fig. 37

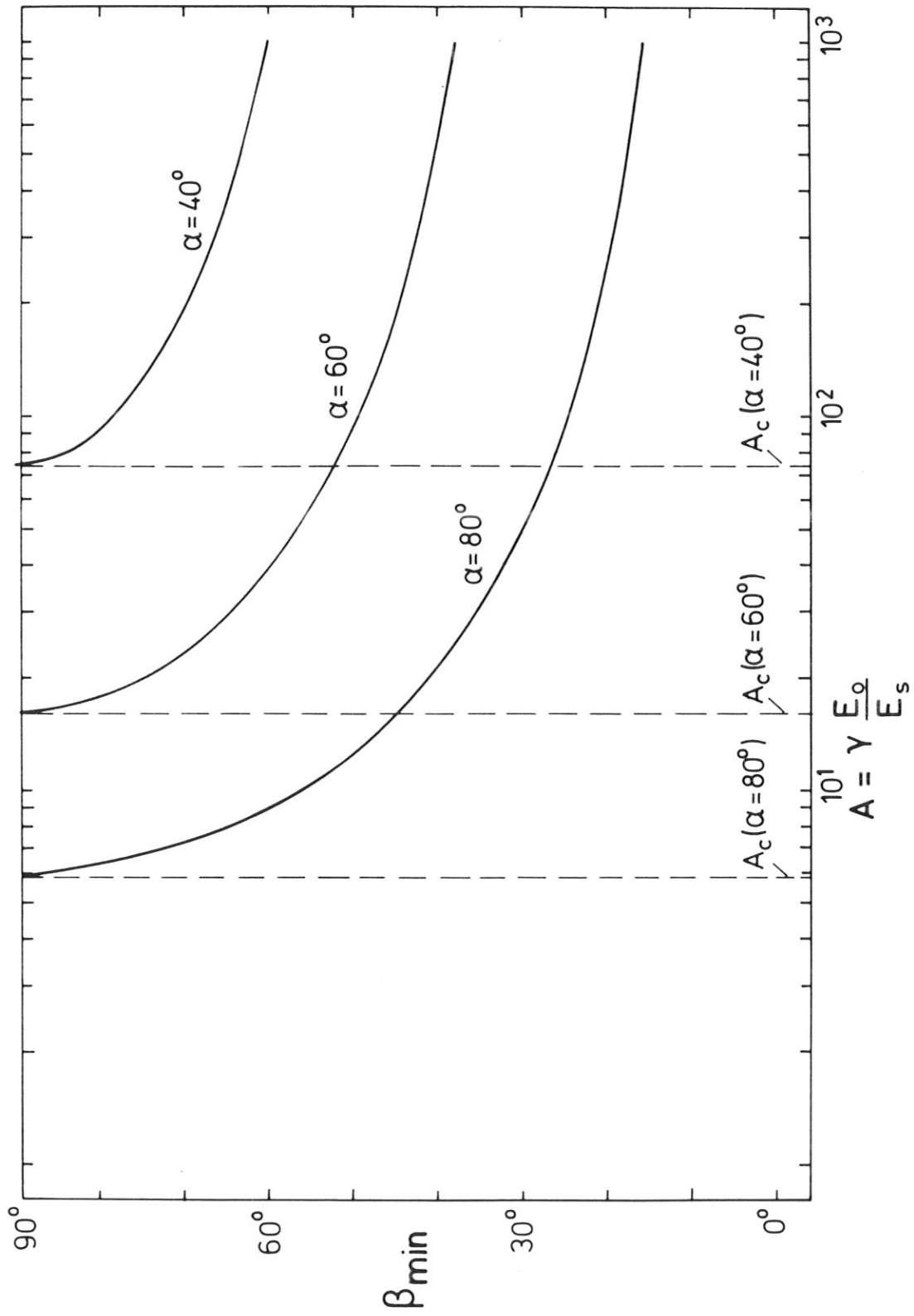
α = 40°
α = 60°
α = 80°
A_c (α = 40°)
A_c (α = 60°)
A_c (α = 80°)
β_min
90°
60°
30°
0°
10^1
10^2
10^3
A = γ E_o / E_s

Fig. 38

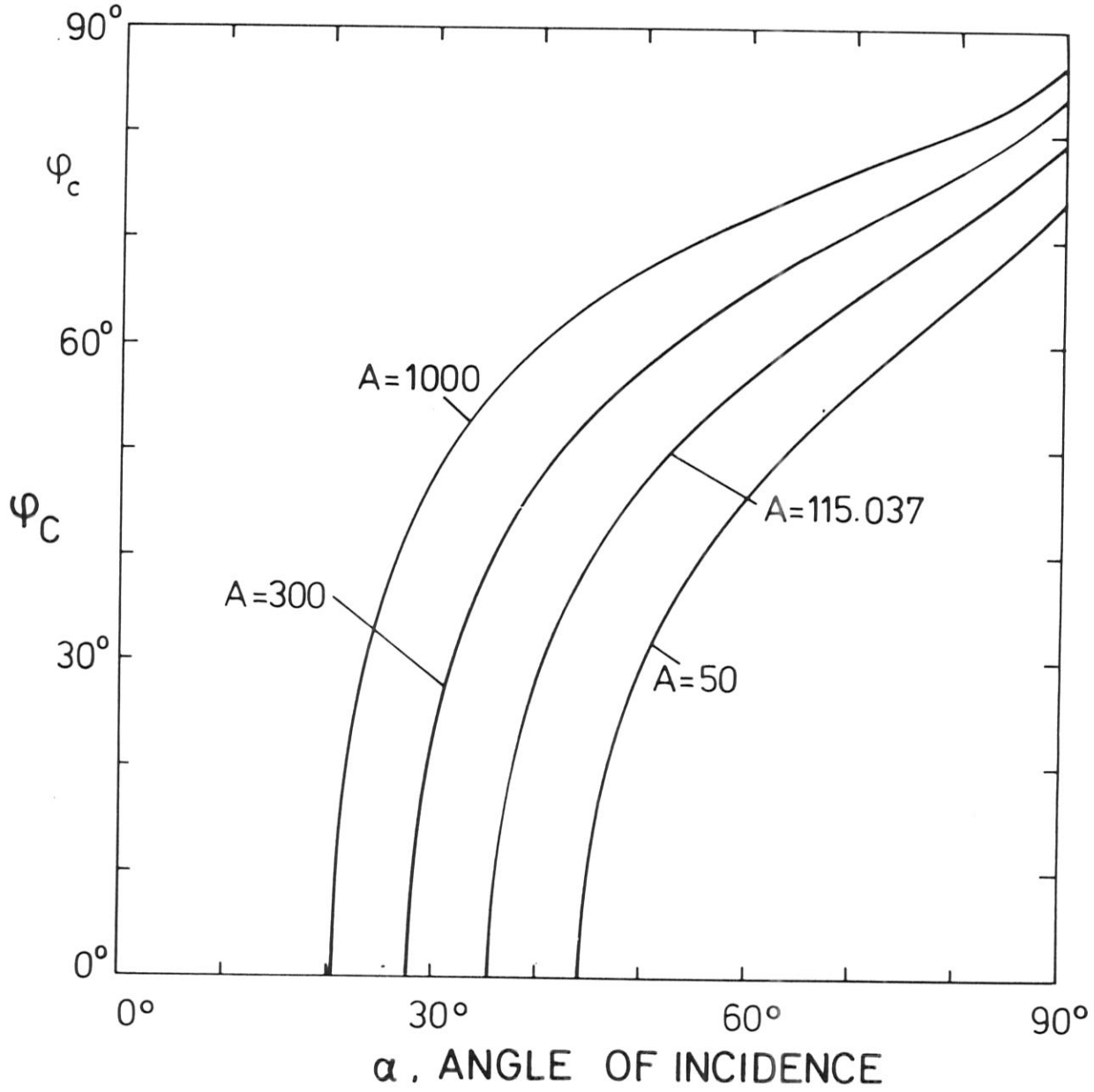
90°
60°
30°
0°
φ_c
φ_C
A=1000
A=300
A=115.037
A=50
0°
30°
60°
90°
α , ANGLE OF INCIDENCE

Fig. 39

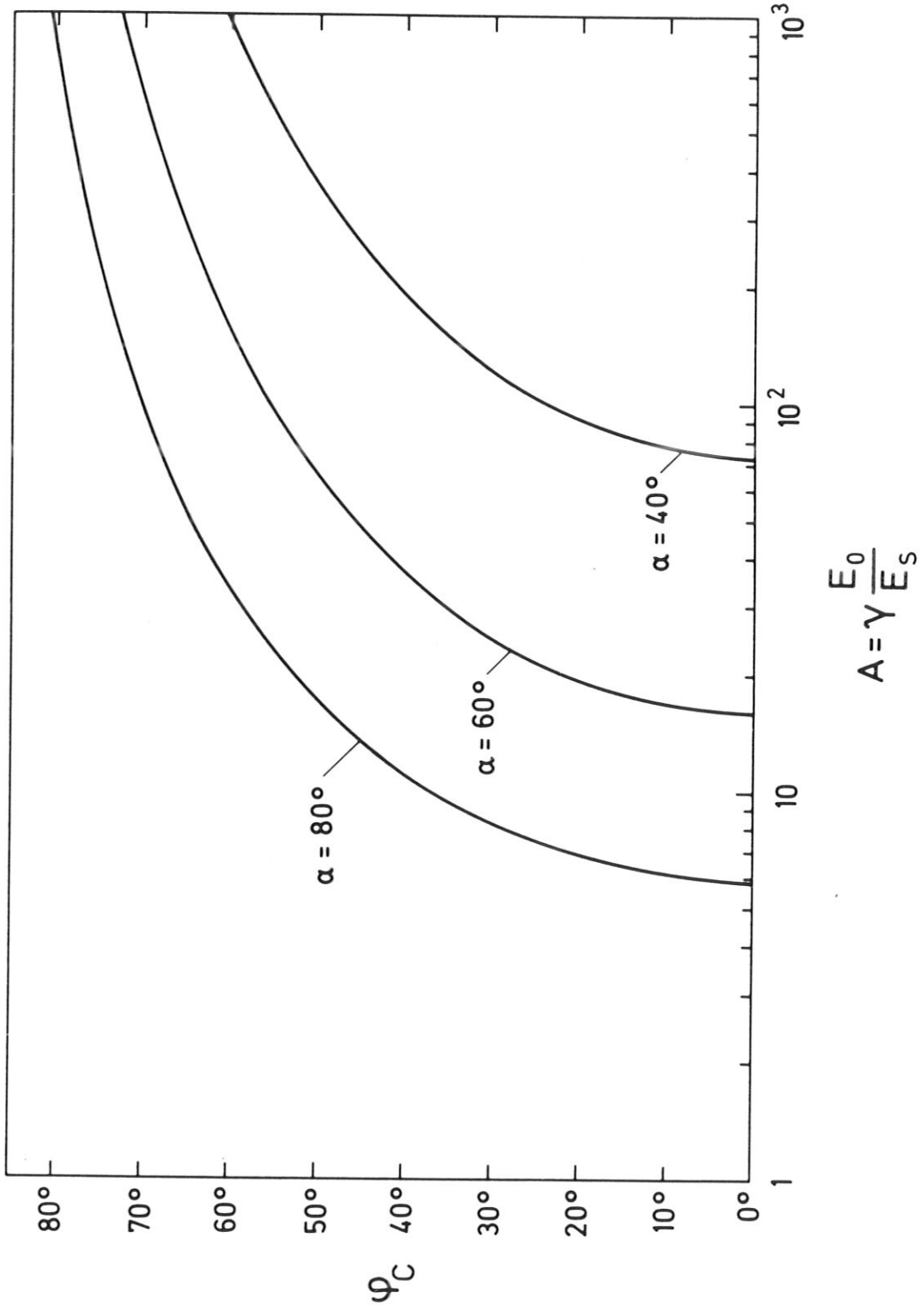
80°
70°
60°
50°
40°
30°
20°
10°
0°
φ_C
1
10
10^2
10^3
$A = \gamma \frac{E_0}{E_S}$
α = 80°
α = 60°
α = 40°

Fig. 40

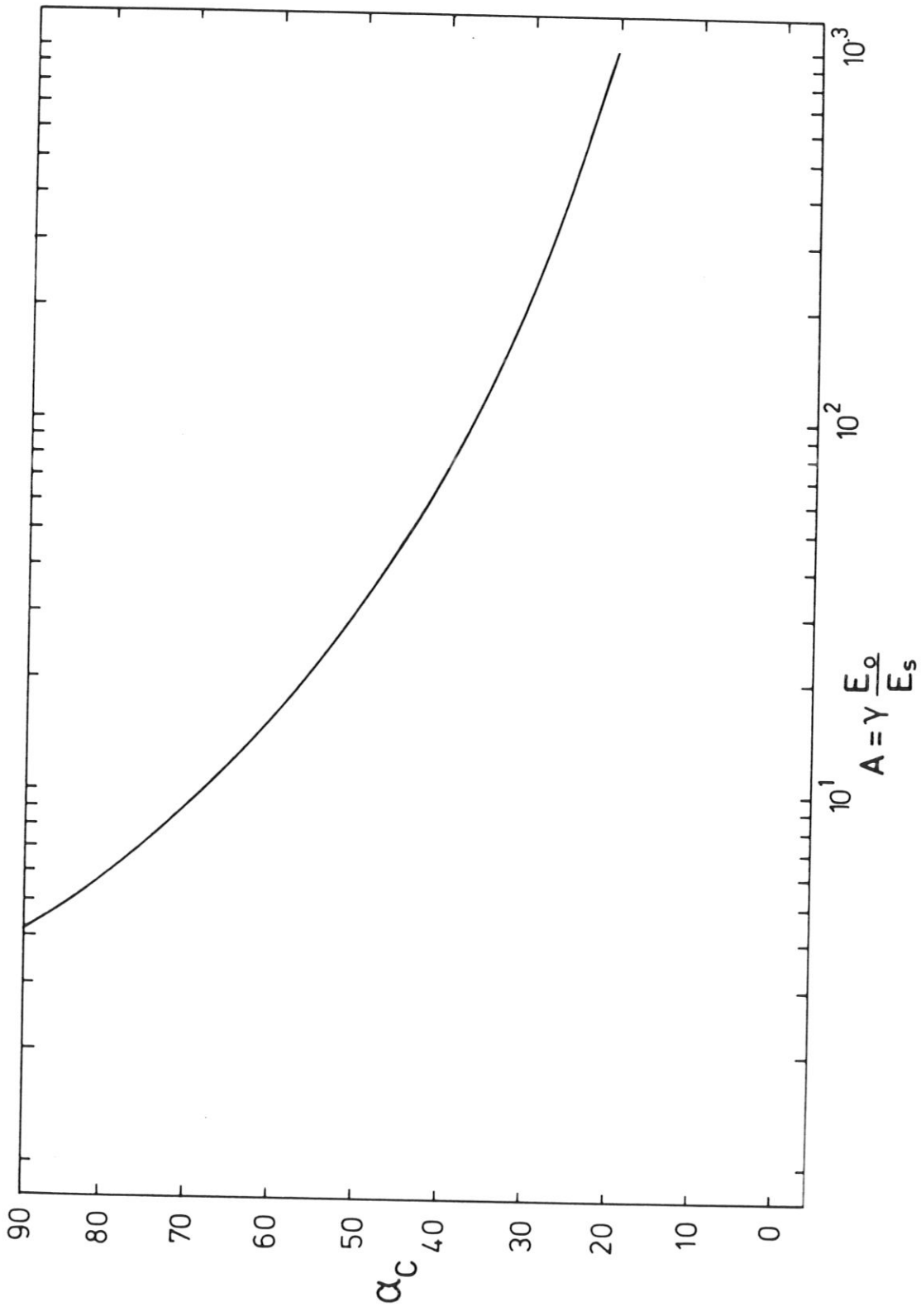

Fig. 41

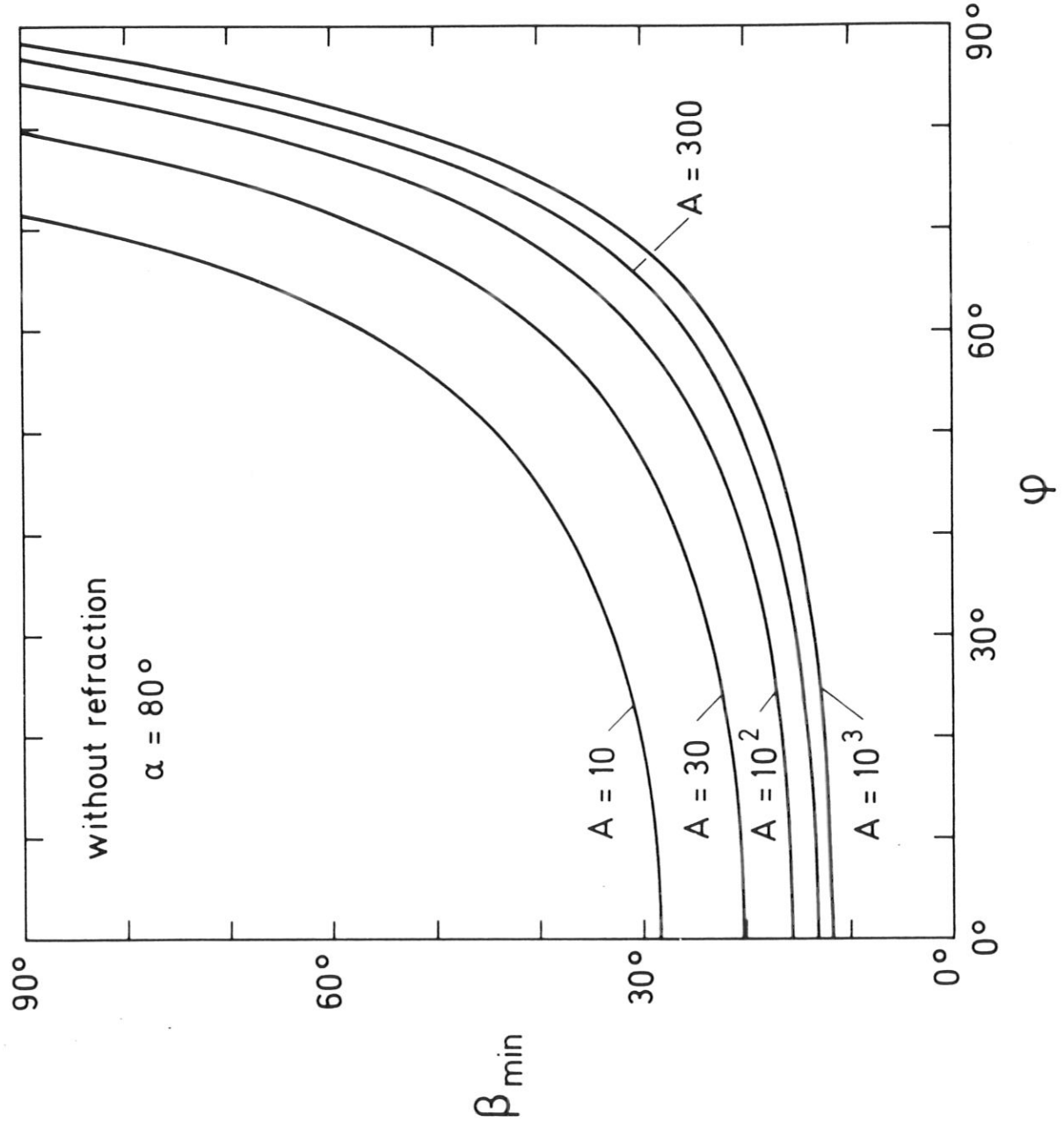
without refraction
α = 80°
A = 10
A = 30
A = 10²
A = 10³
A = 300
90°
60°
30°
0°
β min
φ

Fig. 42

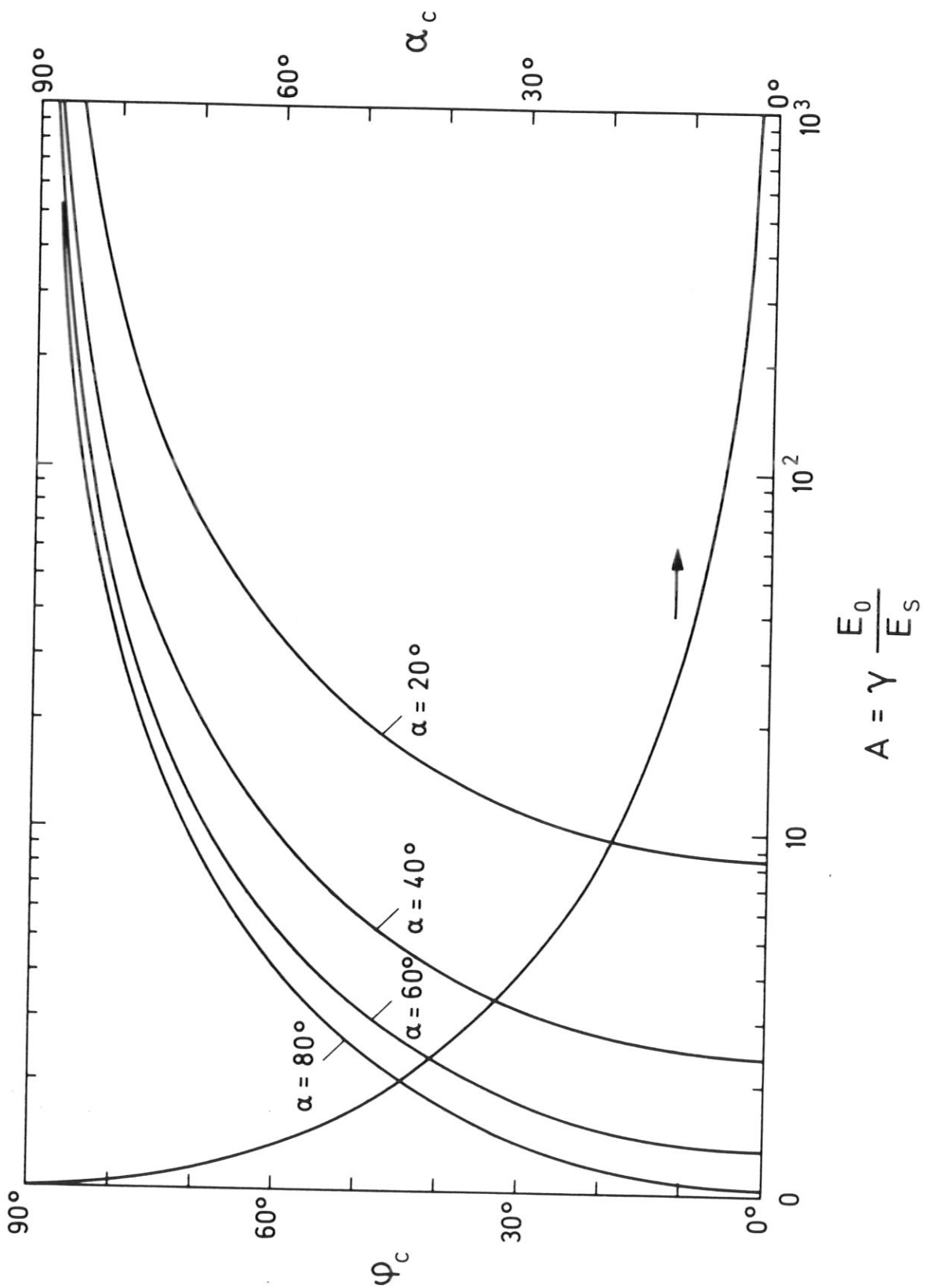
90°
60°
30°
0°
α_c
10^3
10^2
10
0
φ_c
$\alpha = 80°$
$\alpha = 60°$
$\alpha = 40°$
$\alpha = 20°$
$A = \gamma \frac{E_0}{E_s}$

Fig. 43

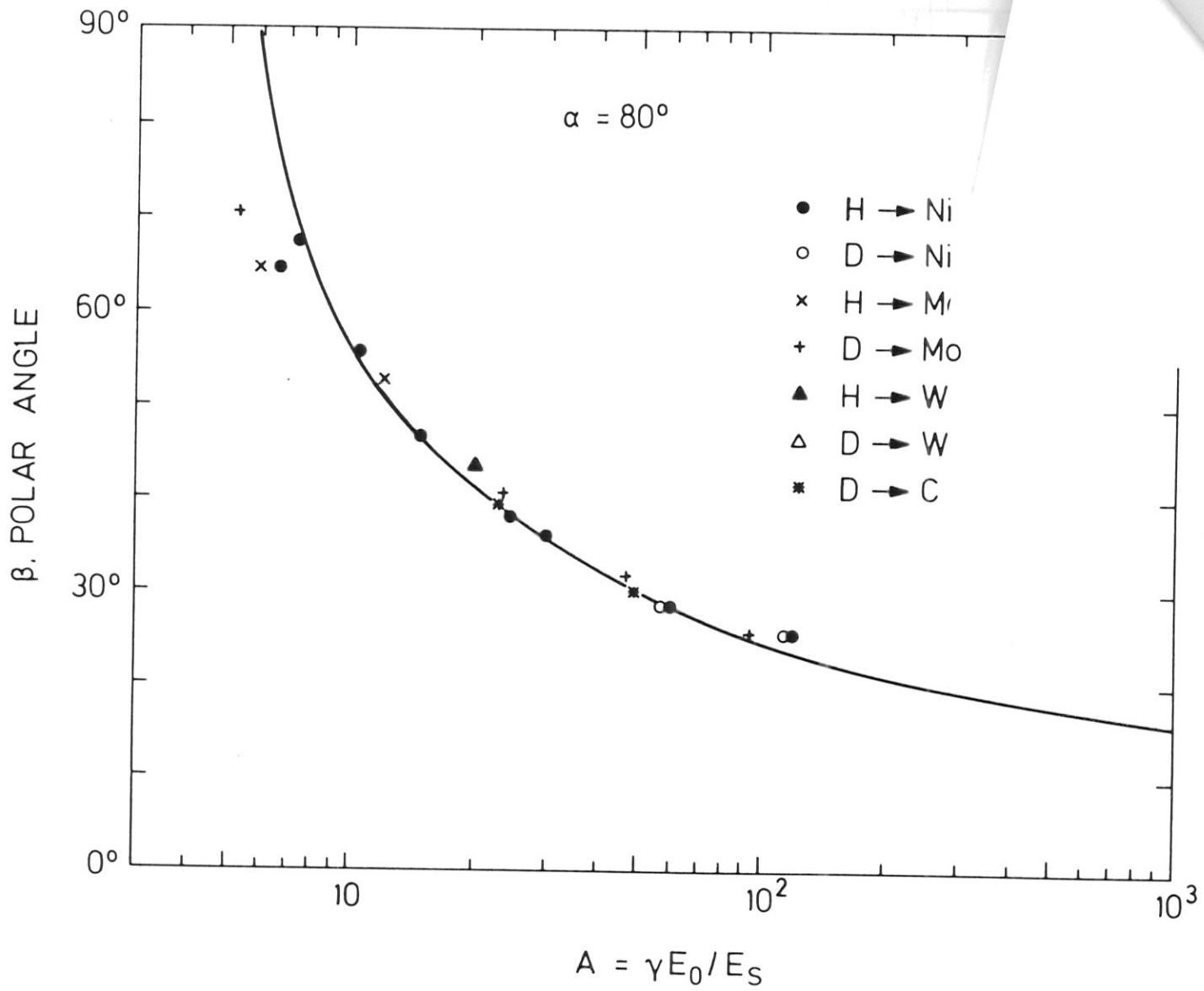
90°
60°
30°
0°
β, POLAR ANGLE
α = 80°
H → Ni
D → Ni
H → M
D → Mo
H → W
D → W
D → C
10
10²
10³
A = γE₀/Eₛ

Fig. 44

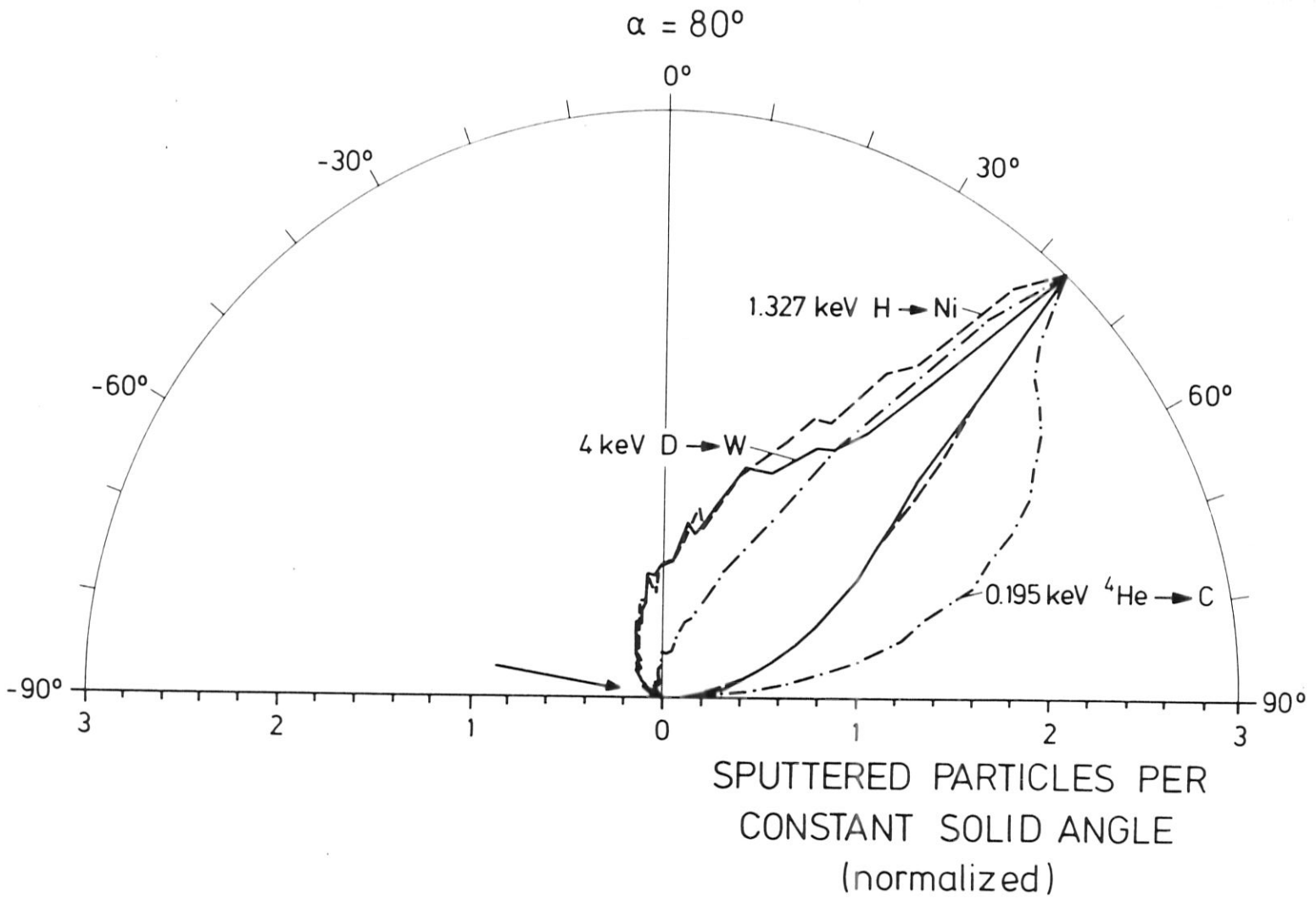
α = 80°
0°
-30°
30°
-60°
60°
-90°
90°
1.327 keV H → Ni
4 keV D → W
0.195 keV ⁴He → C
3
2
1
0
1
2
3
SPUTTERED PARTICLES PER
CONSTANT SOLID ANGLE
(normalized)

Fig. 45

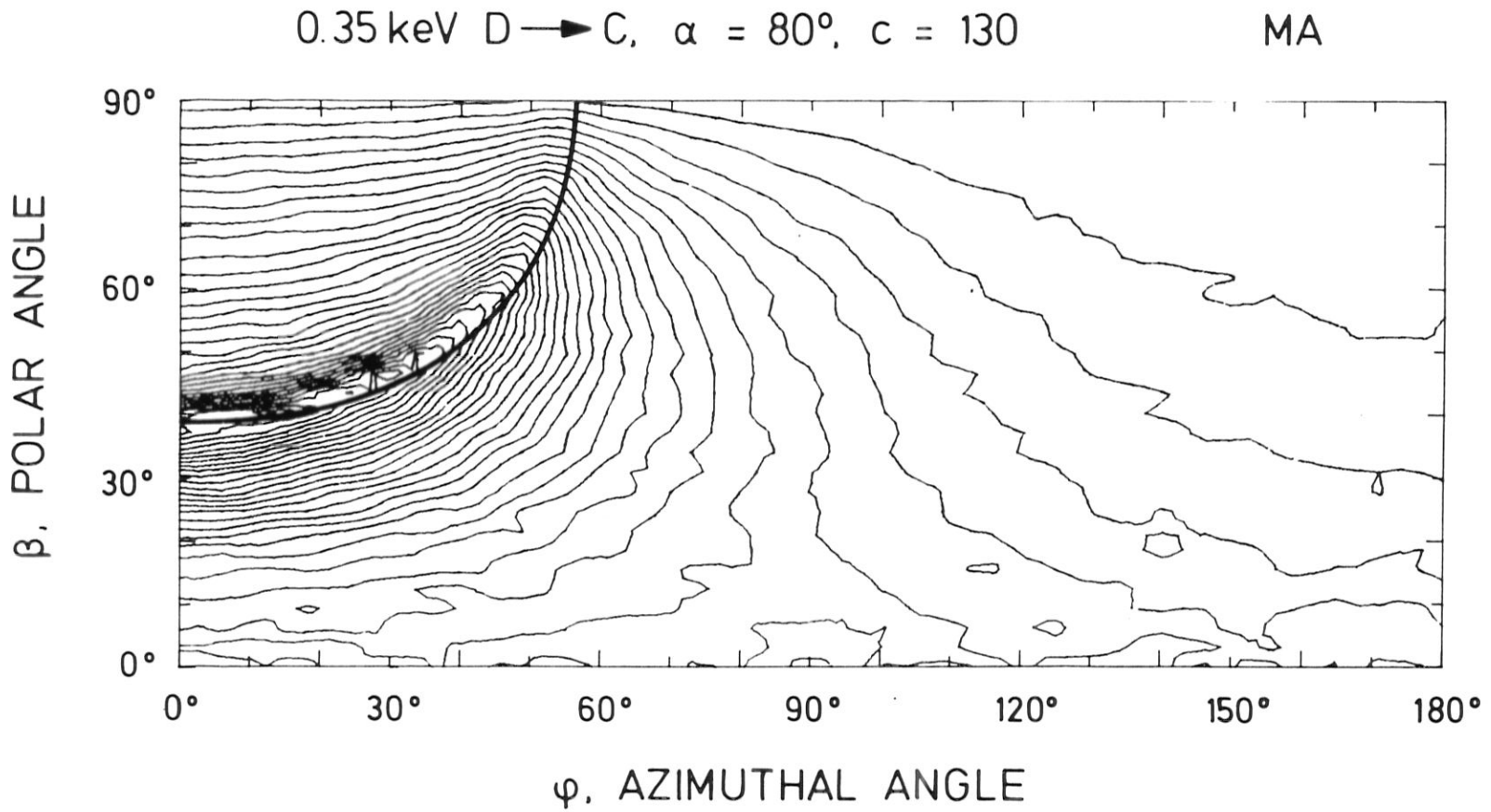
0.35 keV D → C, α = 80°, c = 130
MA
90°
60°
30°
0°
β, POLAR ANGLE
0°
30°
60°
90°
120°
150°
180°
φ, AZIMUTHAL ANGLE

Fig. 46a

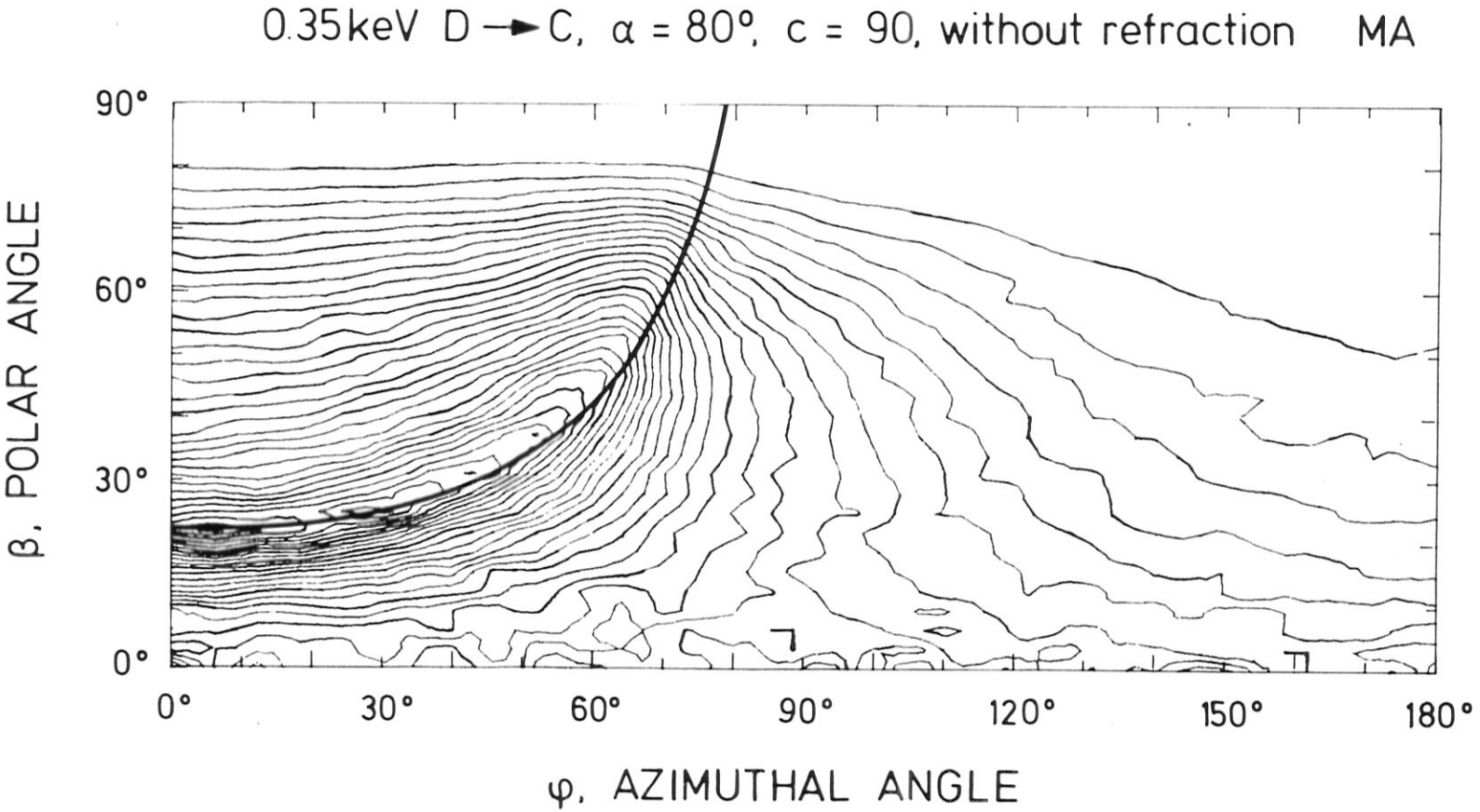
0.35keV D → C, α = 80°, c = 90, without refraction MA
β, POLAR ANGLE
90°
60°
30°
0°
0°
30°
60°
90°
120°
150°
180°
φ, AZIMUTHAL ANGLE

Fig. 46b

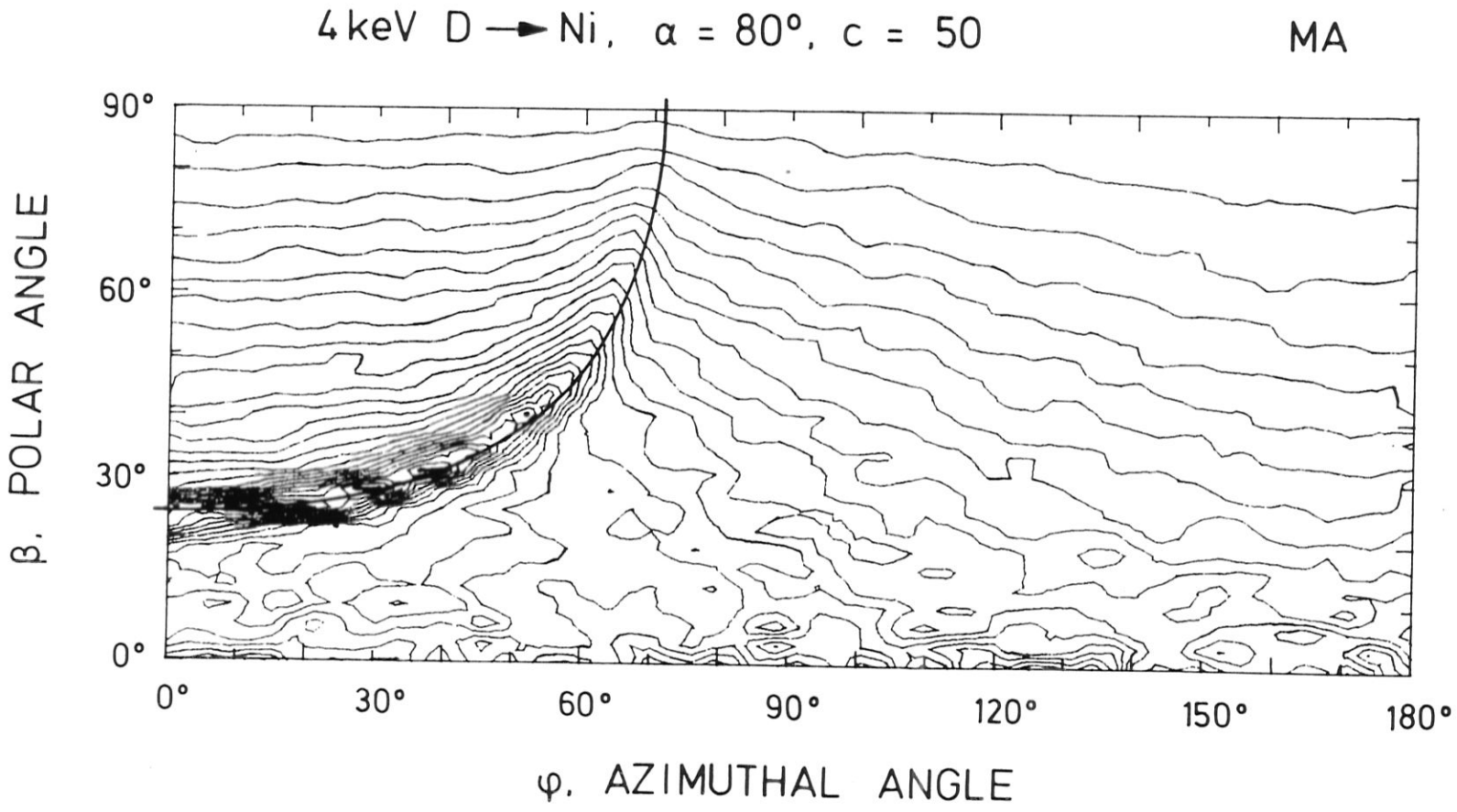
4 keV D → Ni, α = 80°, c = 50
MA
β, POLAR ANGLE
90°
60°
30°
0°
0°
30°
60°
90°
120°
150°
180°
φ, AZIMUTHAL ANGLE

Fig. 47

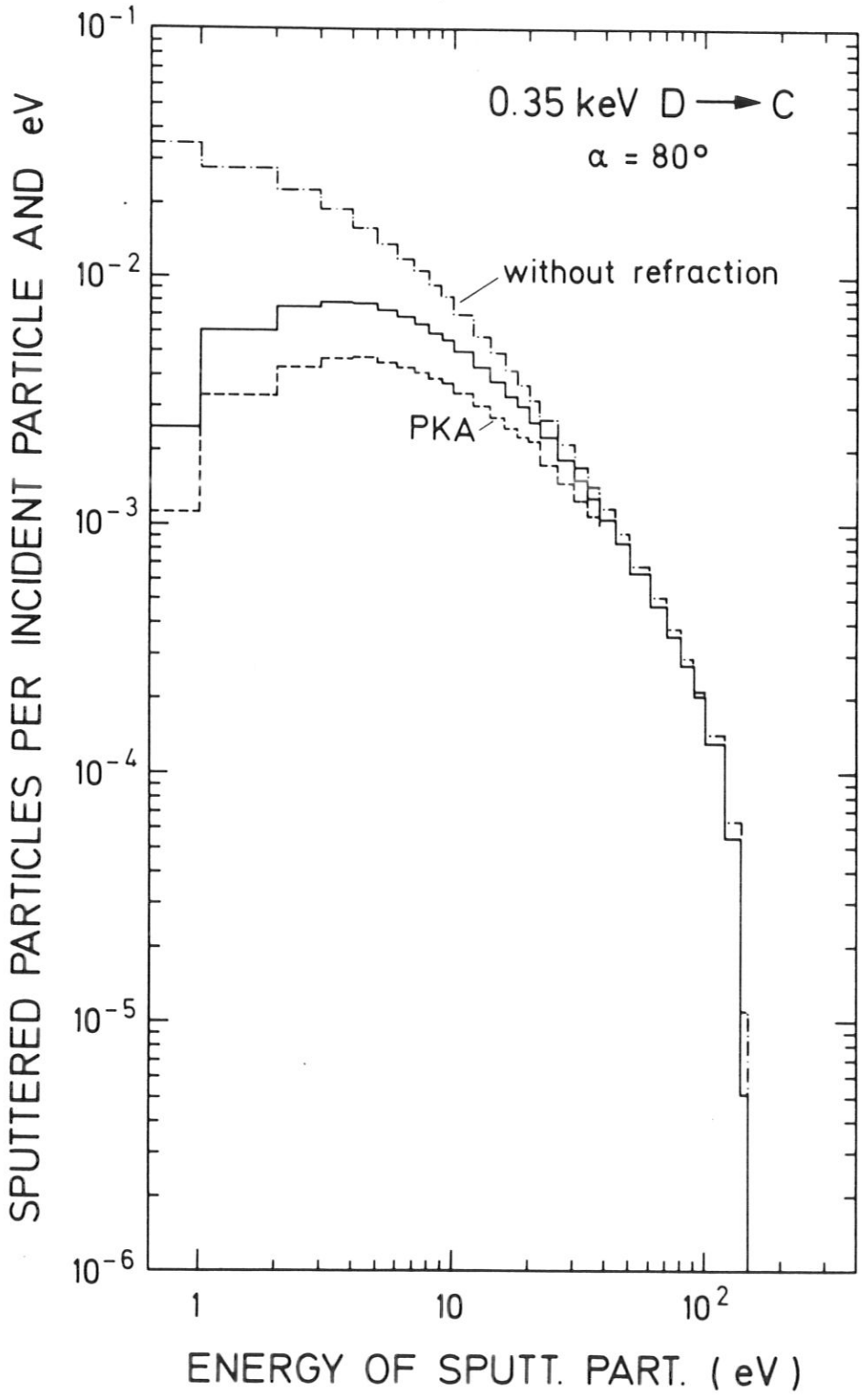
0.35 keV D → C
α = 80°
without refraction
PKA
SPUTTERED PARTICLES PER INCIDENT PARTICLE AND eV
ENERGY OF SPUTT. PART. (eV)
10^-1
10^-2
10^-3
10^-4
10^-5
10^-6
1
10
10^2

Fig. 48

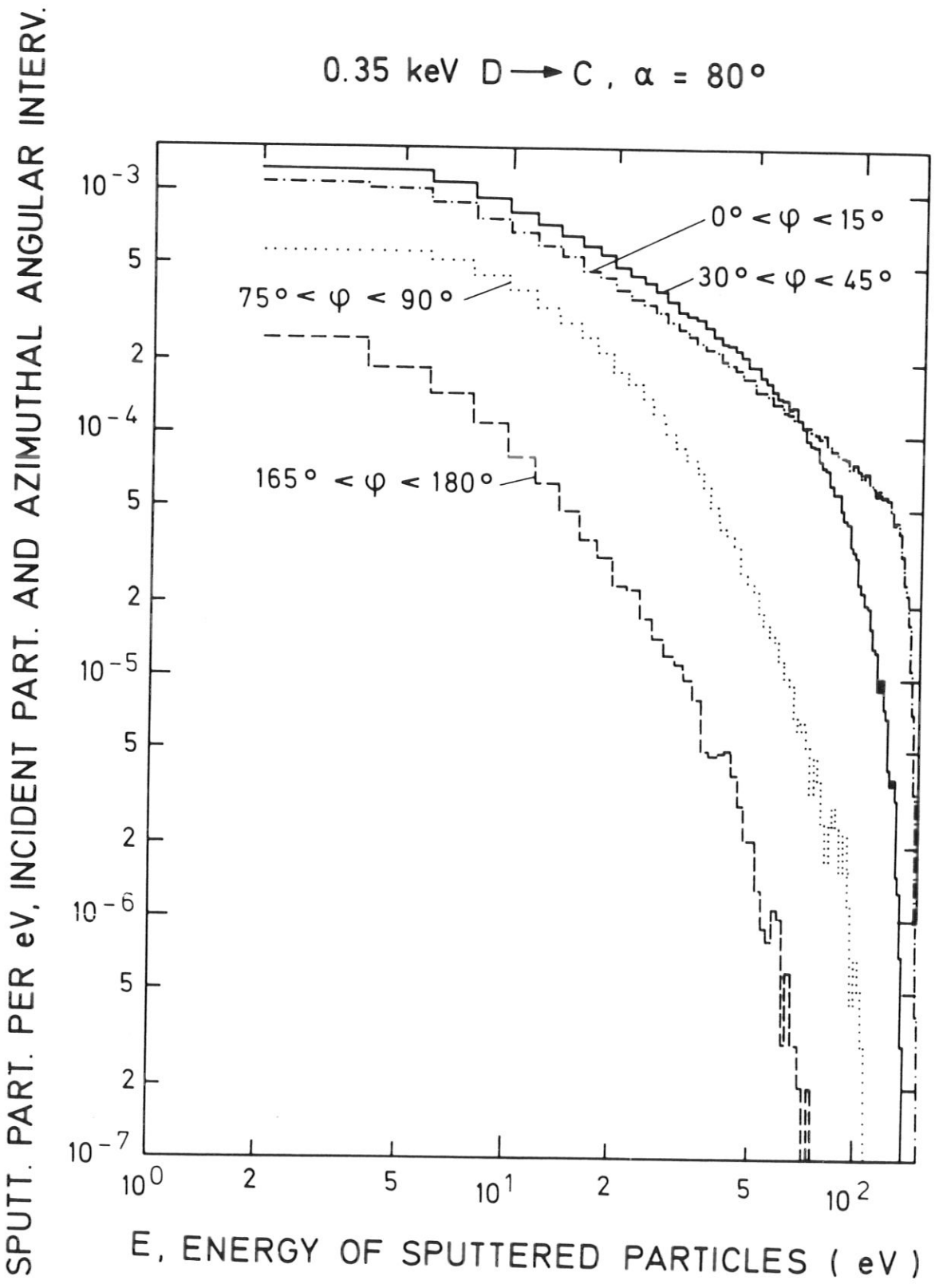
0.35 keV D → C , α = 80°
SPUTT. PART. PER eV, INCIDENT PART. AND AZIMUTHAL ANGULAR INTERV.
E, ENERGY OF SPUTTERED PARTICLES (eV)
0° < φ < 15°
30° < φ < 45°
75° < φ < 90°
165° < φ < 180°
10^-3
5
2
10^-4
5
2
10^-5
5
2
10^-6
5
2
10^-7
10^0
2
5
10^1
2
5
10^2

Fig. 49

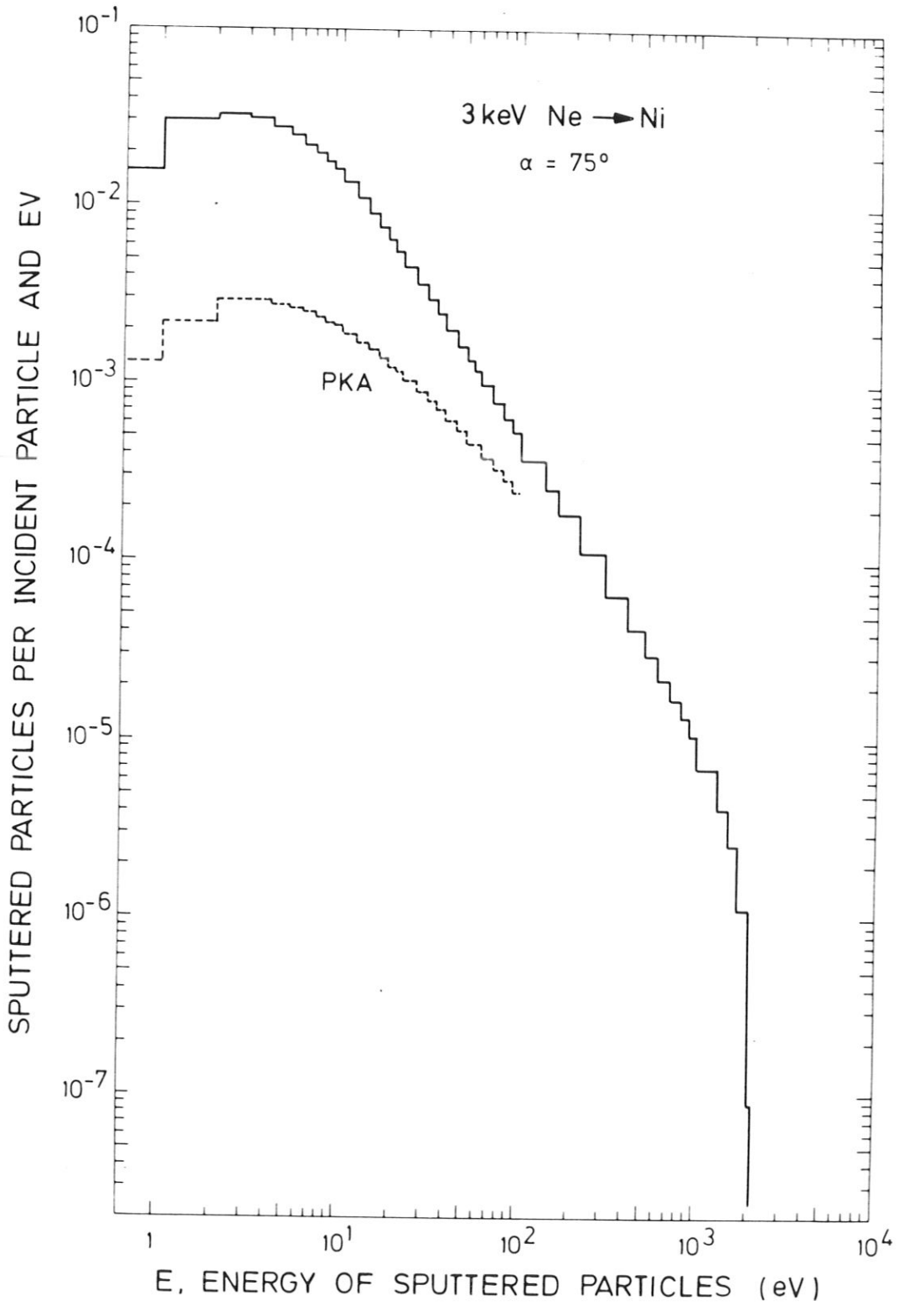
3 keV Ne → Ni
α = 75°
PKA
SPUTTERED PARTICLES PER INCIDENT PARTICLE AND EV
E, ENERGY OF SPUTTERED PARTICLES (eV)
10^-1
10^-2
10^-3
10^-4
10^-5
10^-6
10^-7
1
10^1
10^2
10^3
10^4

Fig. 50

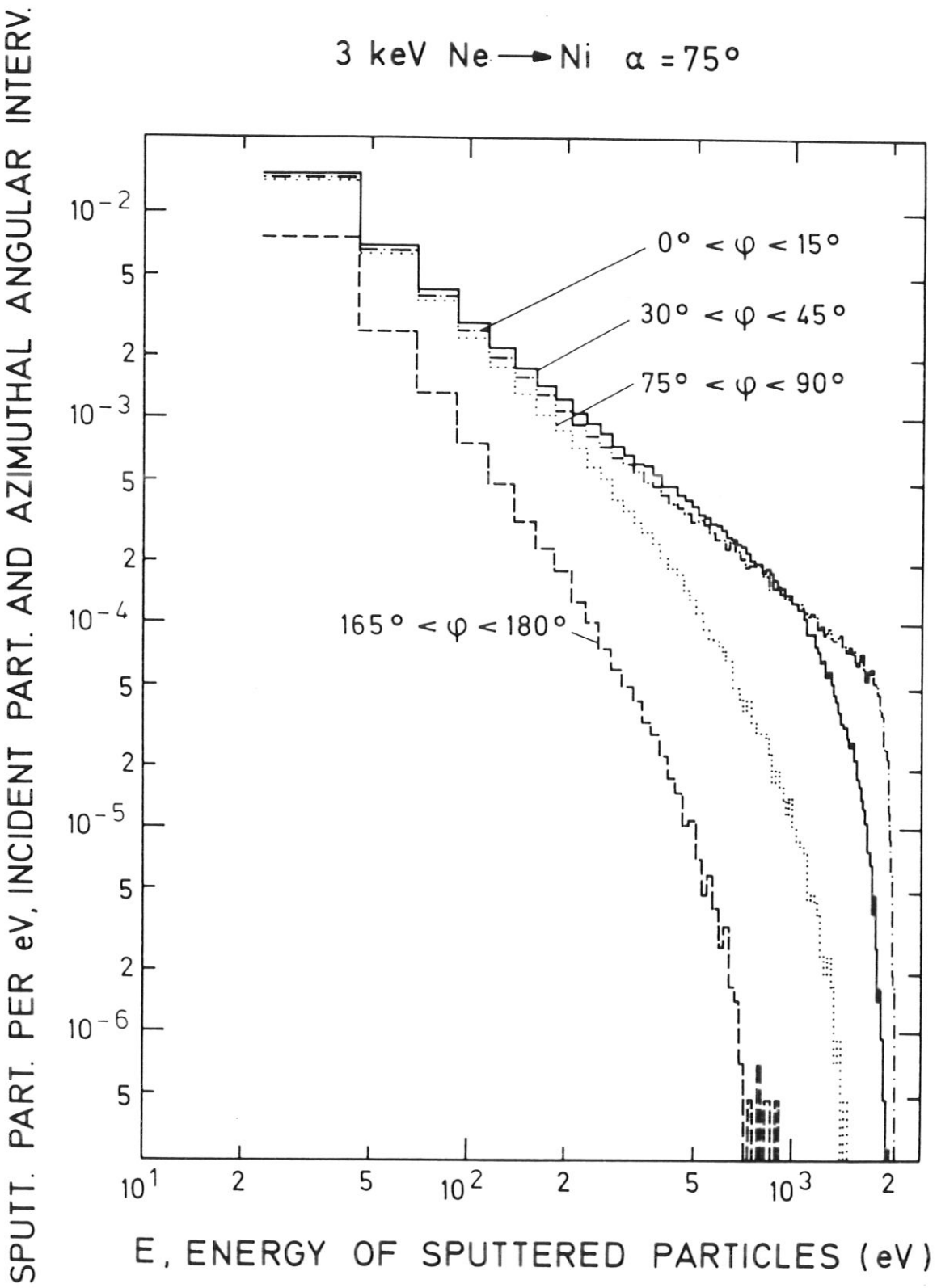
3 keV Ne → Ni α = 75°
SPUTT. PART. PER eV, INCIDENT PART. AND AZIMUTHAL ANGULAR INTERV.
0° < φ < 15°
30° < φ < 45°
75° < φ < 90°
165° < φ < 180°
E, ENERGY OF SPUTTERED PARTICLES (eV)

Fig. 51

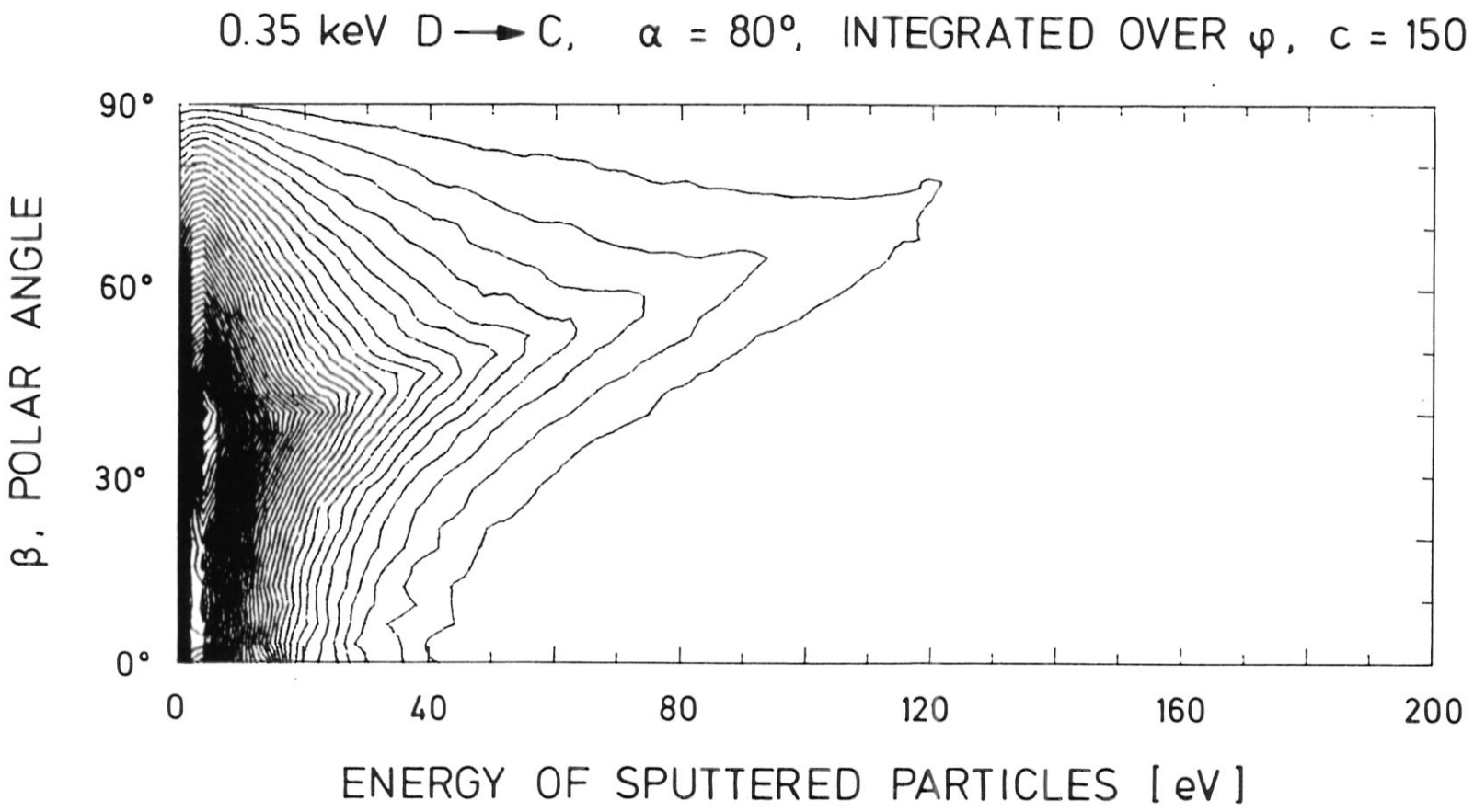
0.35 keV D ⟶ C, α = 80°, INTEGRATED OVER φ, c = 150
β, POLAR ANGLE
90°
60°
30°
0°
0
40
80
120
160
200
ENERGY OF SPUTTERED PARTICLES [eV]

Fig. 52a

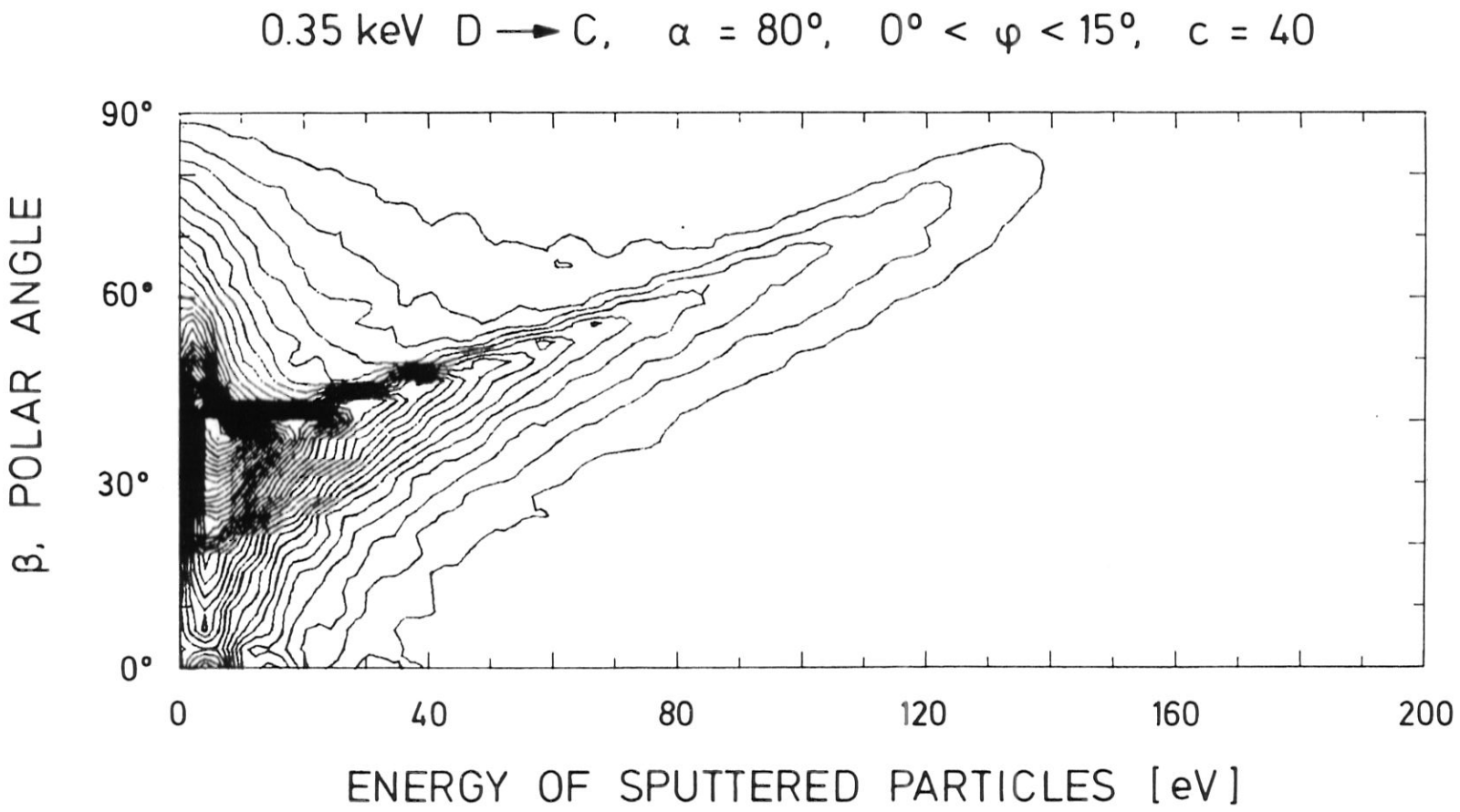
0.35 keV D → C, α = 80°, 0° < φ < 15°, c = 40
β, POLAR ANGLE
90°
60°
30°
0°
0
40
80
120
160
200
ENERGY OF SPUTTERED PARTICLES [eV]

Fig. 52b

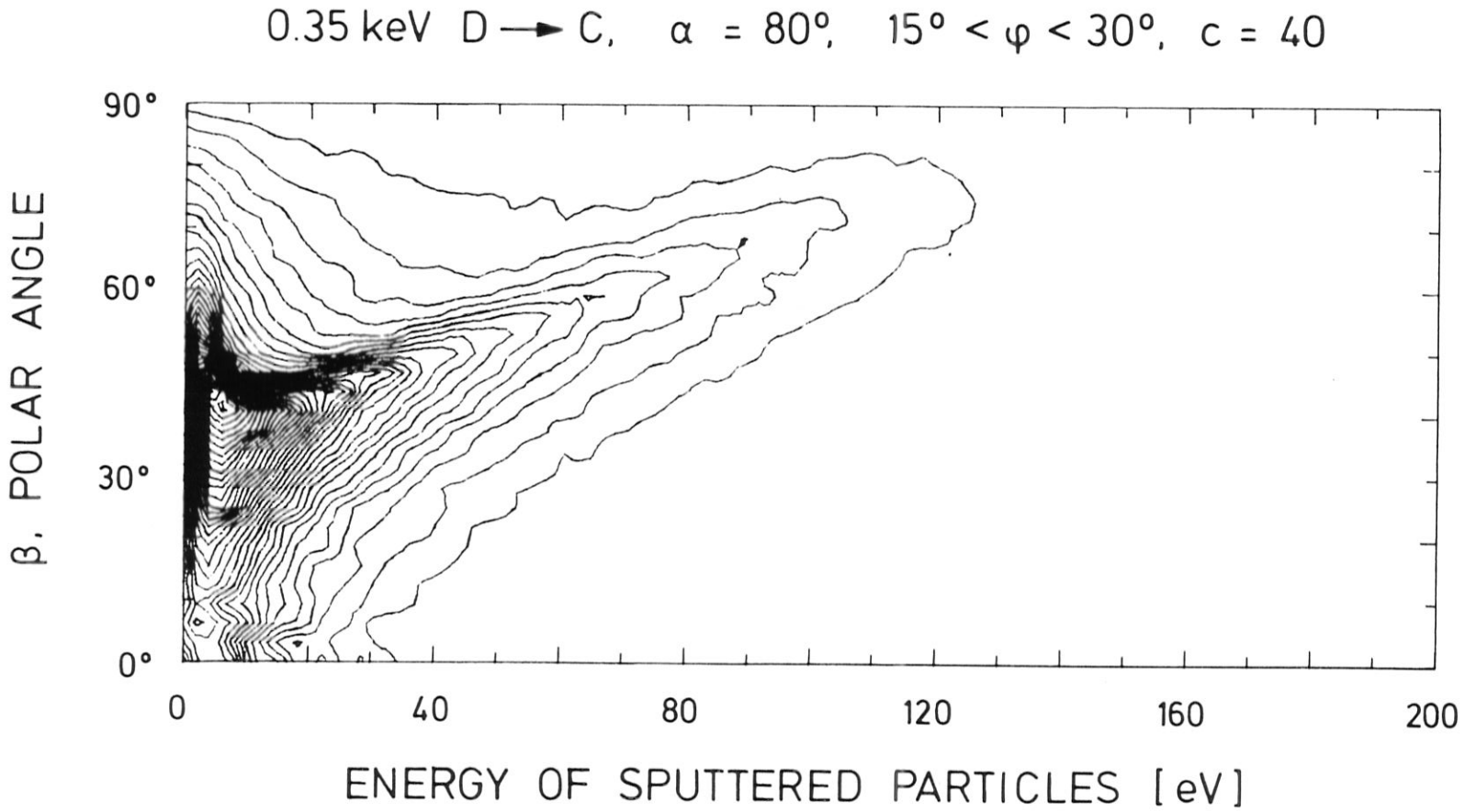
0.35 keV D → C, α = 80°, 15° < φ < 30°, c = 40
β, POLAR ANGLE
90°
60°
30°
0°
0
40
80
120
160
200
ENERGY OF SPUTTERED PARTICLES [eV]

Fig. 52c

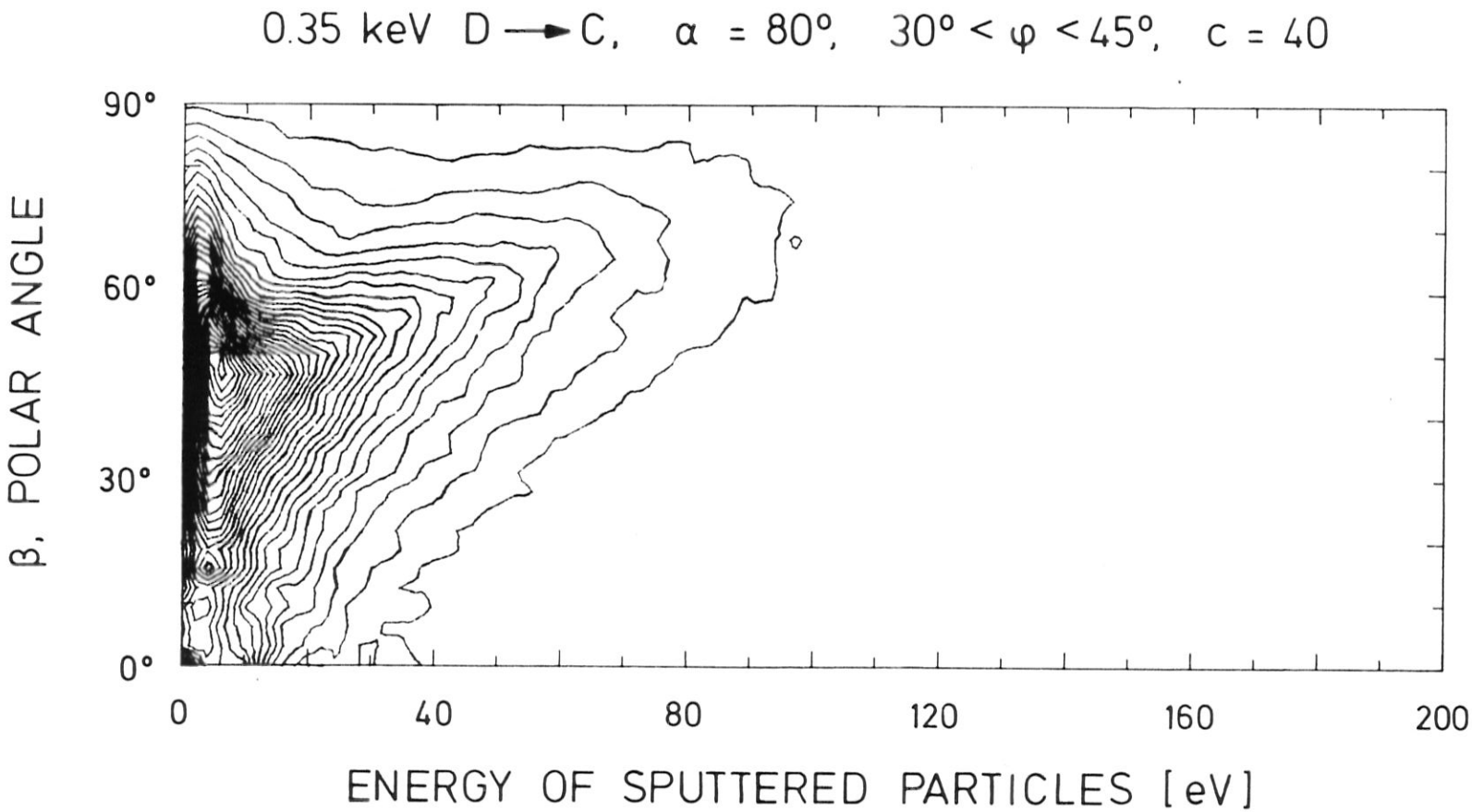
0.35 keV D → C, α = 80°, 30° < φ < 45°, c = 40
β, POLAR ANGLE
90°
60°
30°
0°
0
40
80
120
160
200
ENERGY OF SPUTTERED PARTICLES [eV]

Fig. 52d

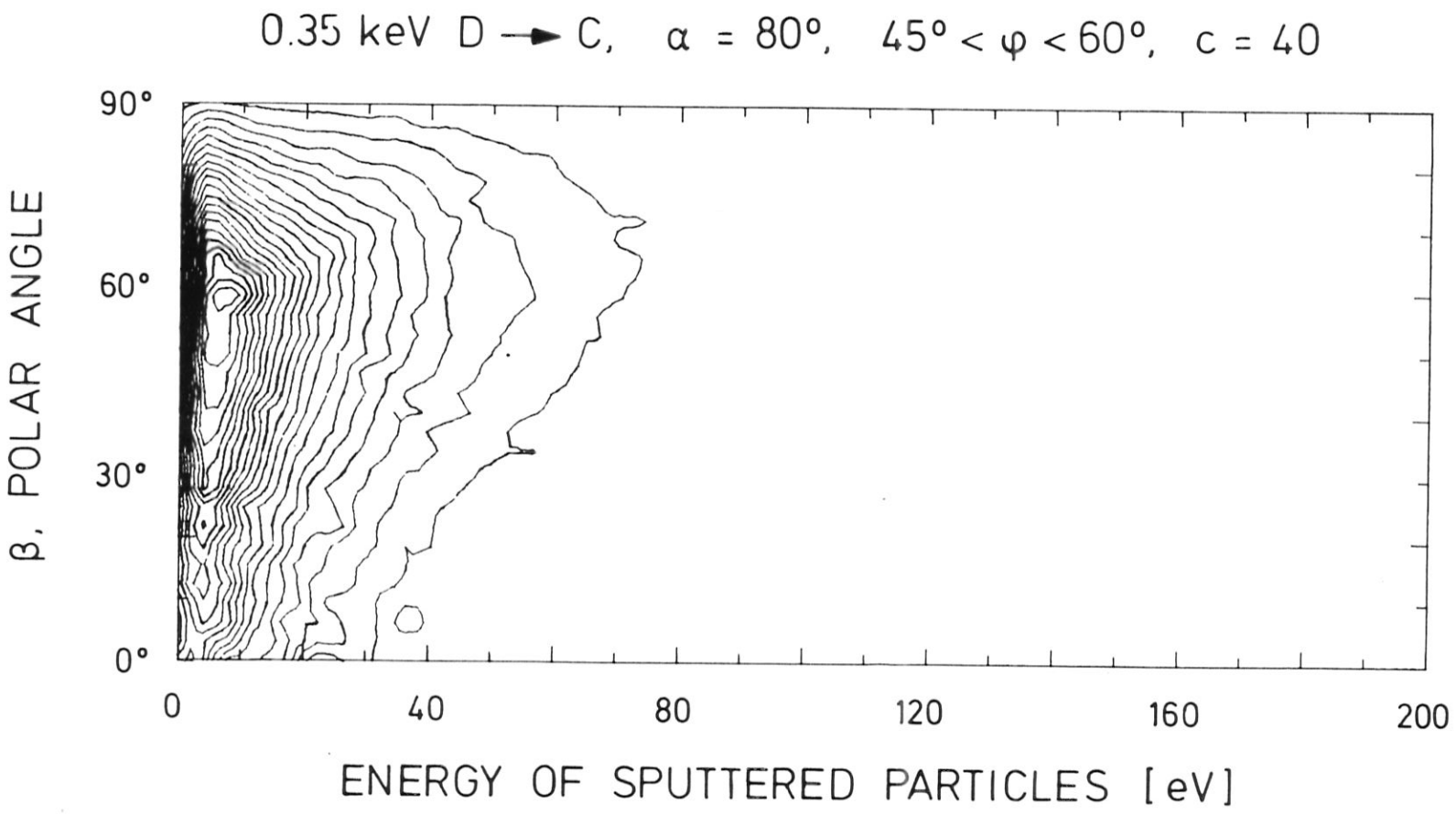
0.35 keV D → C, α = 80°, 45° < φ < 60°, c = 40
β, POLAR ANGLE
90°
60°
30°
0°
0
40
80
120
160
200
ENERGY OF SPUTTERED PARTICLES [eV]

Fig. 52e

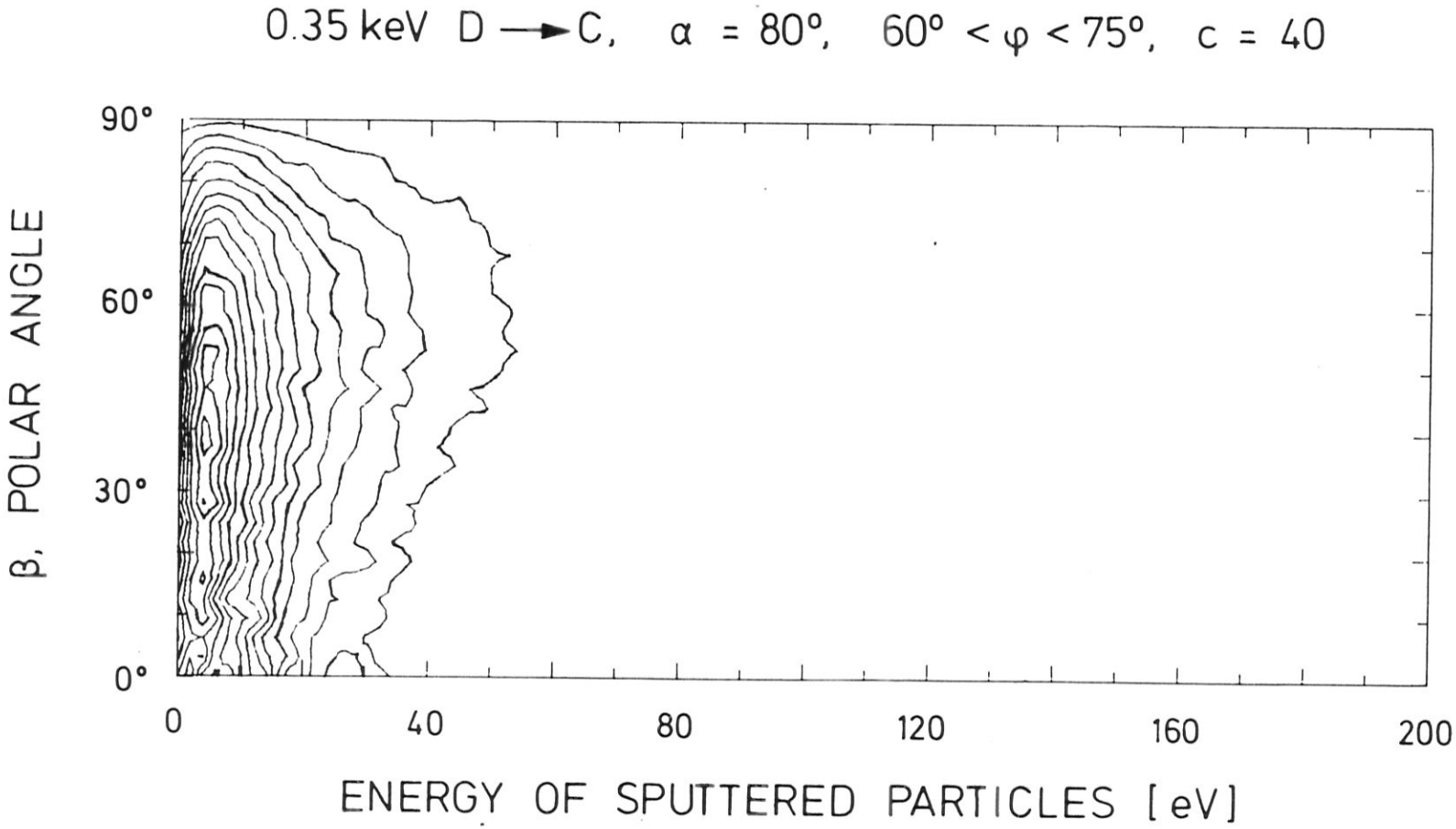
0.35 keV D → C, α = 80°, 60° < φ < 75°, c = 40
β, POLAR ANGLE
90°
60°
30°
0°
0
40
80
120
160
200
ENERGY OF SPUTTERED PARTICLES [eV]

Fig. 52f

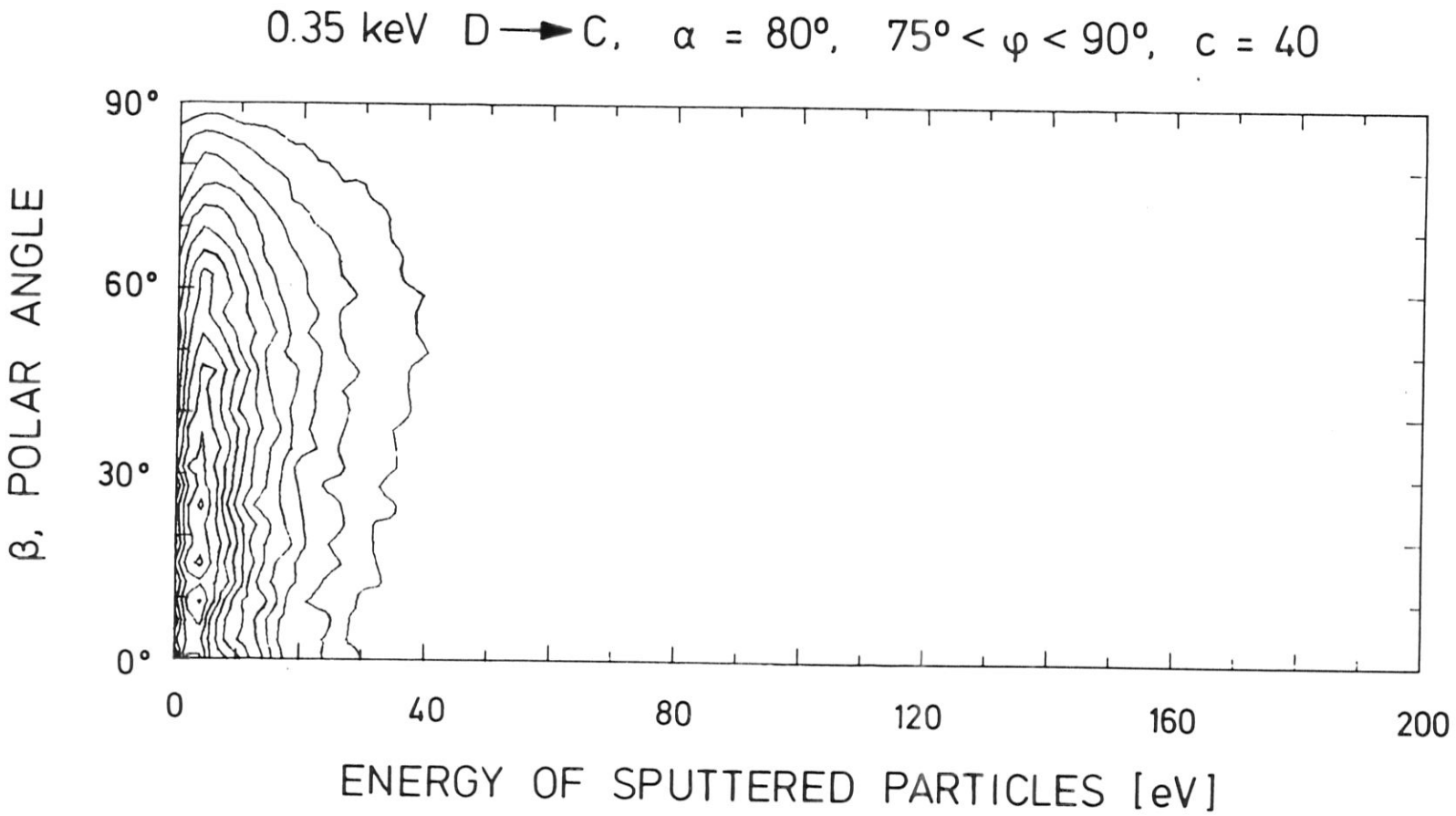
0.35 keV D → C, α = 80°, 75° < φ < 90°, c = 40
β, POLAR ANGLE
90°
60°
30°
0°
0
40
80
120
160
200
ENERGY OF SPUTTERED PARTICLES [eV]

Fig. 52g

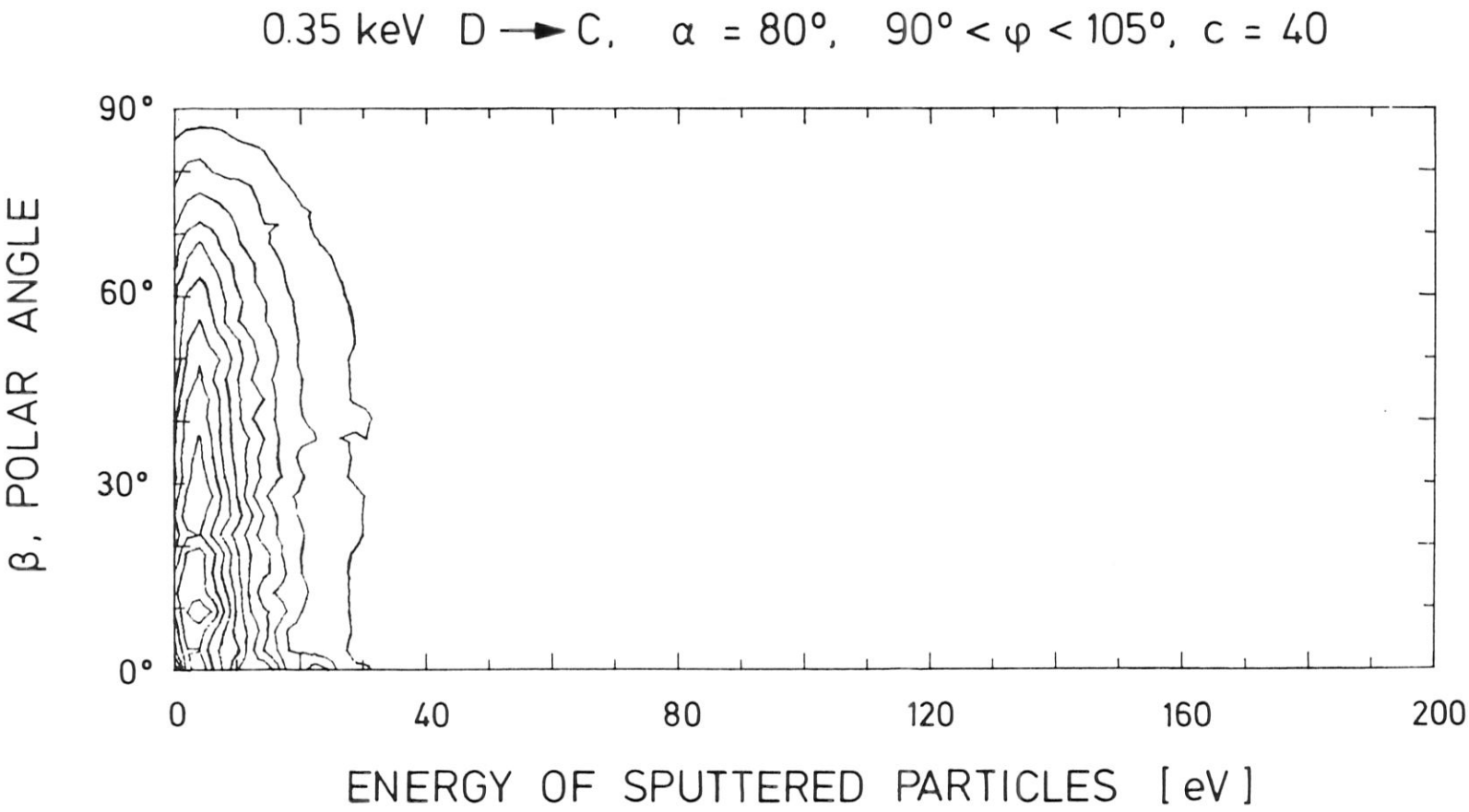
0.35 keV D → C, α = 80°, 90° < φ < 105°, c = 40
β, POLAR ANGLE
90°
60°
30°
0°
0
40
80
120
160
200
ENERGY OF SPUTTERED PARTICLES [eV]

Fig. 52h

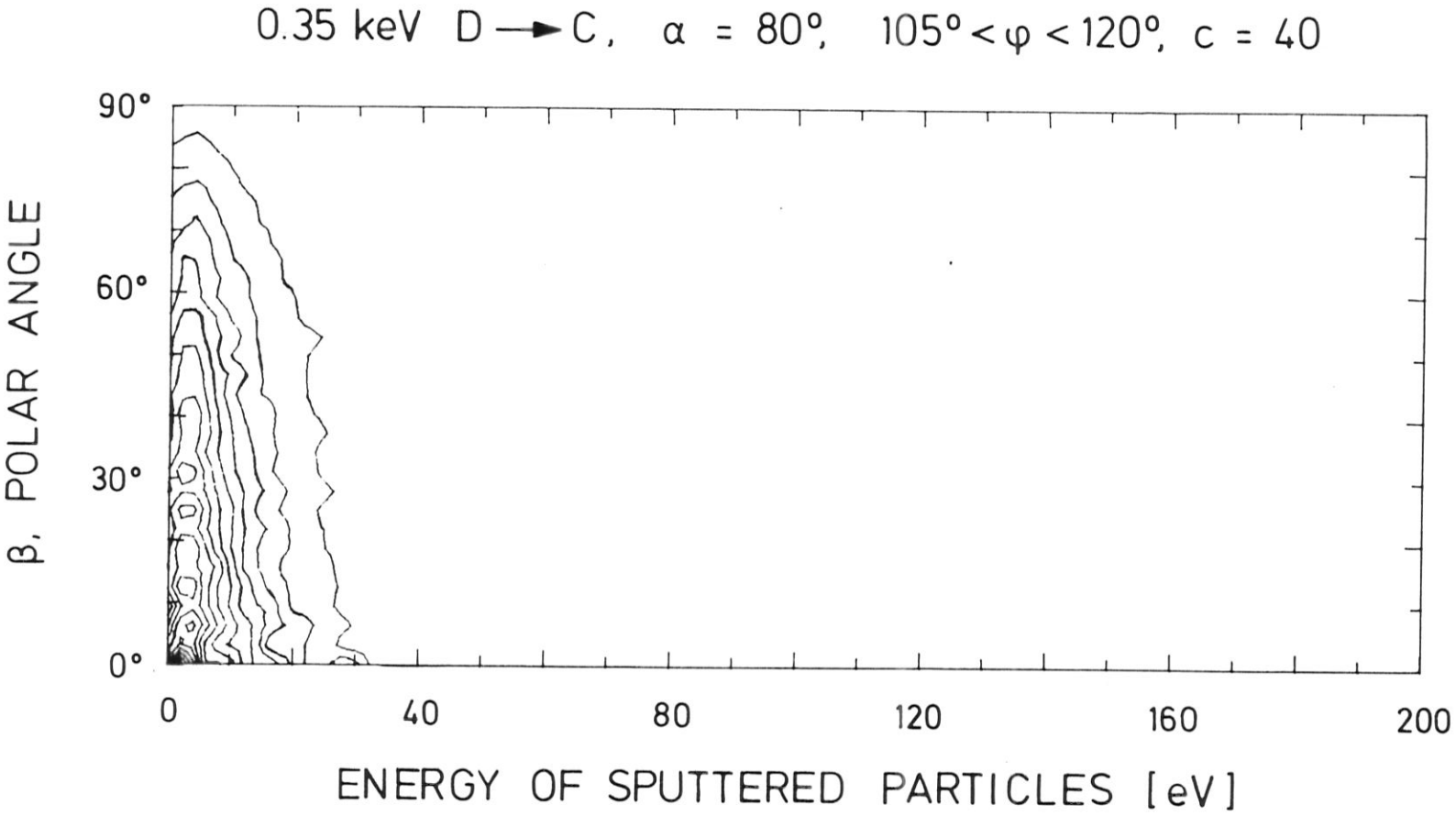
0.35 keV D → C, α = 80°, 105° < φ < 120°, c = 40
β, POLAR ANGLE
90°
60°
30°
0°
0
40
80
120
160
200
ENERGY OF SPUTTERED PARTICLES [eV]

Fig. 52i

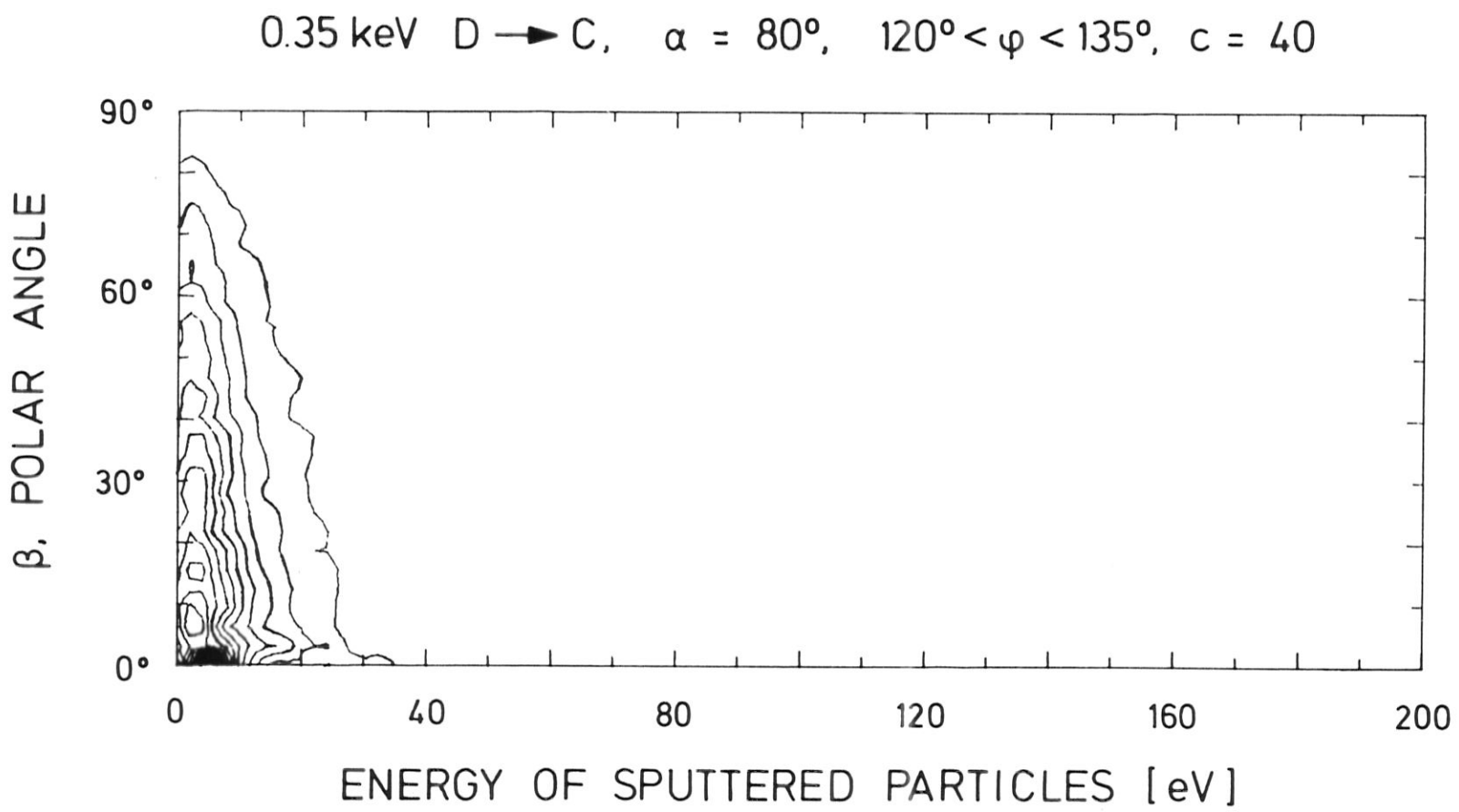
0.35 keV D → C, α = 80°, 120° < φ < 135°, c = 40
β, POLAR ANGLE
90°
60°
30°
0°
0
40
80
120
160
200
ENERGY OF SPUTTERED PARTICLES [eV]

Fig. 52j

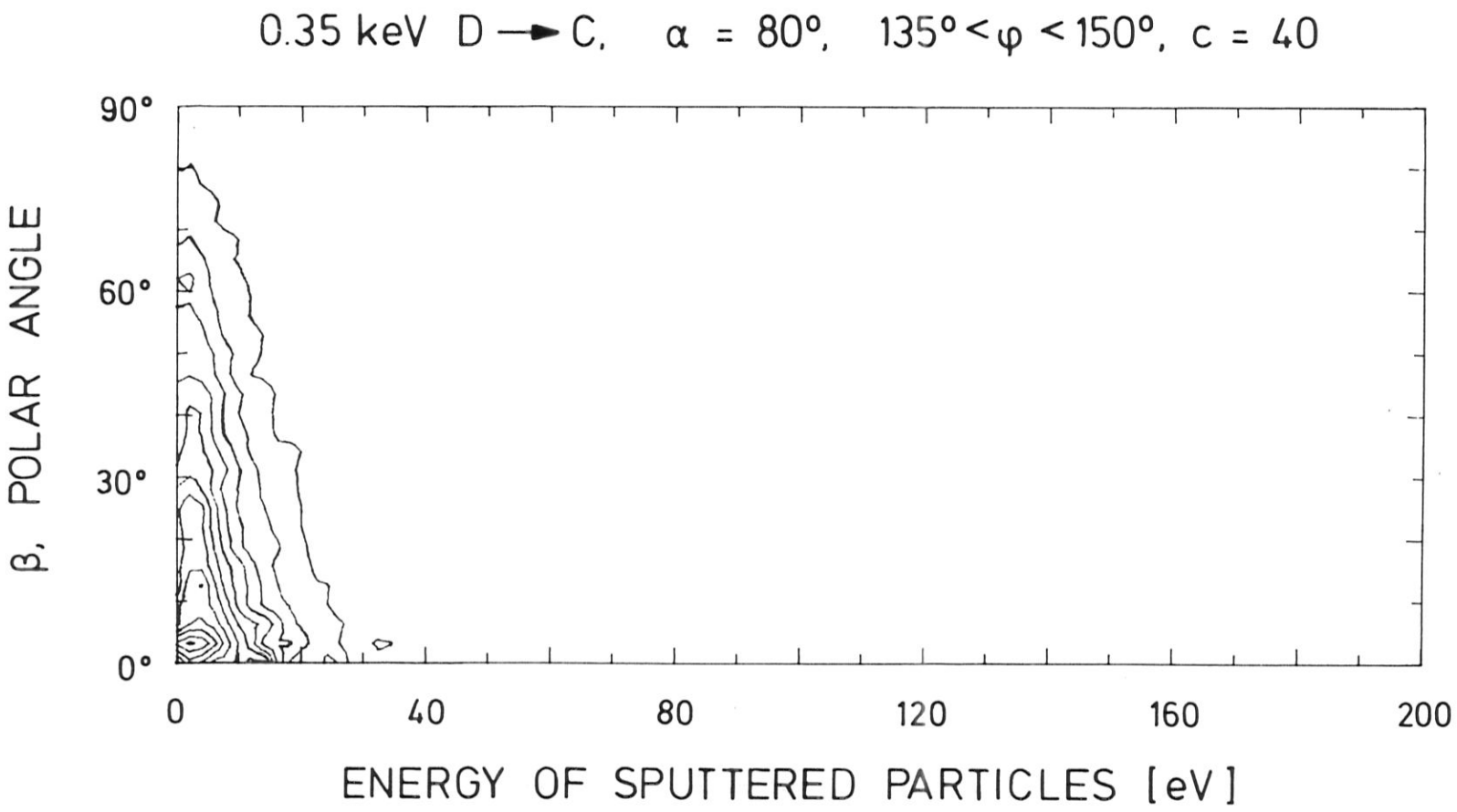
0.35 keV D → C, α = 80°, 135° < φ < 150°, c = 40
90°
60°
30°
0°
β, POLAR ANGLE
0
40
80
120
160
200
ENERGY OF SPUTTERED PARTICLES [eV]

Fig. 52k

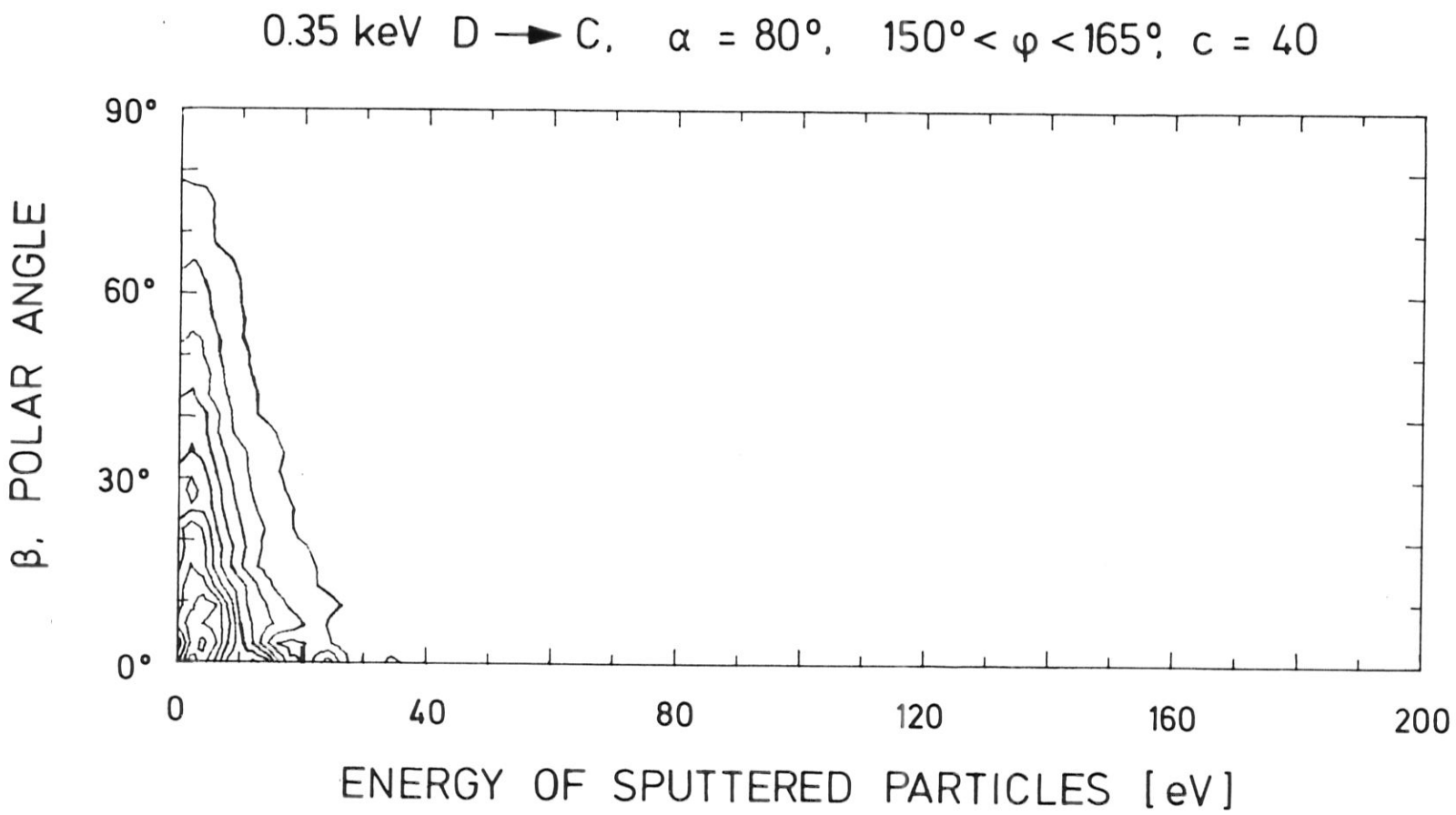
0.35 keV D → C, α = 80°, 150° < φ < 165°, c = 40
β, POLAR ANGLE
90°
60°
30°
0°
0
40
80
120
160
200
ENERGY OF SPUTTERED PARTICLES [eV]

Fig. 521

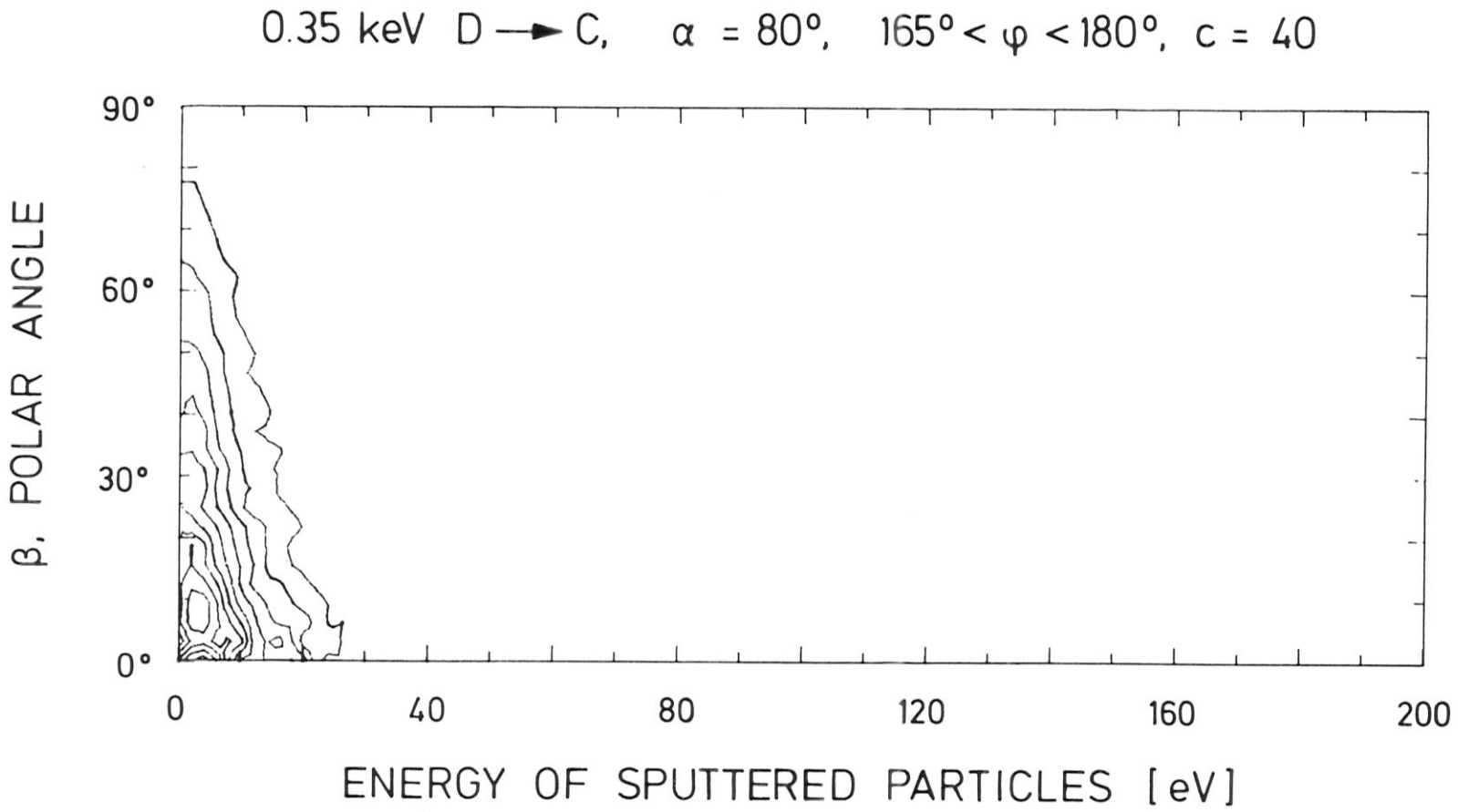
0.35 keV D → C, α = 80°, 165° < φ < 180°, c = 40
β, POLAR ANGLE
90°
60°
30°
0°
0
40
80
120
160
200
ENERGY OF SPUTTERED PARTICLES [eV]

Fig. 52m

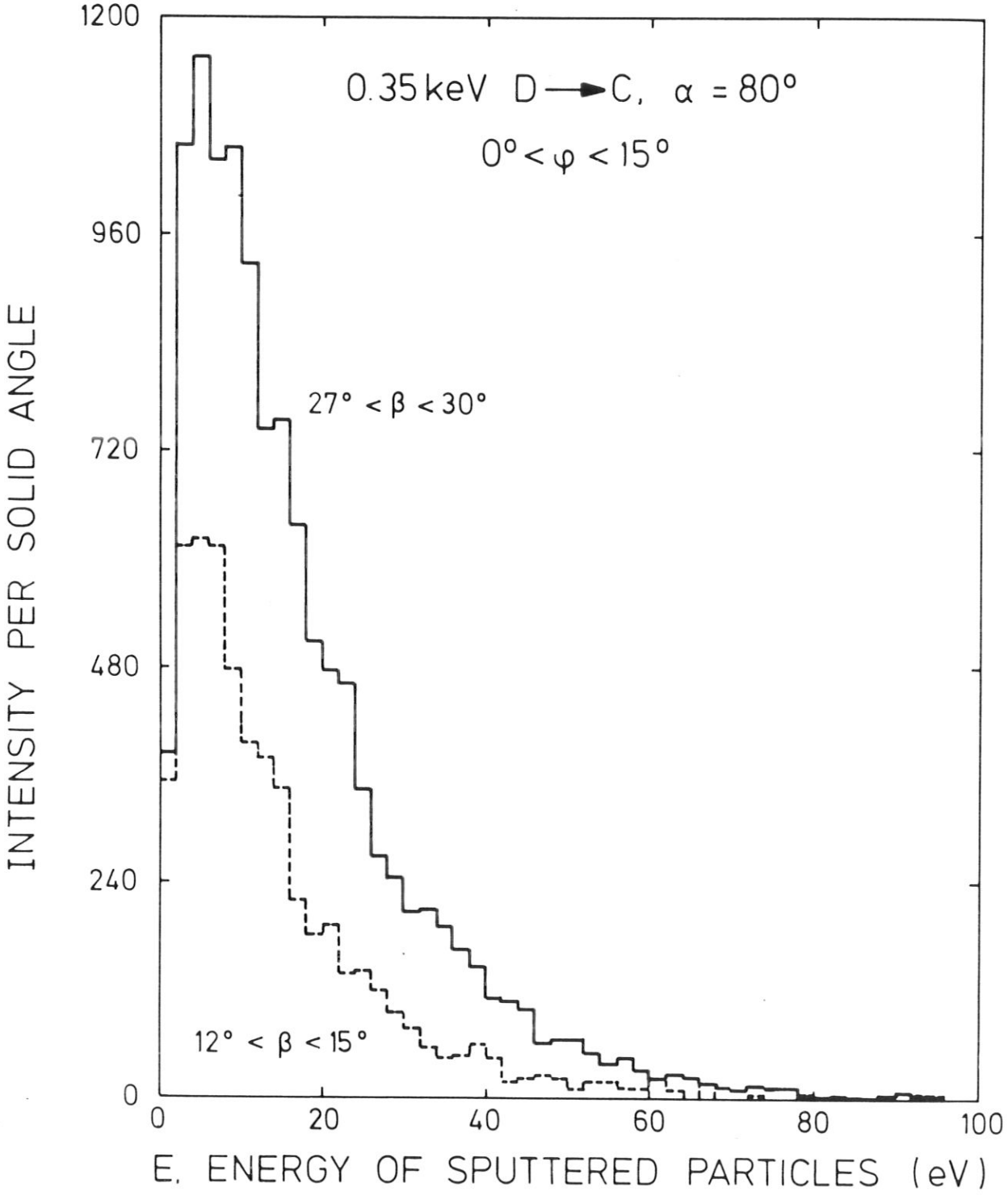
0.35 keV D ⟶ C, α = 80°
0° < φ < 15°
27° < β < 30°
12° < β < 15°
INTENSITY PER SOLID ANGLE
E, ENERGY OF SPUTTERED PARTICLES (eV)
1200
960
720
480
240
0
0
20
40
60
80
100

Fig. 53a

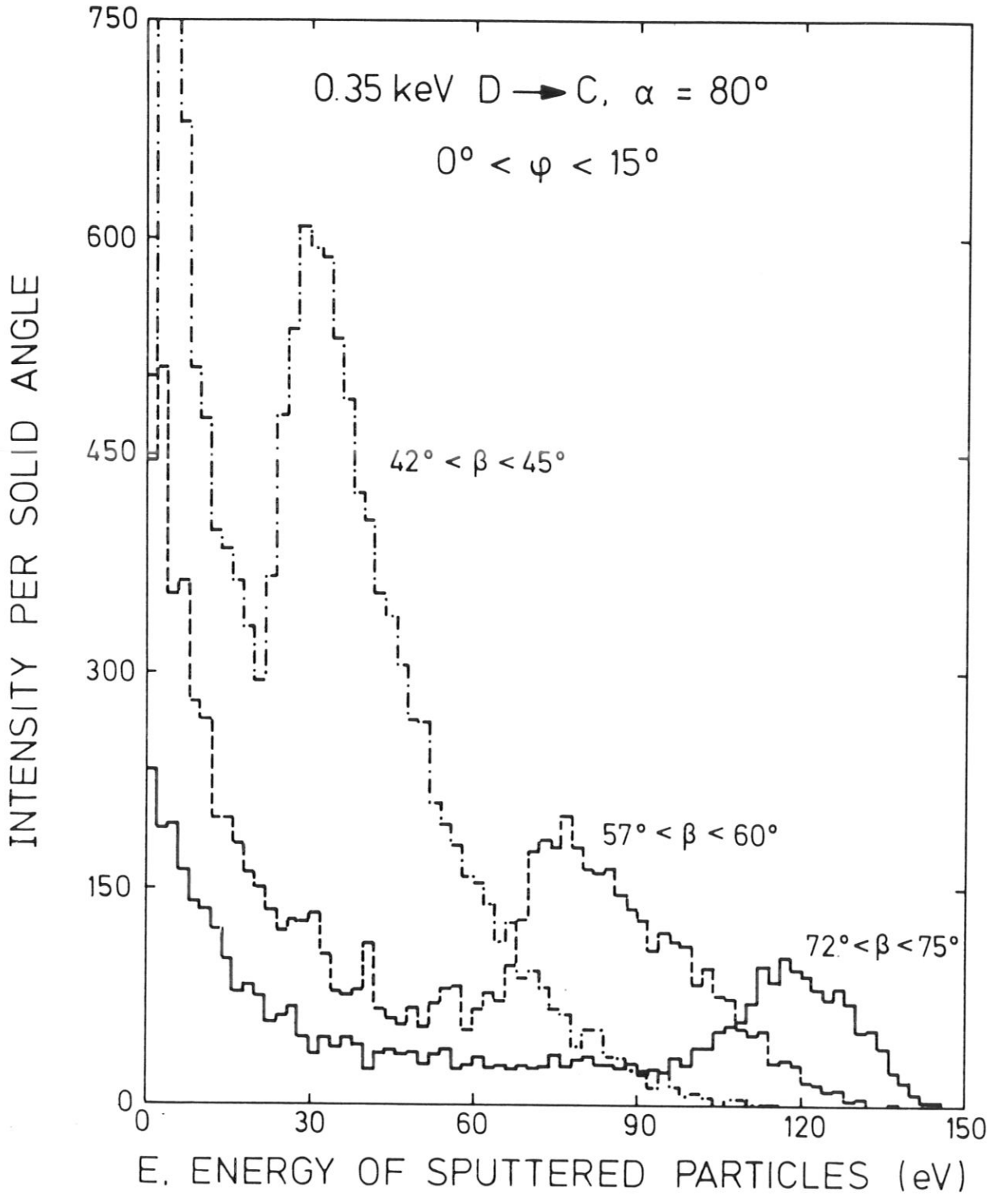
0.35 keV D → C, α = 80°
0° < φ < 15°
42° < β < 45°
57° < β < 60°
72° < β < 75°
INTENSITY PER SOLID ANGLE
E, ENERGY OF SPUTTERED PARTICLES (eV)
750
600
450
300
150
0
0
30
60
90
120
150

Fig. 53b

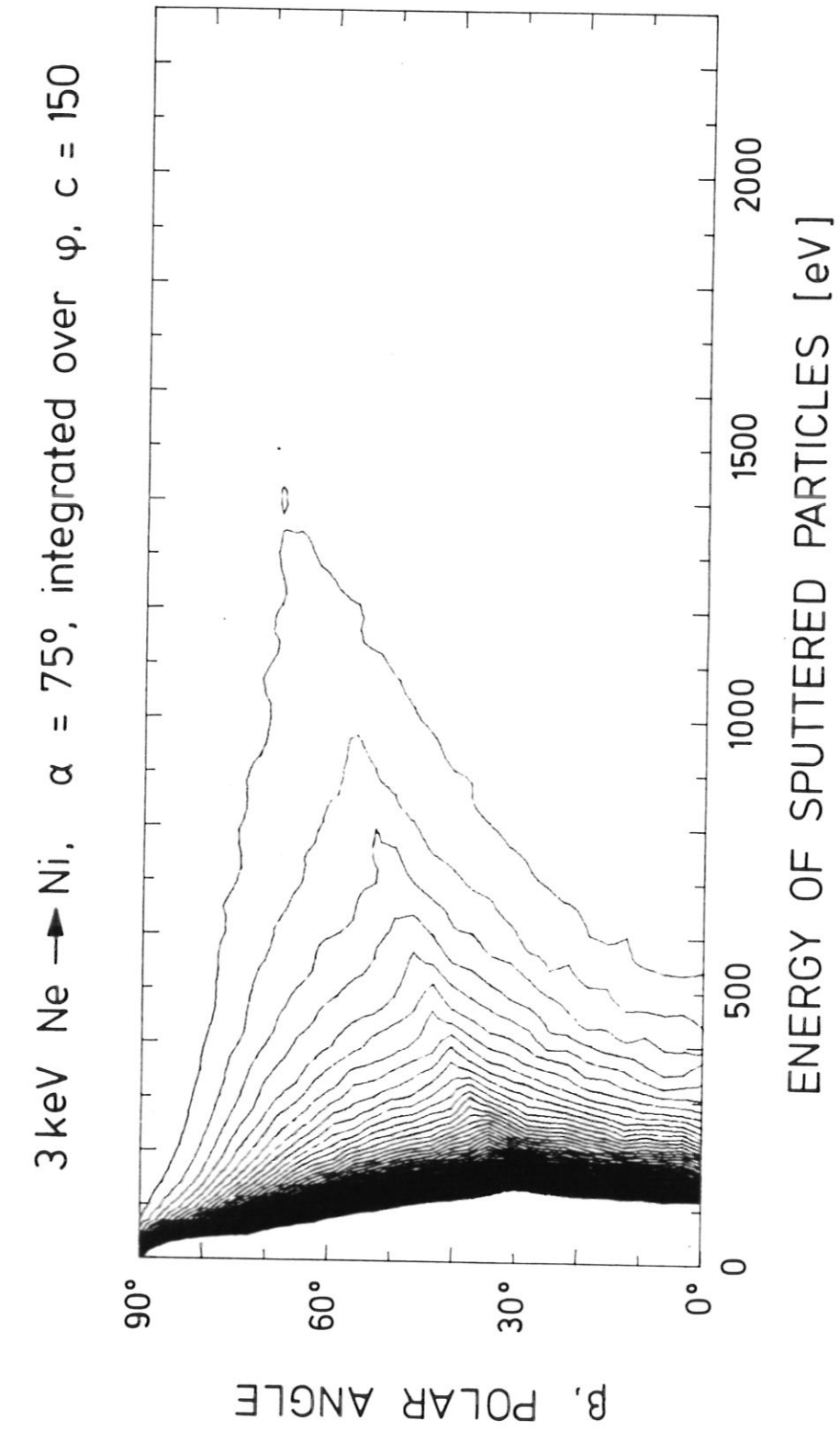
3 keV Ne → Ni, α = 75°, integrated over φ, c = 150
ϑ, POLAR ANGLE
90°
60°
30°
0°
0
500
1000
1500
2000
ENERGY OF SPUTTERED PARTICLES [eV]

Fig. 54a

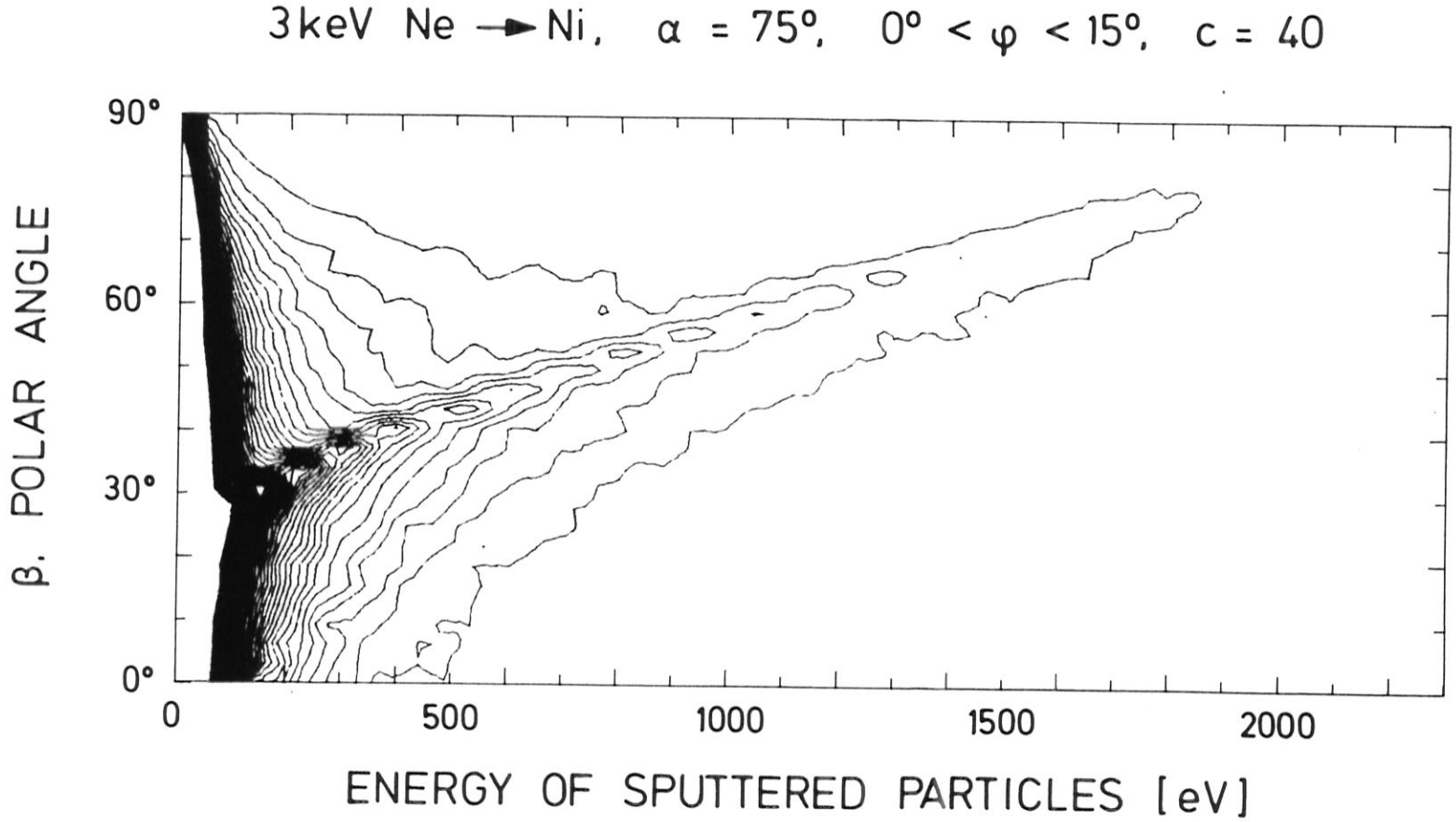
3keV Ne → Ni, α = 75°, 0° < φ < 15°, c = 40
β. POLAR ANGLE
90°
60°
30°
0°
0
500
1000
1500
2000
ENERGY OF SPUTTERED PARTICLES [eV]

Fig. 54b

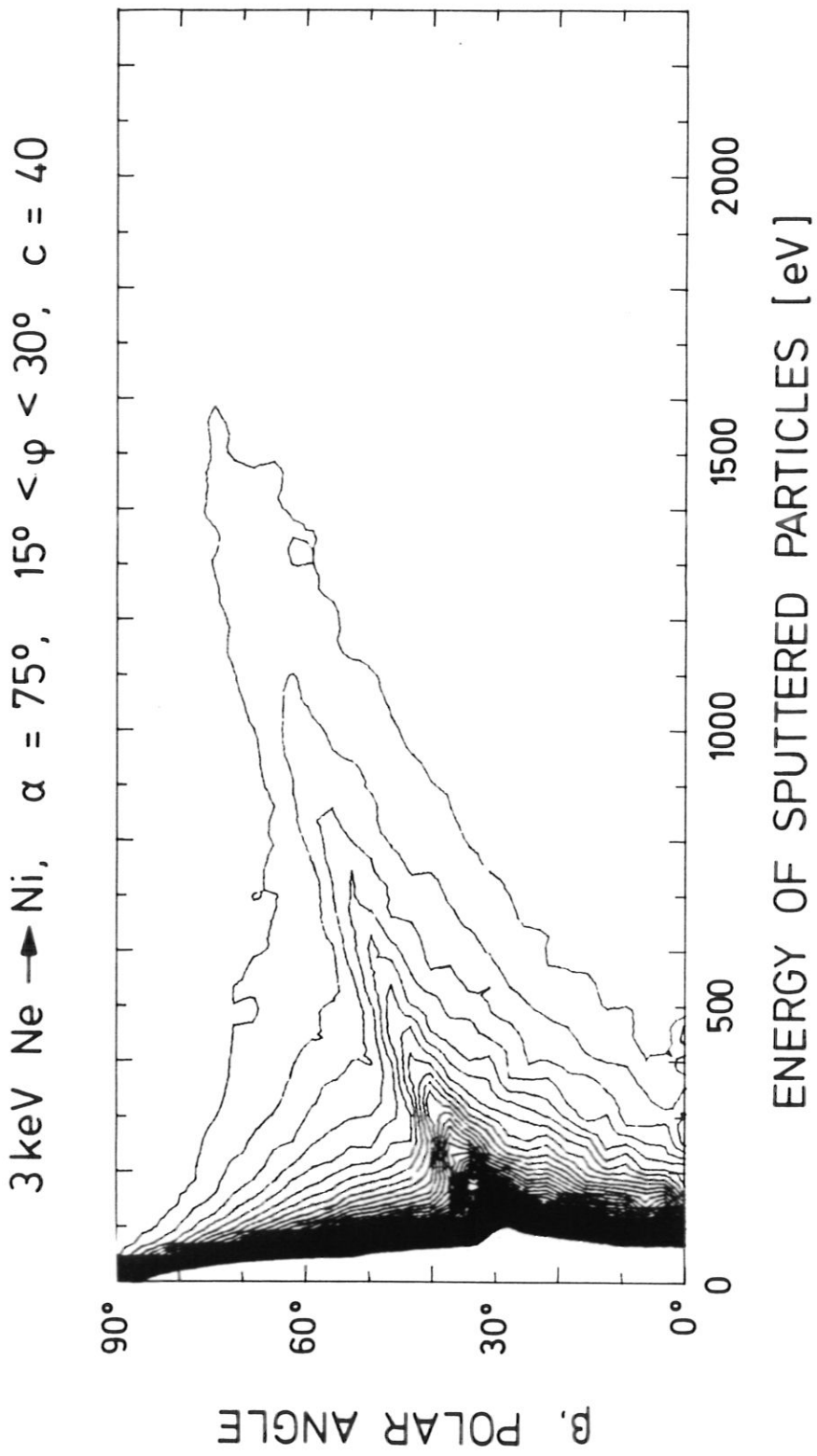
3 keV Ne → Ni, α = 75°, 15° < φ < 30°, c = 40
ENERGY OF SPUTTERED PARTICLES [eV]
0
500
1000
1500
2000
β, POLAR ANGLE
90°
60°
30°
0°

Fig. 54c

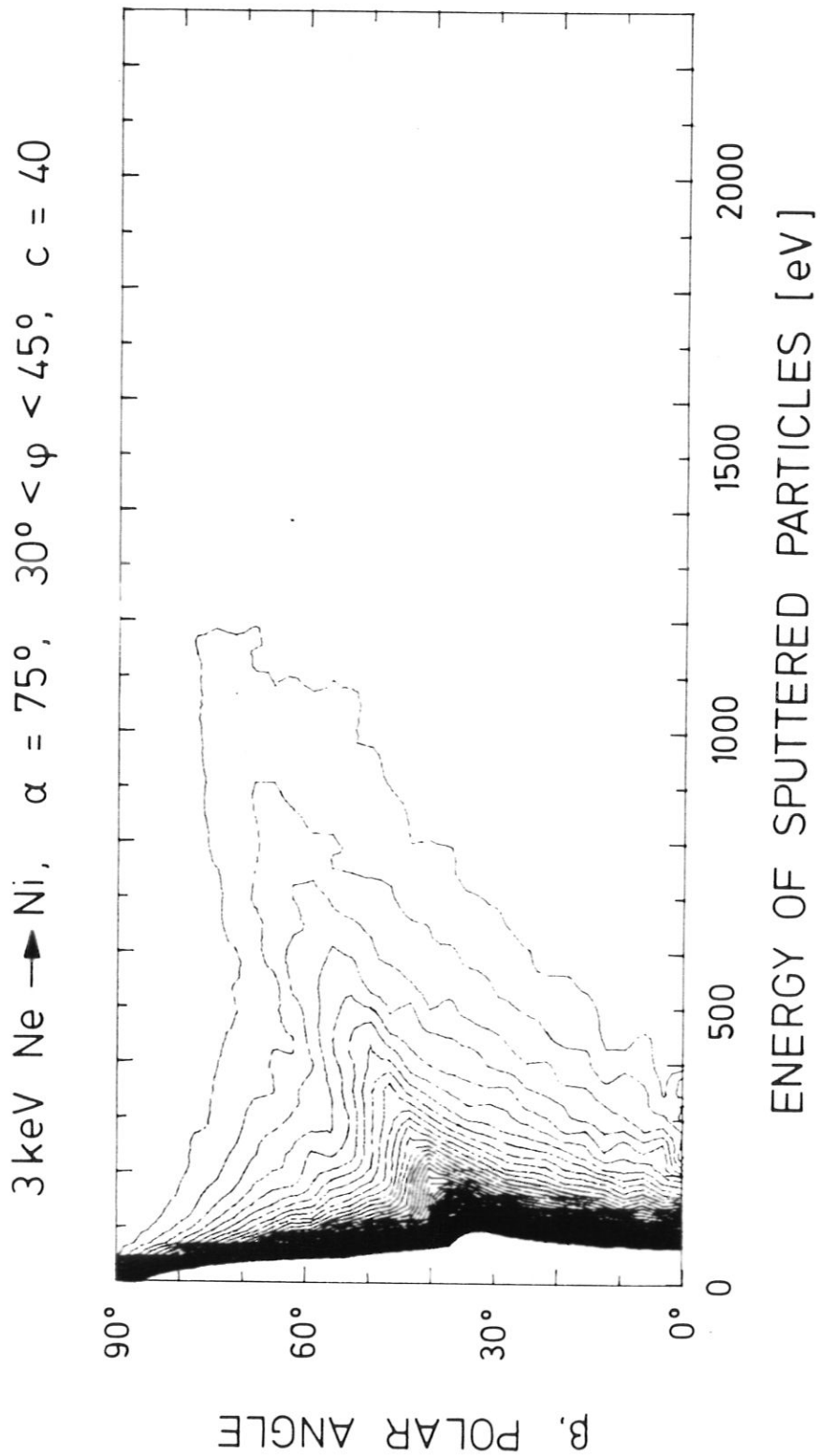
3 keV Ne → Ni, α = 75°, 30° < φ < 45°, c = 40
ENERGY OF SPUTTERED PARTICLES [eV]
0
500
1000
1500
2000
β, POLAR ANGLE
90°
60°
30°
0°

Fig. 54d

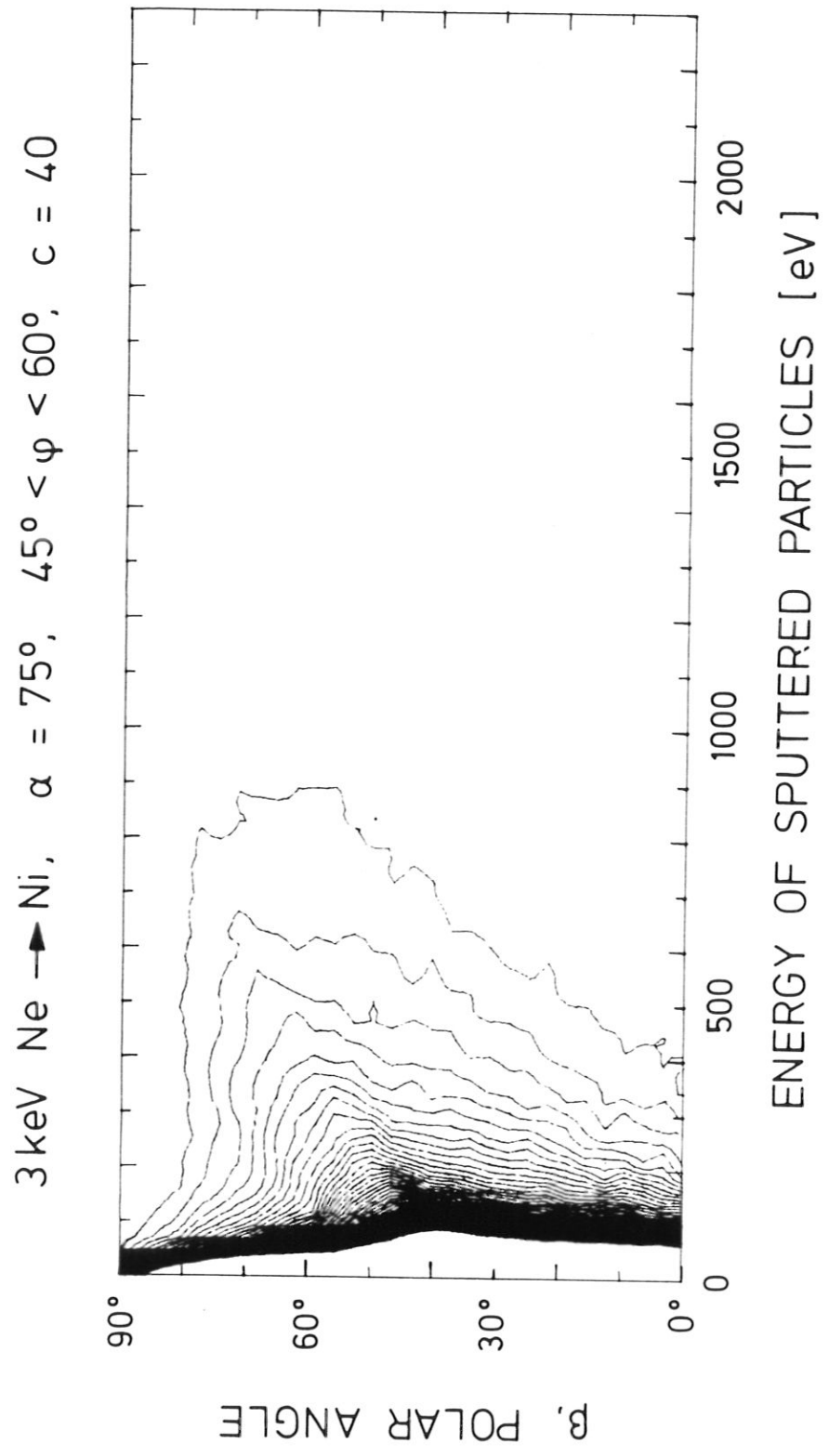
3 keV Ne → Ni, α = 75°, 45° < φ < 60°, c = 40
ENERGY OF SPUTTERED PARTICLES [eV]
0
500
1000
1500
2000
β, POLAR ANGLE
90°
60°
30°
0°

Fig. 54e

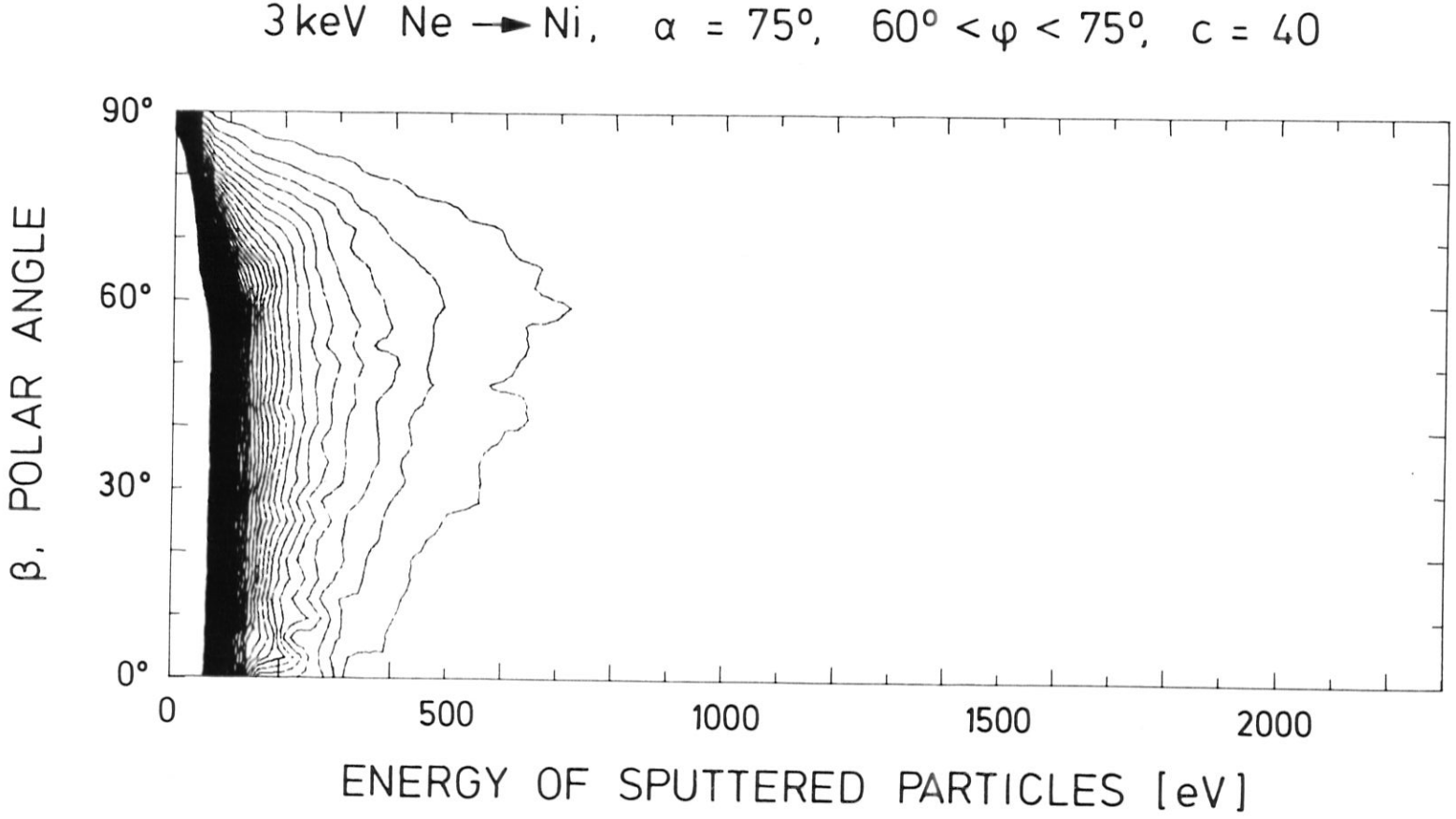
3 keV Ne → Ni, α = 75°, 60° < φ < 75°, c = 40
β, POLAR ANGLE
90°
60°
30°
0°
0
500
1000
1500
2000
ENERGY OF SPUTTERED PARTICLES [eV]

Fig. 54f

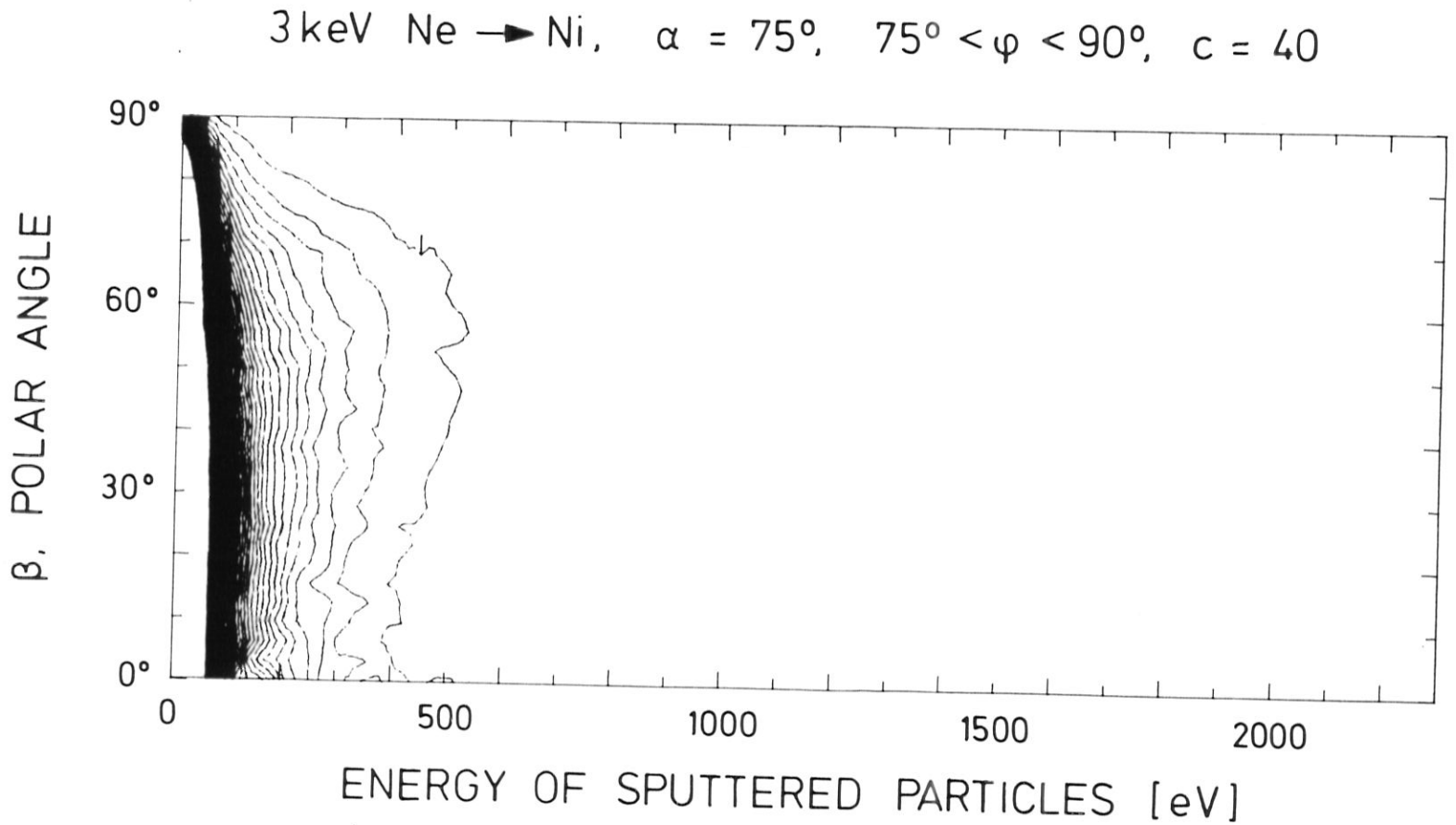
3keV Ne → Ni, α = 75°, 75° < φ < 90°, c = 40
β, POLAR ANGLE
90°
60°
30°
0°
0
500
1000
1500
2000
ENERGY OF SPUTTERED PARTICLES [eV]

Fig. 54g

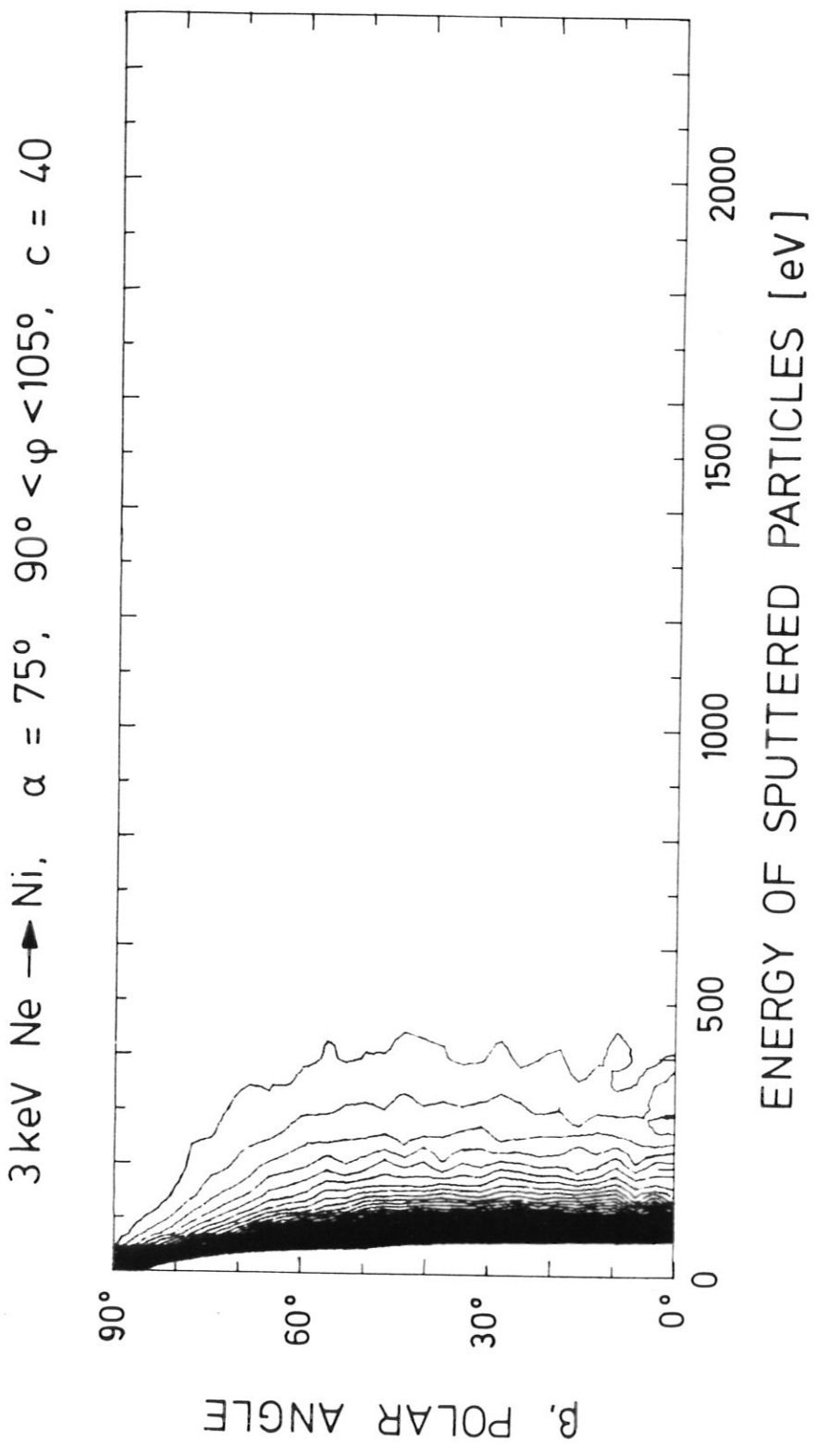
3 keV Ne → Ni, α = 75°, 90° < φ < 105°, c = 40
ENERGY OF SPUTTERED PARTICLES [eV]
0
500
1000
1500
2000
ϑ, POLAR ANGLE
90°
60°
30°
0°

Fig. 54h

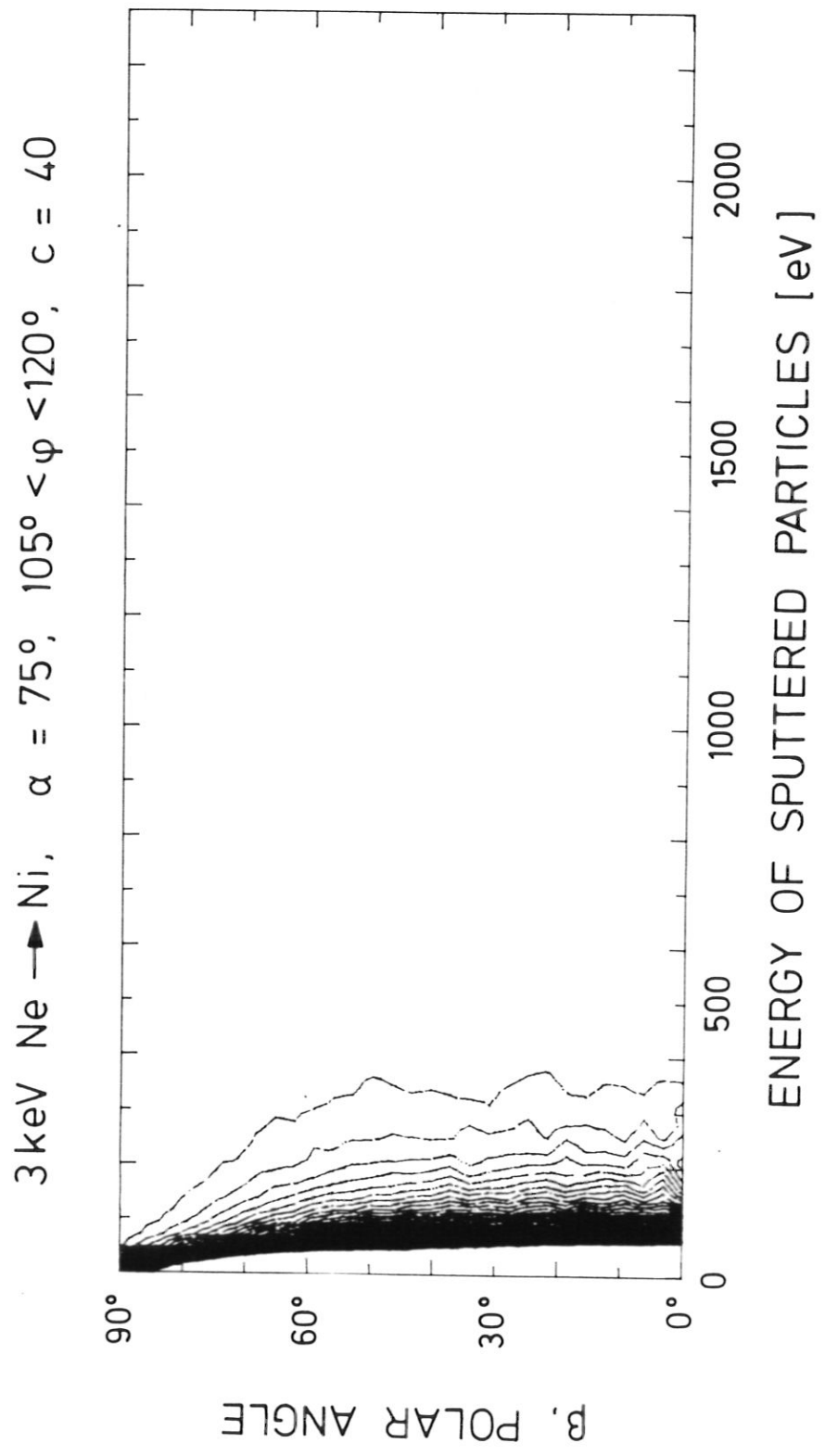
3 keV Ne → Ni, α = 75°, 105° < φ < 120°, c = 40
ENERGY OF SPUTTERED PARTICLES [eV]
0
500
1000
1500
2000
β, POLAR ANGLE
90°
60°
30°
0°

Fig. 54i

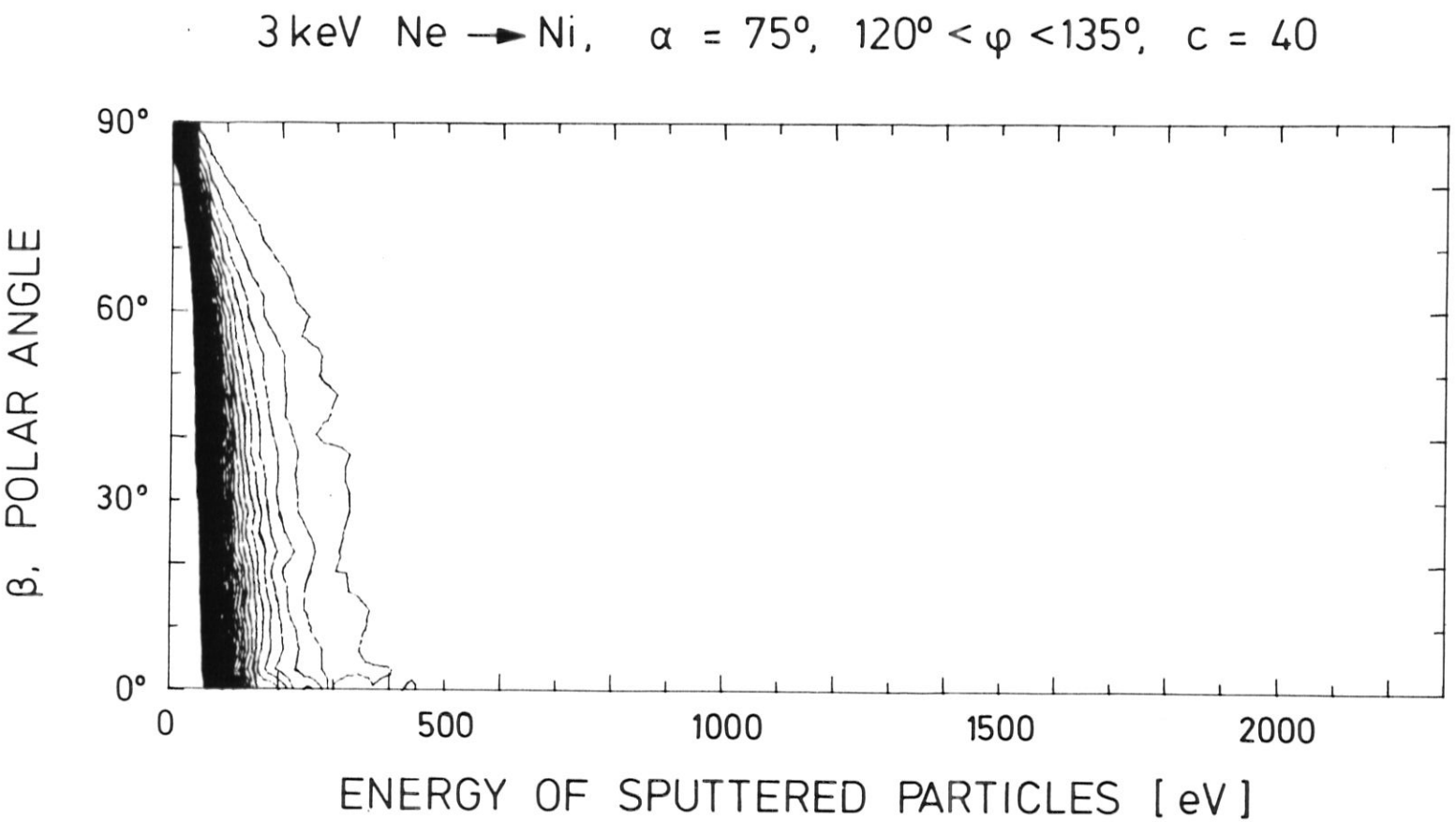
3 keV Ne → Ni, α = 75°, 120° < φ < 135°, c = 40
β, POLAR ANGLE
90°
60°
30°
0°
0
500
1000
1500
2000
ENERGY OF SPUTTERED PARTICLES [eV]

Fig. 54j

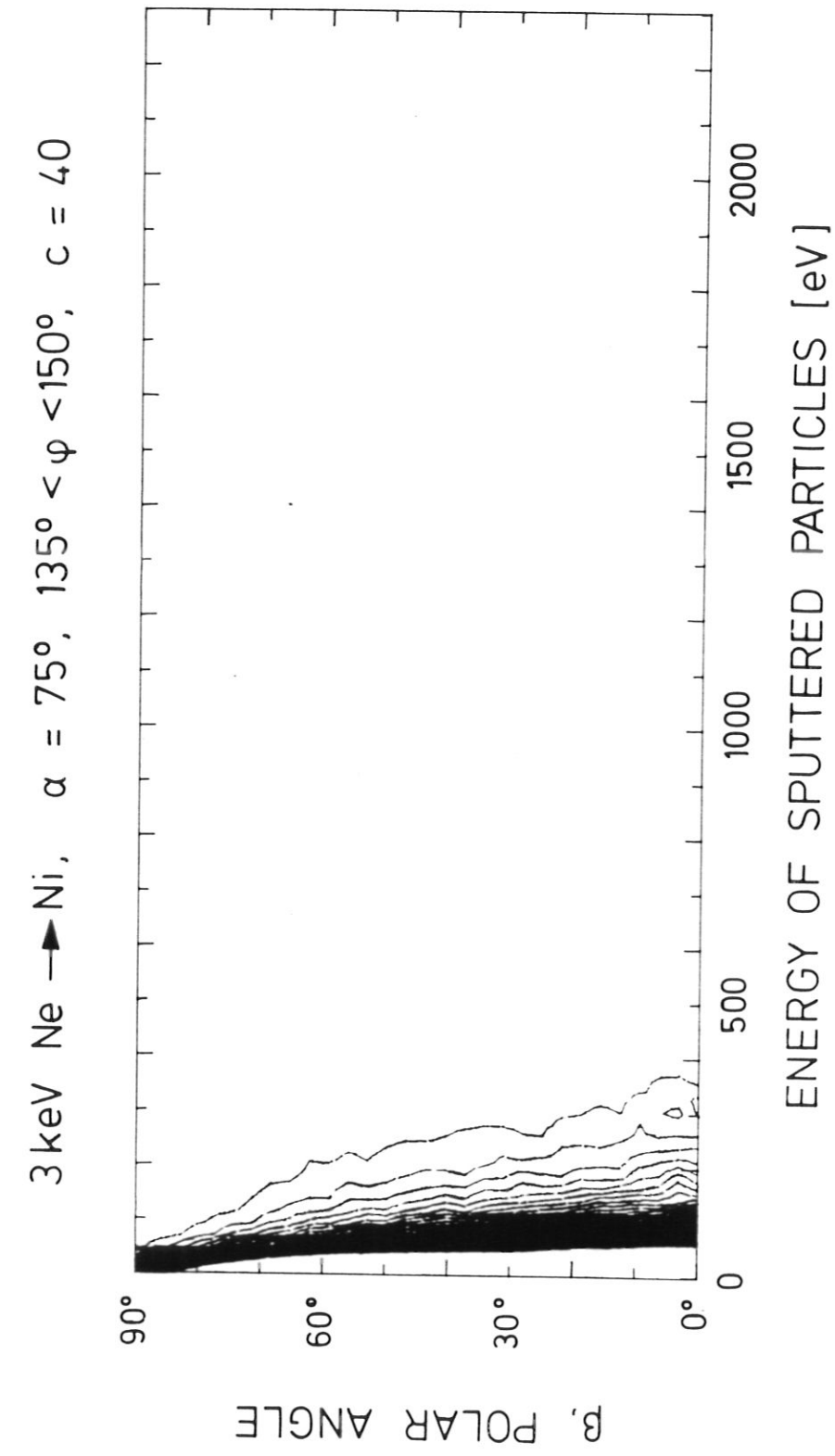
3 keV Ne → Ni, α = 75°, 135° < φ <150°, c = 40
ENERGY OF SPUTTERED PARTICLES [eV]
0
500
1000
1500
2000
β, POLAR ANGLE
90°
60°
30°
0°

Fig. 54k

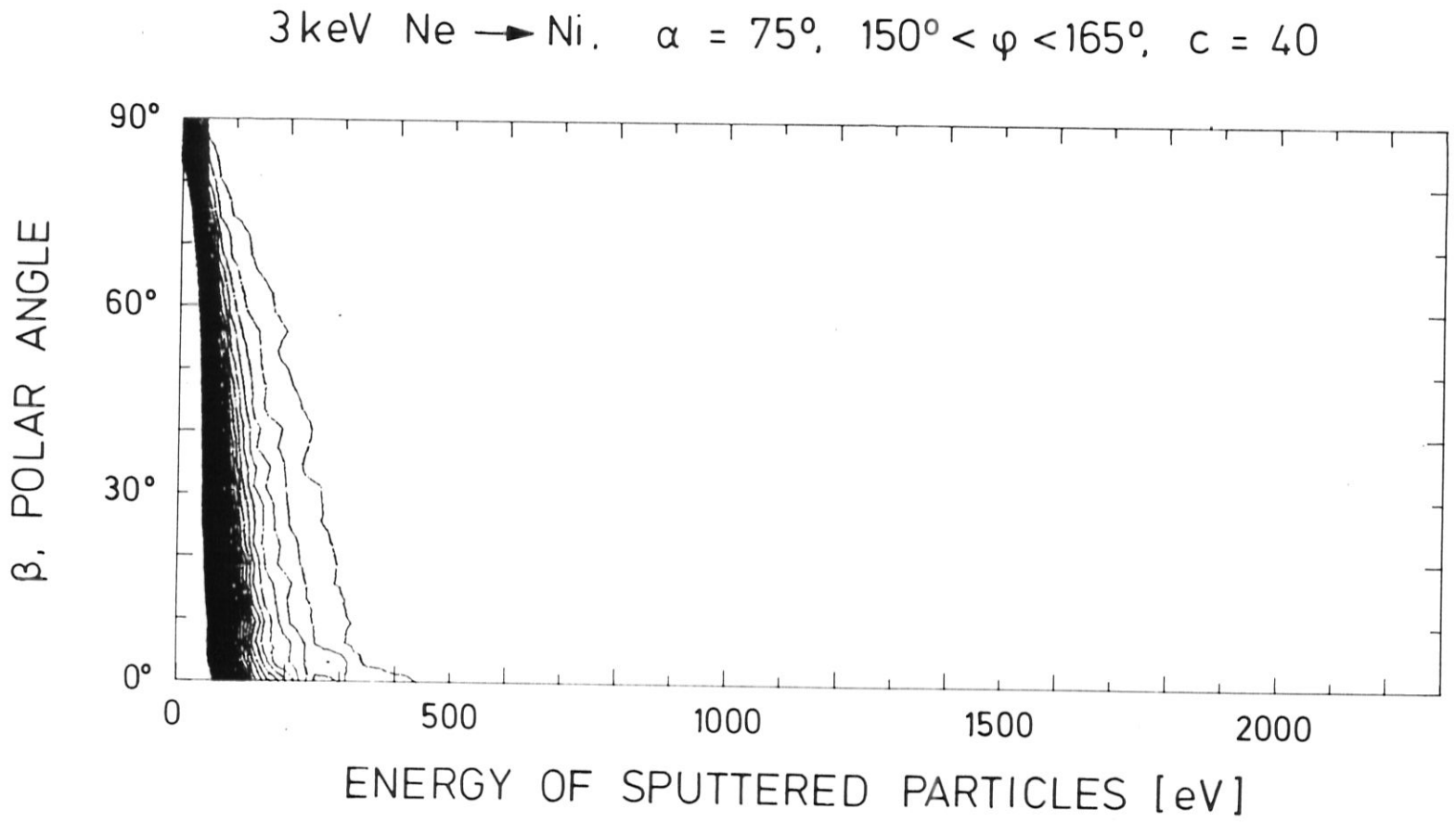
3 keV Ne → Ni. α = 75°, 150° < φ < 165°, c = 40
β, POLAR ANGLE
90°
60°
30°
0°
0
500
1000
1500
2000
ENERGY OF SPUTTERED PARTICLES [eV]

Fig. 541

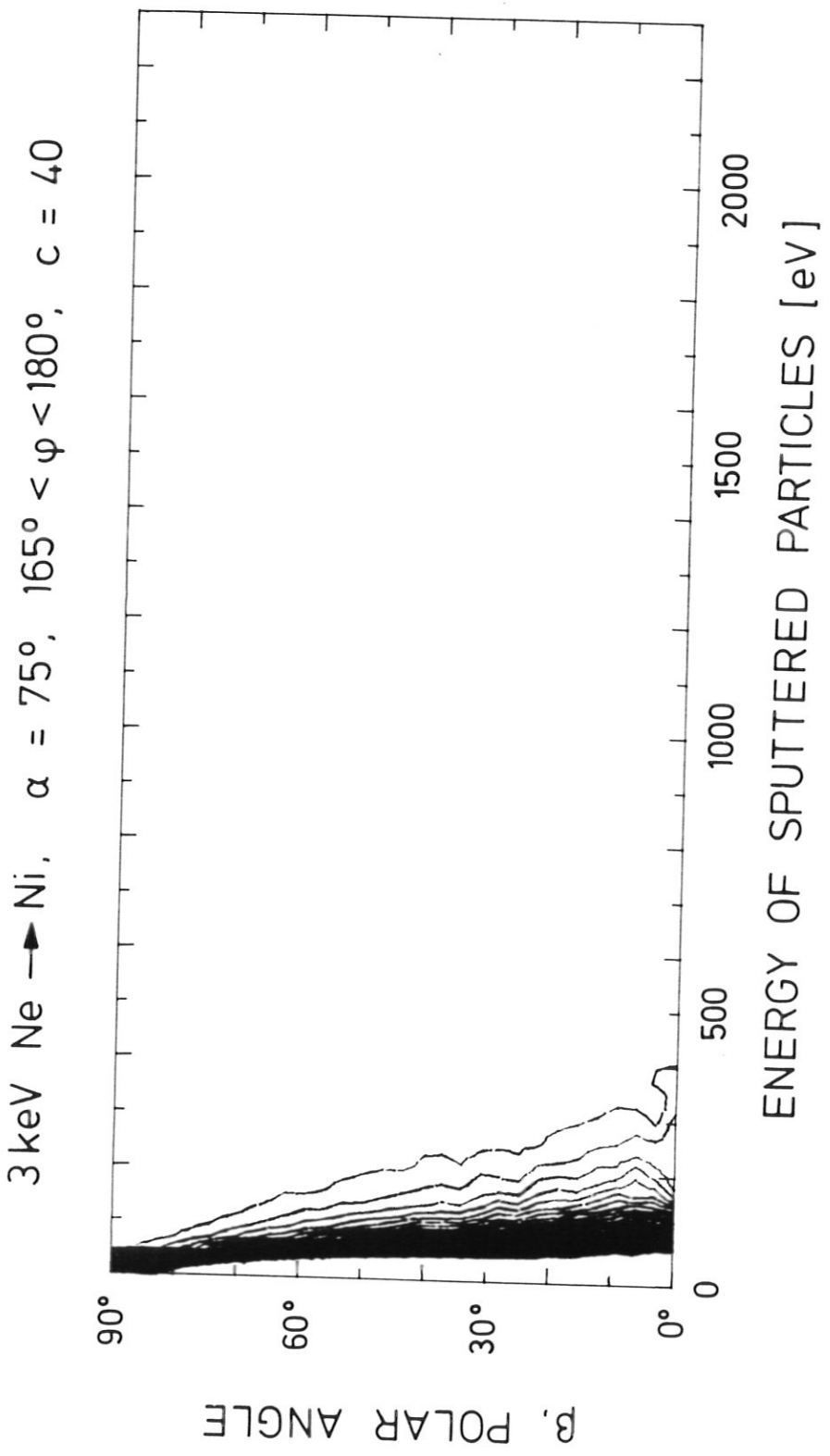
3 keV Ne → Ni, α = 75°, 165° < φ < 180°, c = 40
ENERGY OF SPUTTERED PARTICLES [eV]
0
500
1000
1500
2000
β, POLAR ANGLE
90°
60°
30°
0°

Fig. 54m

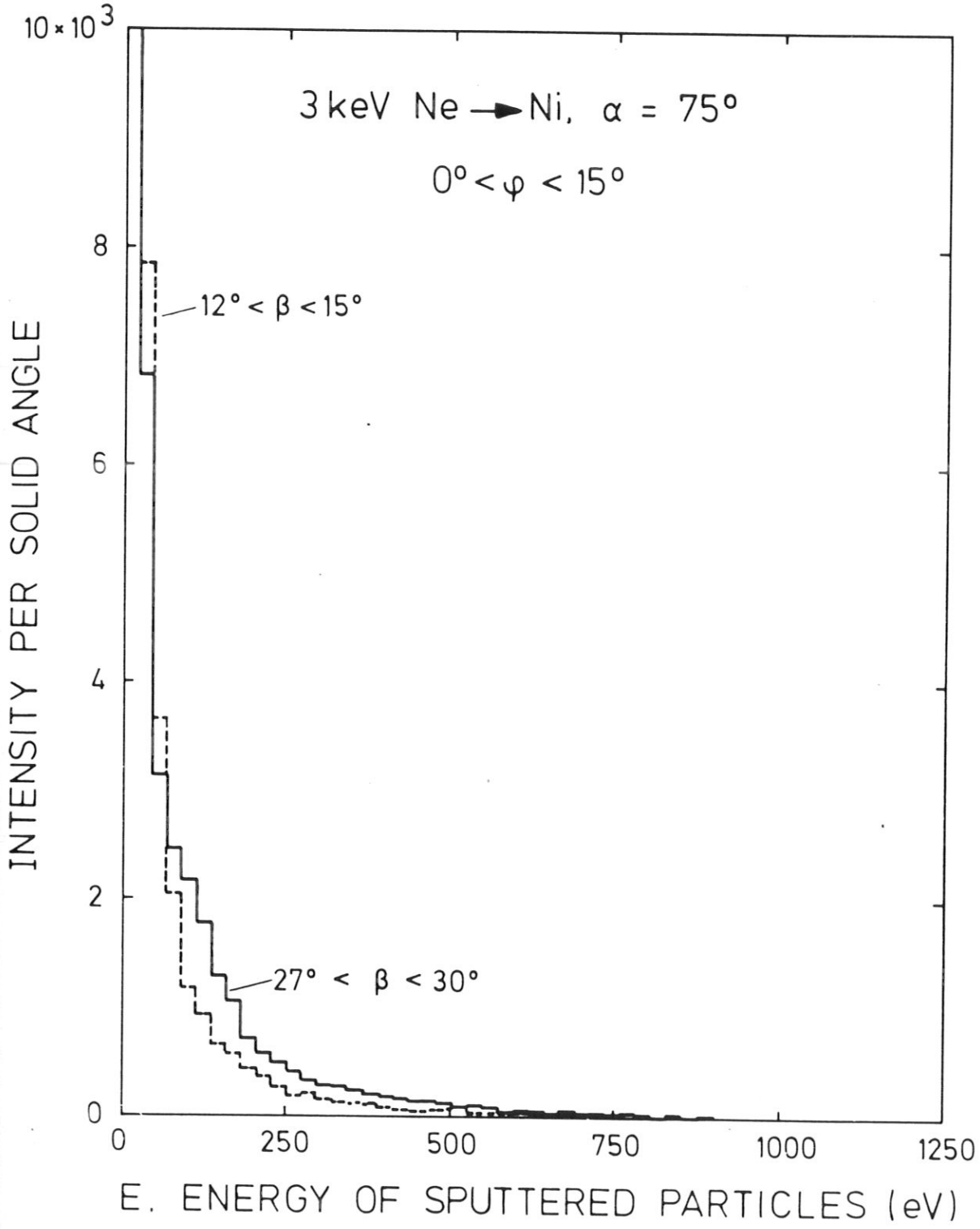
10 × 10^3
3 keV Ne → Ni, α = 75°
0° < φ < 15°
12° < β < 15°
27° < β < 30°
INTENSITY PER SOLID ANGLE
E. ENERGY OF SPUTTERED PARTICLES (eV)
0
2
4
6
8
0
250
500
750
1000
1250

Fig. 55a

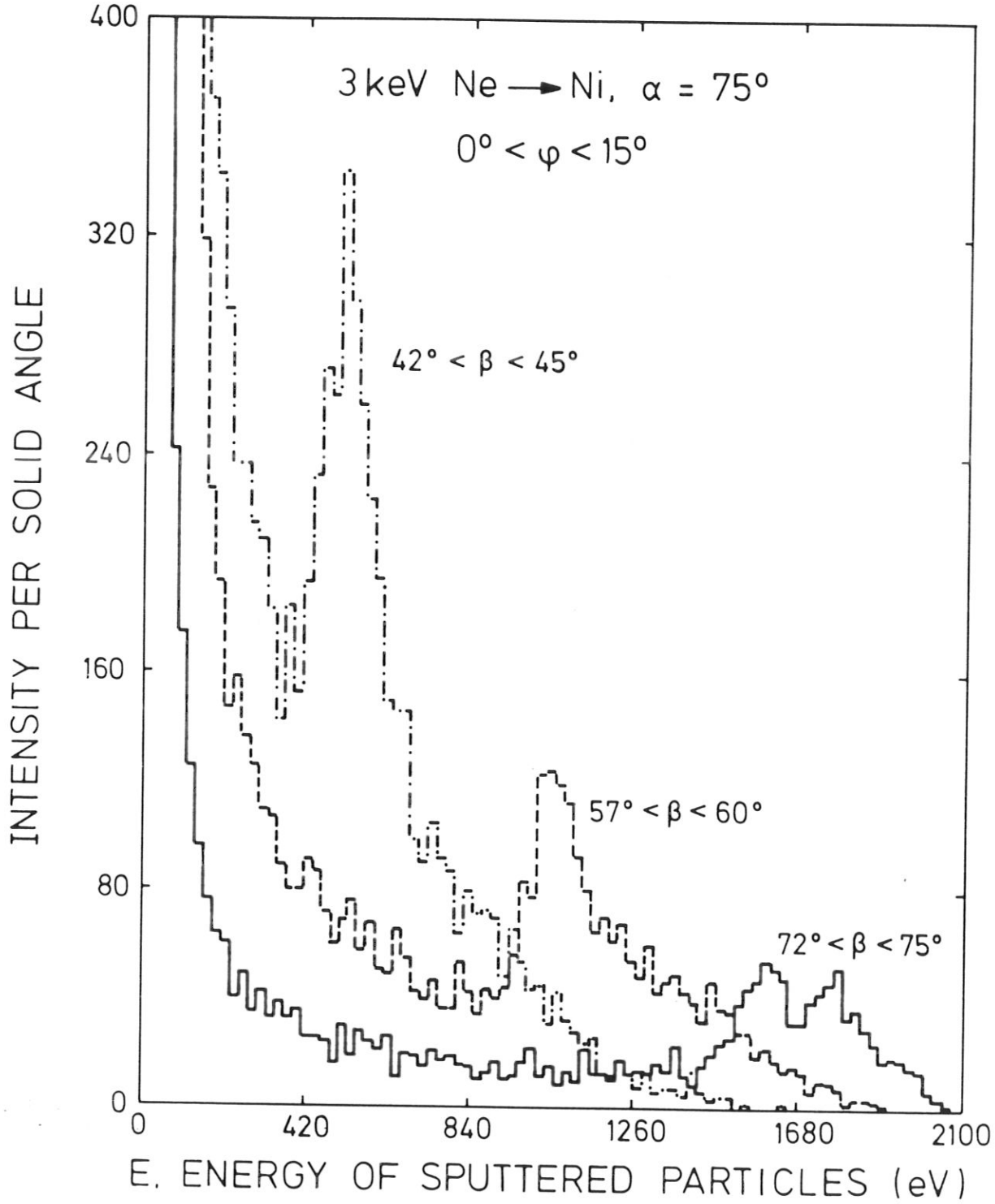
3 keV Ne → Ni, α = 75°
0° < φ < 15°
42° < β < 45°
57° < β < 60°
72° < β < 75°
INTENSITY PER SOLID ANGLE
E. ENERGY OF SPUTTERED PARTICLES (eV)
400
320
240
160
80
0
0
420
840
1260
1680
2100

Fig. 55b

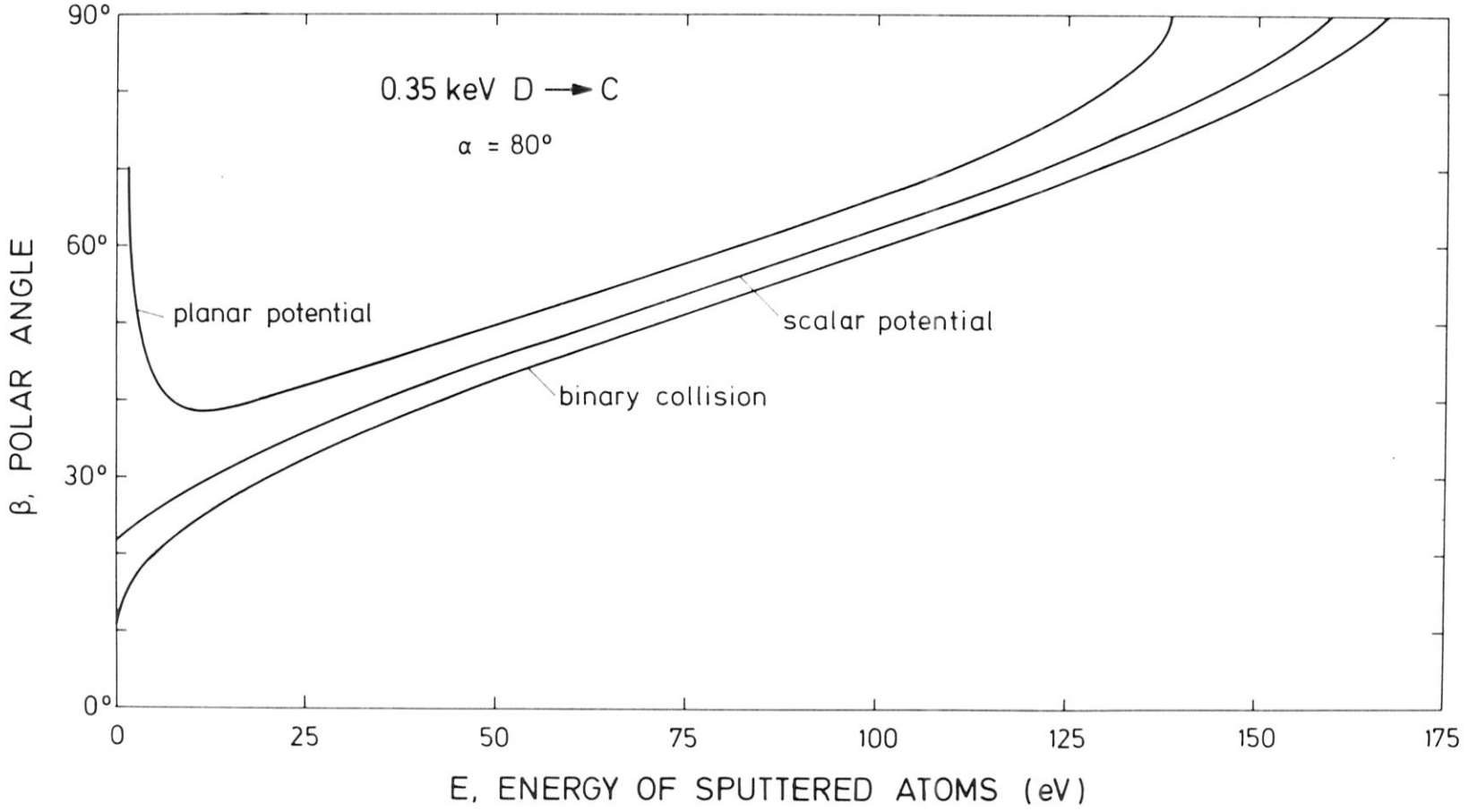
0.35 keV D → C
α = 80°
planar potential
scalar potential
binary collision
β, POLAR ANGLE
E, ENERGY OF SPUTTERED ATOMS (eV)
90°
60°
30°
0°
0
25
50
75
100
125
150
175

Fig. 56

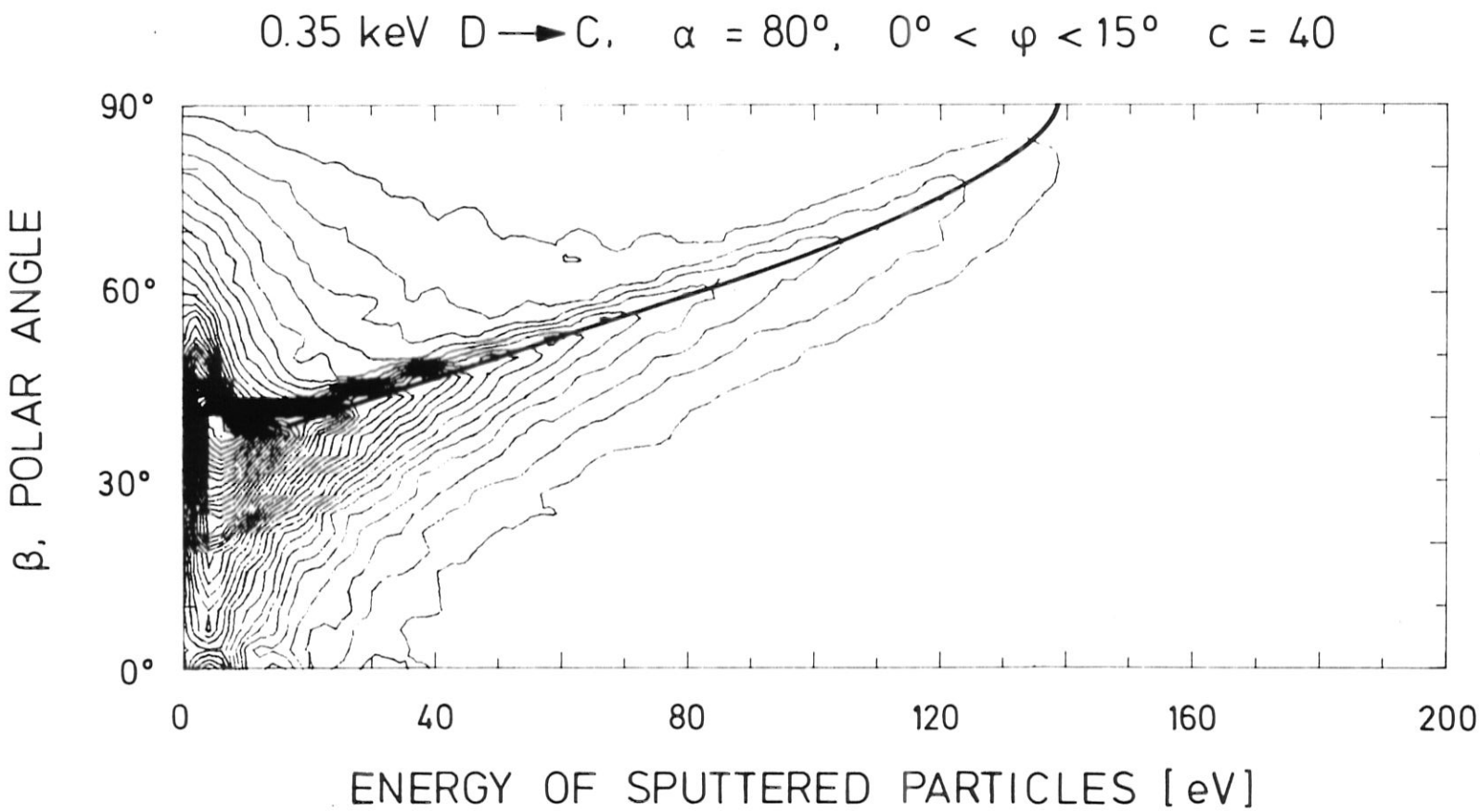
0.35 keV D → C, α = 80°, 0° < φ < 15° c = 40
β, POLAR ANGLE
90°
60°
30°
0°
0
40
80
120
160
200
ENERGY OF SPUTTERED PARTICLES [eV]

Fig. 57a

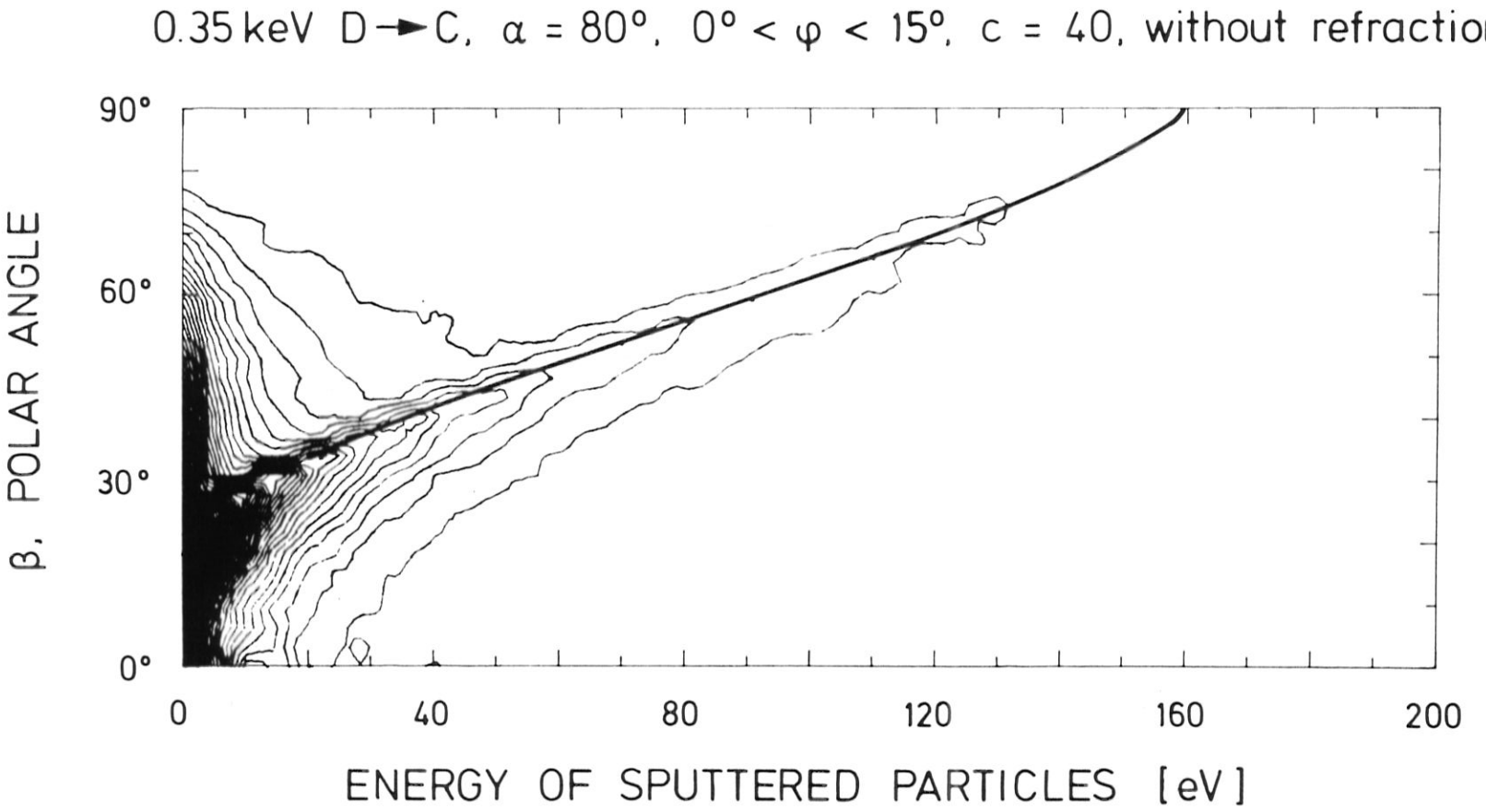
0.35 keV D → C, α = 80°, 0° < φ < 15°, c = 40, without refraction
β, POLAR ANGLE
90°
60°
30°
0°
0
40
80
120
160
200
ENERGY OF SPUTTERED PARTICLES [eV]

Fig. 57b

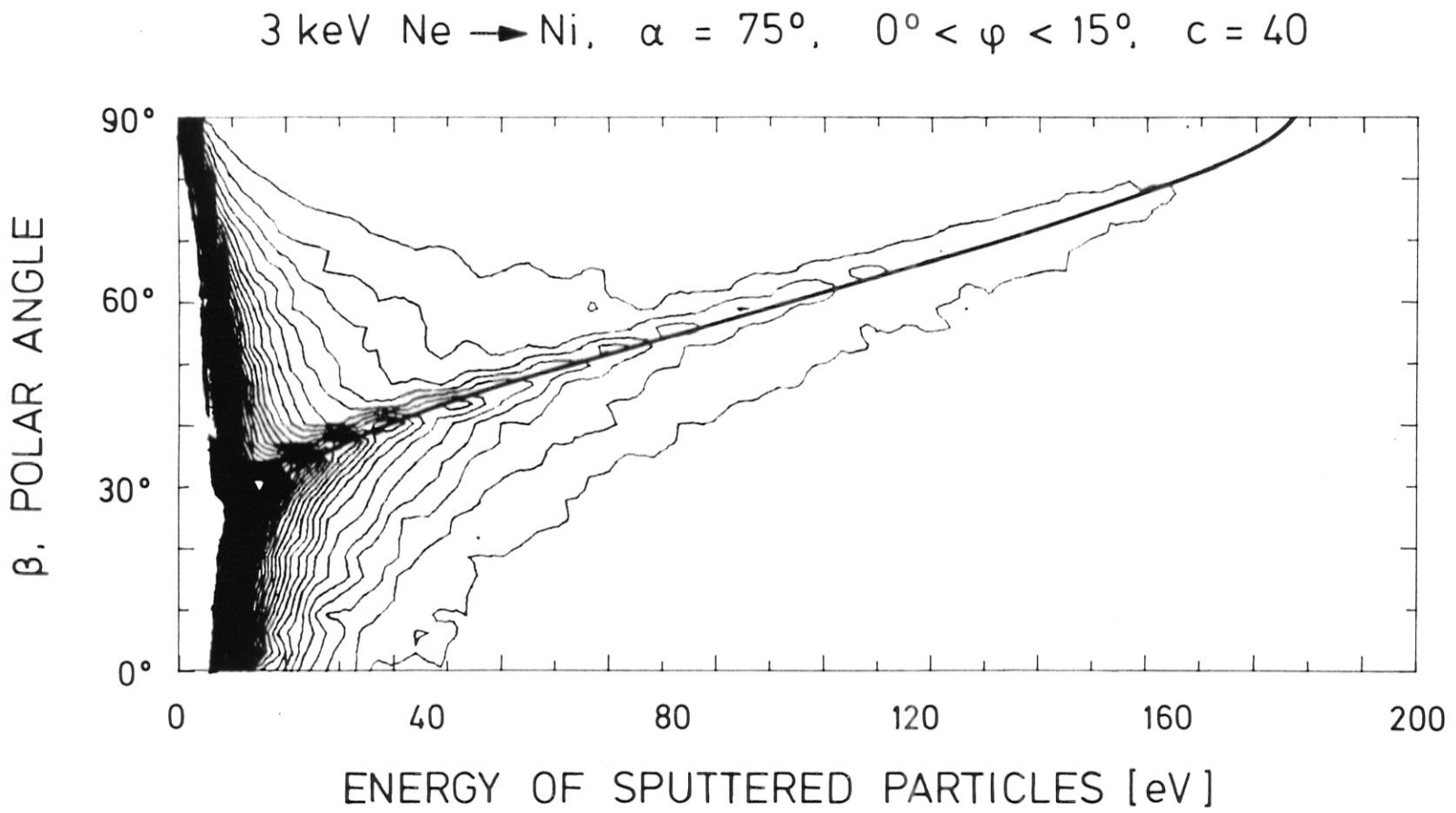
3 keV Ne → Ni, α = 75°, 0° < φ < 15°, c = 40
β, POLAR ANGLE
90°
60°
30°
0°
0
40
80
120
160
200
ENERGY OF SPUTTERED PARTICLES [eV]

Fig. 58

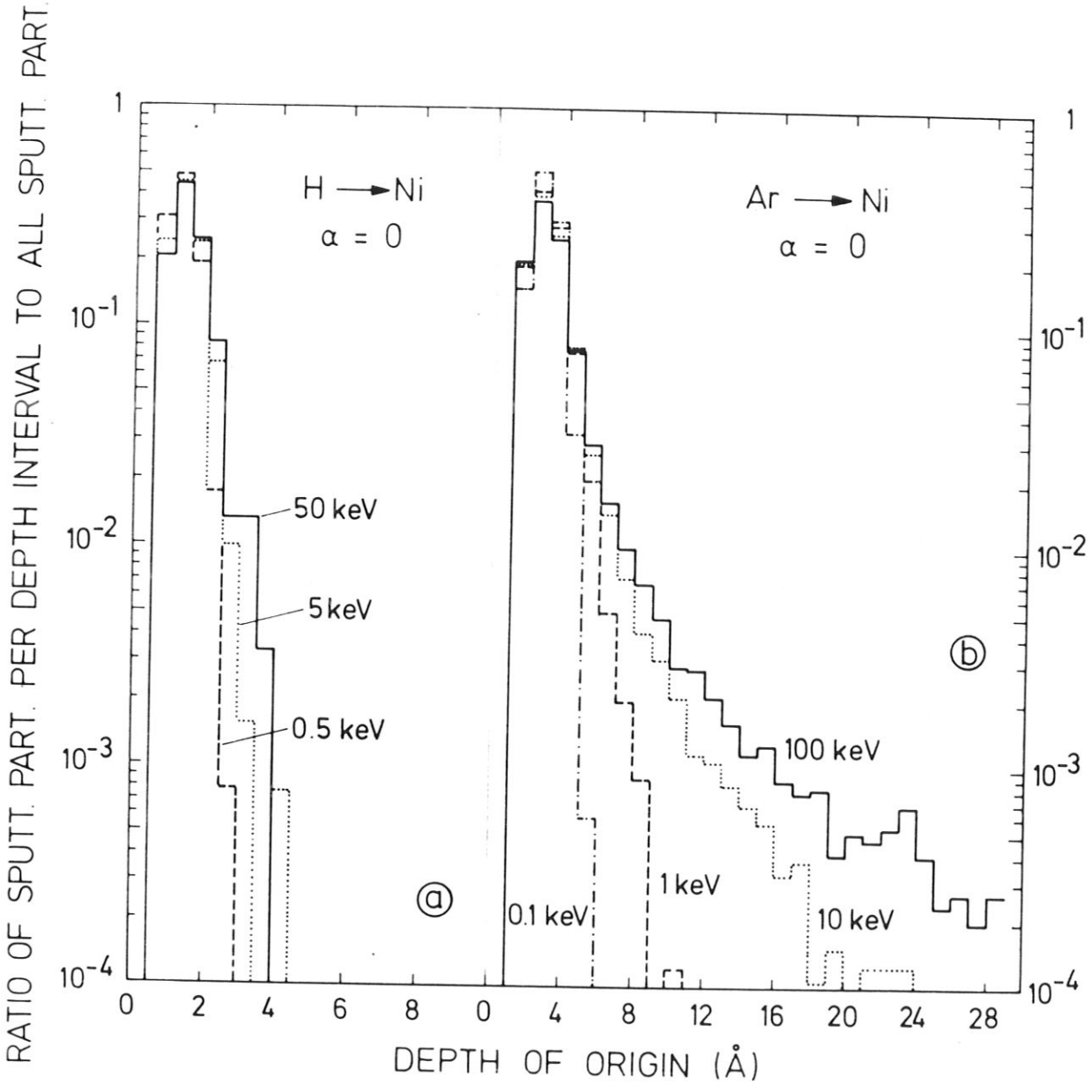
RATIO OF SPUTT. PART. PER DEPTH INTERVAL TO ALL SPUTT. PART.
DEPTH OF ORIGIN (Å)
H → Ni
α = 0
Ar → Ni
α = 0
50 keV
5 keV
0.5 keV
0.1 keV
1 keV
10 keV
100 keV
ⓐ
ⓑ
1
10^{-1}
10^{-2}
10^{-3}
10^{-4}
0
2
4
6
8
0
4
8
12
16
20
24
28

Fig. 59

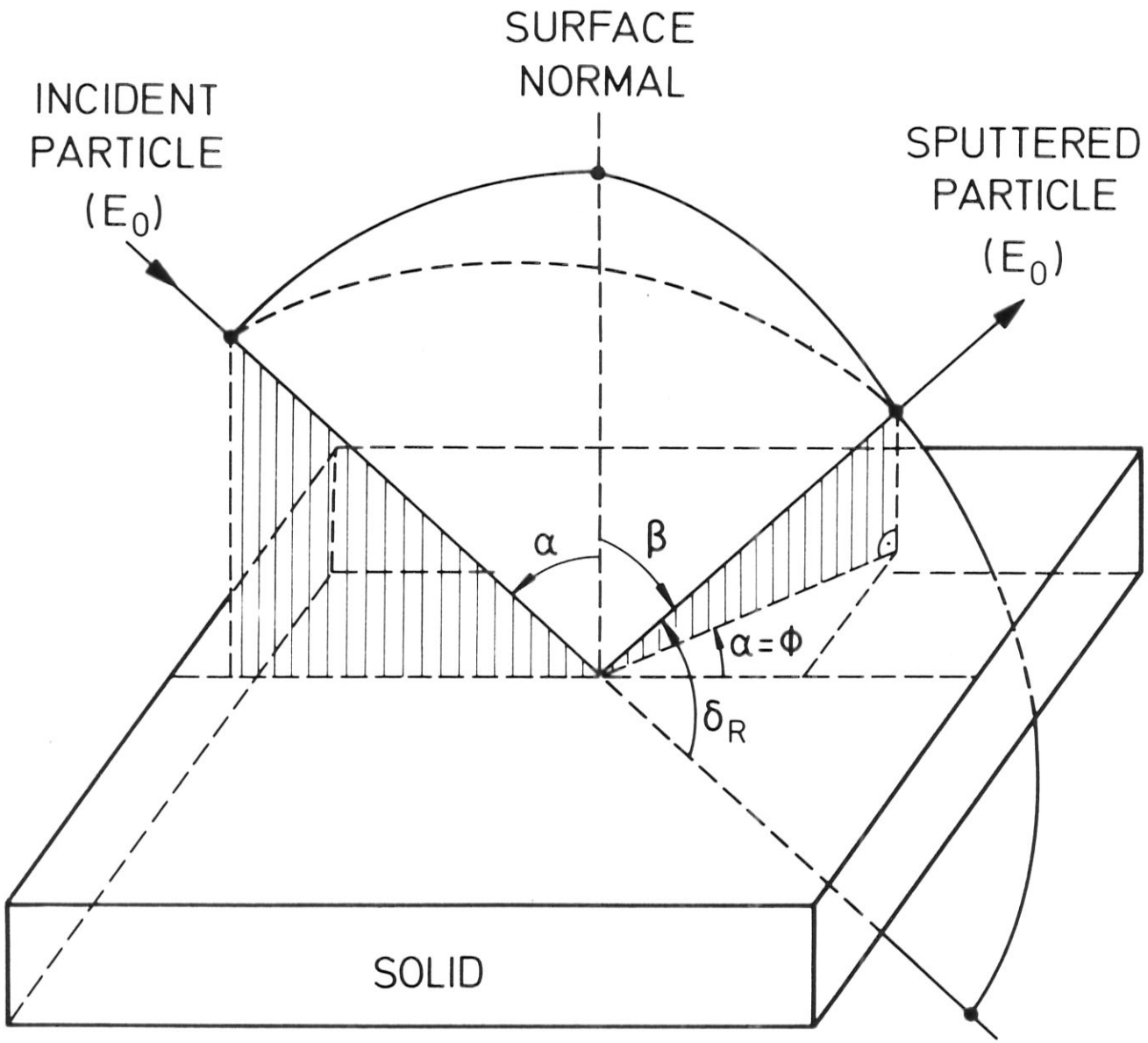
SURFACE
NORMAL
INCIDENT
PARTICLE
(E_0)
SPUTTERED
PARTICLE
(E_0)
α
β
$\alpha = \Phi$
δ_R
SOLID

Fig. 6a

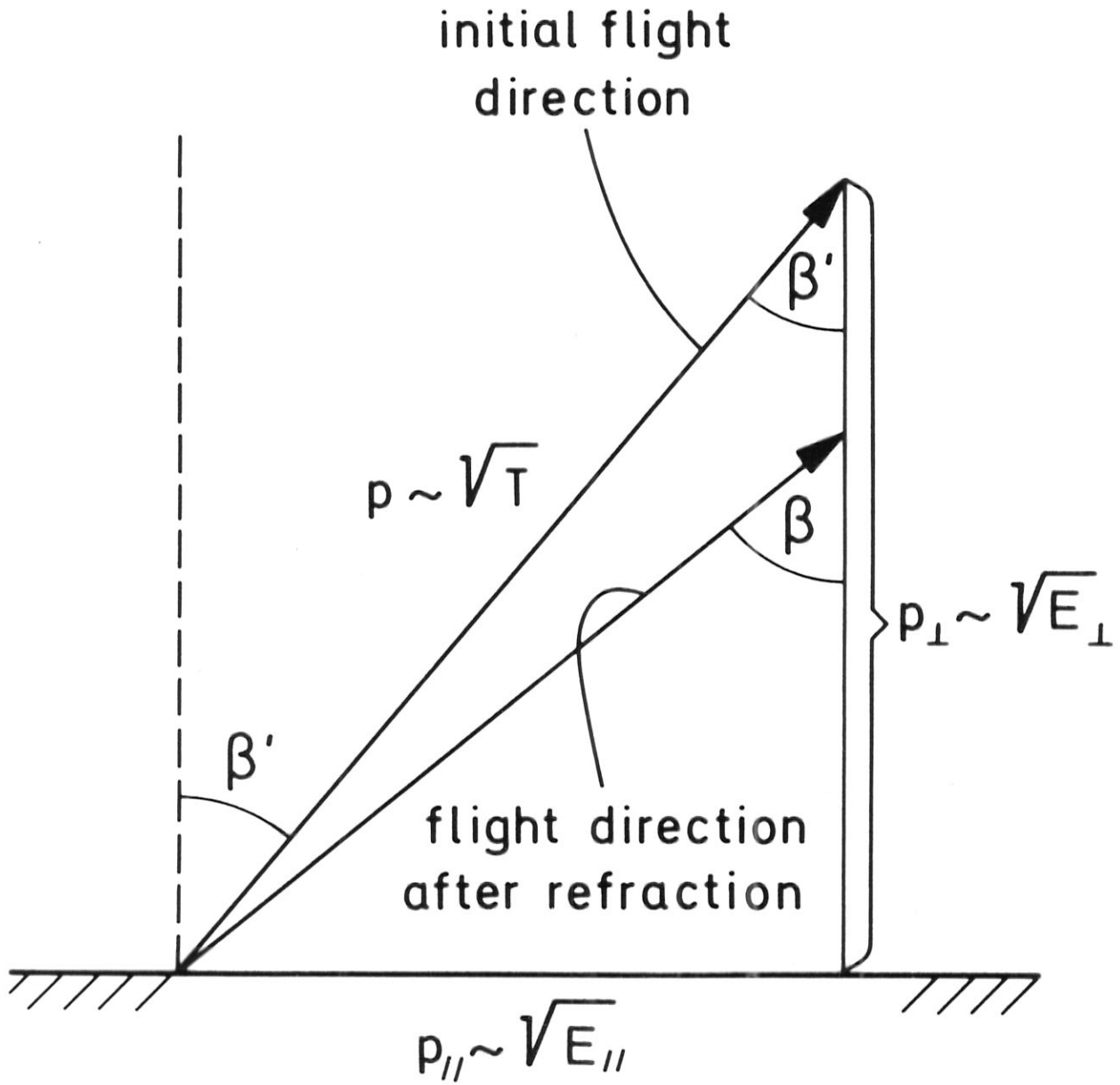
initial flight
direction
β'
p ~ √T
β
p⊥ ~ √E⊥
β'
flight direction
after refraction
p// ~ √E//

Fig. 61